

Detection, attribution, and modeling of climate change: key open issues

Nicola Scafetta^{1*}

June 18, 2025

¹Department of Earth Sciences, Environment and Georesources, University of Naples Federico II, Complesso Universitario di Monte S. Angelo, Naples, Italy.

*Corresponding author: nicola.scafetta@unina.it

Abstract

The Coupled Model Intercomparison Project (CMIP) global climate models (GCMs) assess that nearly 100% of global surface warming observed between 1850–1900 and 2011–2020 is attributable to anthropogenic drivers like greenhouse gas emissions. These models also generate future climate projections based on shared socio-economic pathways (SSPs), aiding in risk assessment and the development of costly “Net-Zero” climate mitigation strategies. Yet, as this study discusses, the CMIP GCMs face significant scientific challenges in attributing and modeling climate change, particularly in capturing natural climate variability over multiple timescales throughout the Holocene. Other key concerns include the reliability of global surface temperature records, the accuracy of solar irradiance models, and the robustness of climate sensitivity estimates. Global warming estimates may be overstated due to uncorrected non-climatic biases, and the GCMs may significantly underestimate solar and astronomical influences on climate variations. The equilibrium climate sensitivity (ECS) to radiative forcing could be lower than commonly assumed; empirical findings suggest ECS values lower than 3°C and possibly even closer to 1.1 ± 0.4 °C. Empirical models incorporating natural variability suggest that the 21st-century global warming may remain moderate, even under SSP scenarios that do not necessitate Net-Zero emission policies. These findings raise important questions regarding the necessity and urgency of implementing aggressive climate mitigation strategies. While GCMs remain essential tools for climate research and policymaking, their scientific limitations underscore the need for more refined modeling approaches to ensure accurate future climate assessments. Addressing uncertainties related to climate change detection, natural variability, solar influences, and climate sensitivity to radiative forcing will enhance predictions and better inform sustainable climate strategies.

Keywords: Climate change detection, attribution and hazard assessment; Climate model validation; Anthropogenic vs. natural climate drivers; Equilibrium climate sensitivity; Solar cycles and influence on climate.

Cite as: Scafetta, N.: 2025. Detection, attribution, and modeling of climate change: Key open issues. Gondwana Research. <https://doi.org/10.1016/j.gr.2025.05.001>

Highlights:

This paper argues that climate science still faces unresolved key issues. Global Climate models struggle in reproducing natural variability at all time scales and may exaggerate warming. Global Climate models likely exaggerate the ECS and significantly underestimate solar influences. Empirical models project moderate warming challenging strict net-zero climate policies. New climate models that better reflect natural climate drivers and variations are needed.

Detection, attribution, and modeling of climate change



key open issues



Climate issues

- Past climate change and natural climate variability are poorly understood and poorly modeled.
- The equilibrium climate sensitivity to radiative forcing is highly uncertain.
- Global surface temperature records are likely to be affected by non-climatic warming biases, such as uncorrected UHI contamination.
- Cloud formation must be modeled with very high precision to understand climate change.

Expectations

- **Fact: current CMIP6 global climate models (GCMs) do not properly model natural climate variability and overestimate the climate sensitivity to radiative forcing (i.e. to CO₂ increase).**
- **The Sun is likely to play an important role in climate change, which remains poorly understood and modeled.**
- **Future climate change is likely to be moderate under realistic socio-economic pathways that do not require Net-Zero policies.**

Solar issues

- It is possible to approximately reconstruct multidecadal, secular, and millennial changes in total solar irradiance in phase and frequency, but not in absolute amplitude.
- It is plausible that the Sun significantly influences climate change through variations in its luminosity, and through a poorly understood mechanism related to variations in particle fluxes reaching Earth.

1 Introduction

Throughout human history, climate change has profoundly influenced both the natural environment and societal structures, leaving a lasting imprint through its wide-ranging positive and negative effects. The negative impacts encompass a range of potential threats, including diminished food production, increased transmission of diseases, and the disruption of ecosystems and infrastructure caused by extreme weather events such as heatwaves, floods, hurricanes, sea level rise, and droughts (IPCC, 2023). Importantly, the effects of climate change are unevenly distributed across the globe, with socio-economic disparities accentuating differences in exposure and vulnerability. Marginalized communities, particularly those facing economic constraints, are disproportionately affected by climate-related hazards. Such disparities underscore the enduring concern humanity has had regarding climate change. Nevertheless, the science underpinning climate change, its causative factors, and the reliability of future climate projections remain subjects of significant scientific uncertainty (Curry, 2023). This contrasts with prevalent public assertions claiming that climate change is “*settled science*”.

The United Nations Intergovernmental Panel on Climate Change (IPCC) has published a series of Assessment Reports (ARs) since 1990, which address the detection and attribution of climate change (IPCC, 1990, 1995, 2001, 2007, 2013, 2021). These reports are regarded by many scientists, policymakers, and members of the public as providing robust evidence of a significant anthropogenic contribution to unprecedented global warming since the pre-industrial period of 1850–1900. Fossil fuel combustion — resulting in the release of greenhouse gases, particularly carbon dioxide (CO₂) — is identified as the primary driver of increased radiative forcing leading to rising global surface temperatures. Global climate models (GCMs) process a number of radiative forcing inputs and simulate global temperature increases, attributed in gran part to the activation of allegedly-positive climatic feedback mechanisms. The outputs of these GCMs are subsequently employed to assess future climate scenarios based on hypothetical shared socioeconomic pathways (SSPs) and associated hazards. This information forms the basis for the IPCC recommendations aimed at guiding policymakers in crafting comprehensive and costly climate mitigation strategies to avert projected adverse climate change outcomes (IPCC, 2023).

For instance, the European Union has adopted the “*Green Deal*”, a policy initiative targeting at least a 55% reduction in net greenhouse gas emissions by 2030 (compared to 1990 levels) and achieving carbon neutral-

ity, or “Net-Zero”, by 2050 (European Union, 2024). This policy framework seeks to balance greenhouse gas emissions with their removal via natural absorption processes and emerging carbon sequestration technologies. The overarching goal of the Net-Zero policies is to keep the “increase in the global average temperature to well below 2°C above pre-industrial levels” with efforts “to limit the temperature increase to 1.5°C above pre-industrial levels” (Paris Agreement, 2016). Strategies include transitioning from fossil fuels to renewable energy sources (geothermal, hydroelectric, solar, and wind power) and replacing internal combustion vehicles with electric alternatives.

However, the implementation of the Green Deal policies entails significant economic investments, potentially jeopardizing industrial development and economic growth. Therefore, a thorough evaluation of the feasibility of these policies and the underlying scientific justifications is imperative.

Serious economic challenges render Net-Zero targets difficult, if not impossible to achieve. As of 2023, the European Union’s 27 member states collectively contributed only 6.08% of global greenhouse gas emission, which continues to grow globally by approximately 2% annually, despite reductions in Europe (European Commission, 2024). The continued global reliance on fossil fuels — evident in the approximately 1,000 coal-fired power plants across Asia currently under construction or planned, particularly in China and India (Global Coal Plant Tracker, 2024) — suggests that achieving Net-Zero emissions may remain impractical throughout the 21st century (Climate Action Tracker, 2024; Hausfather and Peters, 2020; IEA, 2024). Also the depletion of critical metals essential for low-carbon technologies and electric vehicles (e.g., Co, Ni, Cu, Se, Ag, Cd, In, Te, and Pt) by 2060 could hinder further technological advancements (Groves et al., 2023). Furthermore, economic meta-analyses indicate that the costs associated with implementing Net-Zero policies to meet the targets of the Paris Agreement could outweigh the anticipated benefits even in the most favorable scenario (Tol, 2023). The above findings suggest the need of a meticulous evaluation of energy and climate policies by carefully weighing their potential advantages and disadvantages (ÓhAiseadha et al., 2020).

To accurately assess the risks associated with projected climate changes and the effectiveness of mitigation policies, it is essential to first evaluate the reliability of current climate science. The IPCC Assessment Reports directly address this point by explaining in great details how the Coupled Model Intercomparison Project (CMIP6) rigorously tests global climate models (GCMs) against historical climate records. These models undergo thorough a number of statistical validation in an attempt to ensure that their confidence intervals align well with the observed temperature trends. Additionally, climate models are cross-checked with paleoclimate data from ice cores and tree rings, as well as insights from oceanography, atmospheric physics, and geophysics. By integrating evidence from multiple disciplines, the IPCC attempts to maintain consistency between climate projections and real-world observations.

However, unresolved major scientific questions regarding the science of climate change persist. In fact, contrary to some popular perception, climate science remains unsettled and highly debated. Recent research highlights persistent uncertainties in the detection, attribution, and prediction of climate change, and advocate for a more cautious approach to this multifaceted complex issue.

Scientific challenges in climate detection, attribution, and modeling stem from three primary issues:

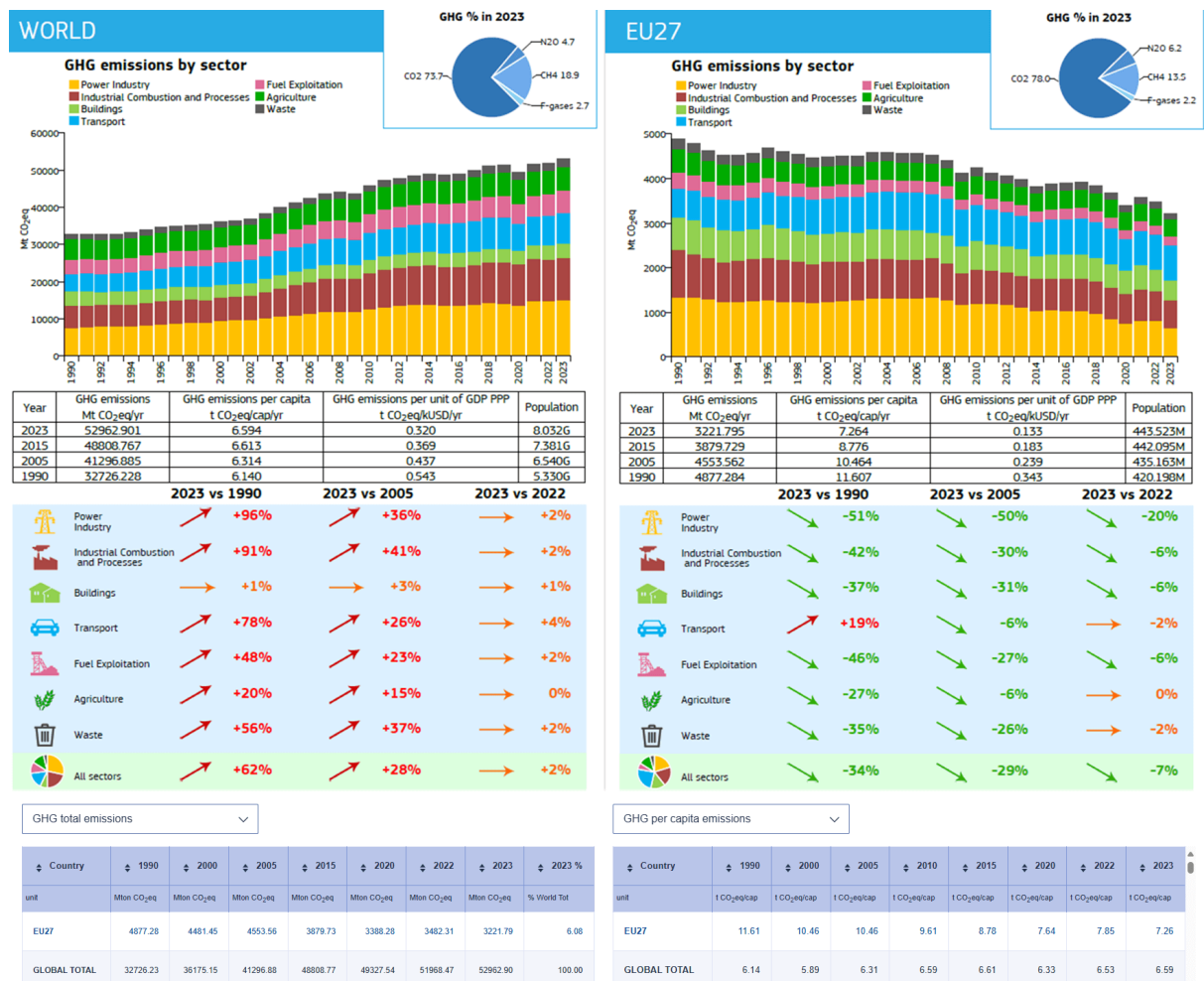
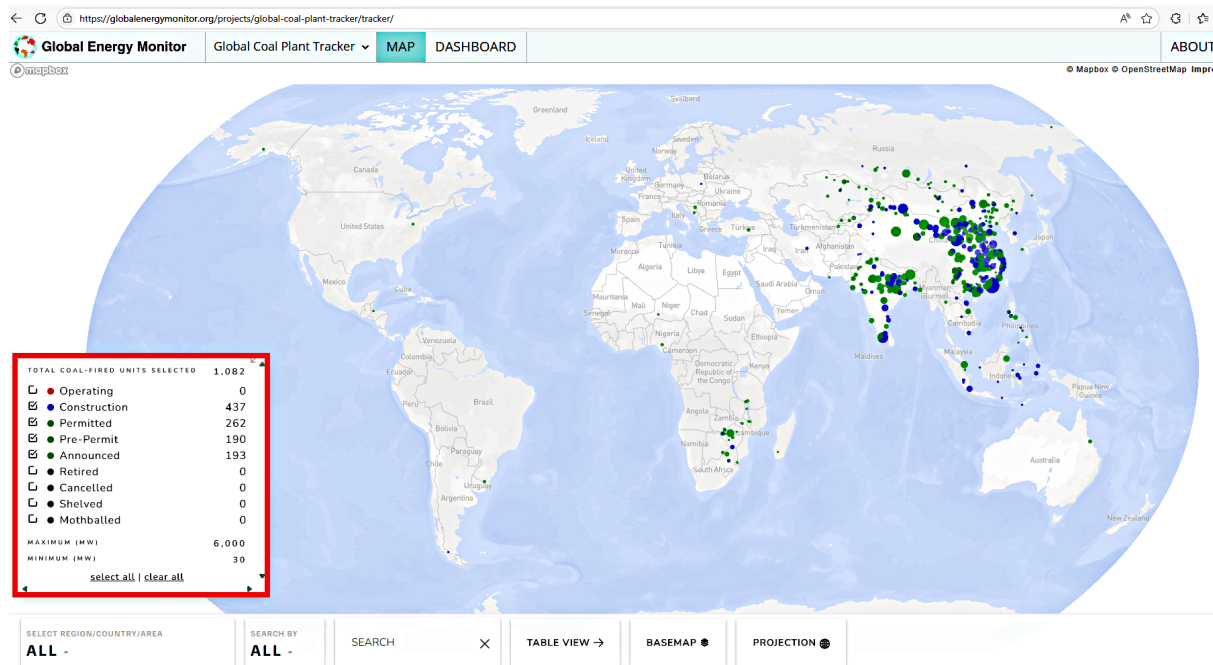
1. the inherent uncertainty of what measurements really indicate complicates the detection of climate change and its causative factors;
2. the anthropogenic contribution is superimposed to natural climate variability, necessitating comprehensive understanding and accurate modeling of the latter;
3. key physical processes, such as cloud formation and solar contributions to climate dynamics, remain poorly characterized.

Anthropogenic climate change becomes meaningful only if it is significant relative to expected natural variability. Accurate attributions require precise modeling of external forcing mechanisms and climate responses. However, ongoing uncertainties in these areas continue to impede the accurate attribution of observed climatic changes to either natural or human influences (Curry, 2023).

Appendix A.

(Top) The figure illustrates that there are the approximately 1,000 coal-fired power plants across Asia currently under construction or planned, particularly in China and India (Global Coal Plant Tracker, 2024).

(Bottom) The figure illustrates that as of 2023, the European Union's 27 member states collectively contributed only 6.08% of global greenhouse gas emission, which continues to grow globally by approximately 2% annually, despite reductions in Europe. Data from the "JRC SCIENCE FOR POLICY REPORT GHG EMISSIONS OF ALL WORLD COUNTRIES 2024" (European Commission, 2024).



Section 2 of this paper outlines the evolution of the “*Anthropogenic Global Warming Theory*” (AGWT) as presented in the IPCC Assessment Reports published from 1990 to 2023 (IPCC, 1990, 1995, 2001, 2007, 2013, 2021). Sections 3 and 4 critically examine uncertainties surrounding the reliability of global temperature records, the extent of solar influences on climate change, and climate sensitivity to radiative forcing. Evidence suggests that estimates of global surface warming since the pre-industrial period may have been exaggerated (e.g.: Scafetta and Ouyang, 2019; Scafetta, 2021a; Katata et al., 2023; Soon et al., 2023) and that solar and astronomical contributions to climate dynamics may have been underestimated (e.g.: Connolly et al., 2023; Scafetta, 2023a). Additionally, contemporary GCMs remain insufficiently validated, and climate sensitivity parameters may be lower than previously anticipated (e.g.: Lewis, 2023; Scafetta, 2022, 2023b).

Empirical models incorporating natural variability are discussed in Section 5 and suggest that global warming during the 21st century under realistic SSPs may be moderate (e.g.: Connolly et al., 2020; Scafetta, 2024) and not as severe as projected by the IPCC (2021, 2023). Consequently, it is investigated whether the risks associated with future climate change have been overestimated, underscoring the need to address several physical uncertainties prior to develop and implement effective climate policies.

2 The Anthropogenic Global Warming Theory (AGWT)

This section outlines the key arguments supporting the Intergovernmental Panel on Climate Change’s theory of anthropogenic global warming, and traces the evolution of the AGWT from the 1990s to the most recent assessment report (AR6, IPCC, 2021, 2023).

2.1 The IPCC Assessment Reports from 1990 to 2023

The IPCC’s Sixth Assessment Report (AR6, 2023) claims definitive evidence linking human activities to the observed global warming. According to the report: “*Global surface temperature was 1.09 [0.95 to 1.20] °C higher in 2011–2020 than 1850–1900, with larger increases over land (1.59 [1.34 to 1.83] °C) than over the ocean (0.88 [0.68 to 1.01] °C)*”; further, “*It is unequivocal that human influence has warmed the atmosphere, ocean and land*” owing to “*observed increases in well-mixed greenhouse gas (GHG) concentrations since around 1750 are unequivocally caused by human activities*”. The report concludes: “*The likely range of total human-caused global surface temperature increase from 1850–1900 to 2010–2019 is 0.8°C to 1.3°C, with a best estimate of 1.07°C*”. These statements support the conclusion that nearly 100% of the global surface warming observed from the pre-industrial period (1850–1900) to 2011–2020 is attributable to anthropogenic drivers, which forms the basis of the Anthropogenic Global Warming Theory (AGWT). However, the IPCC’s attribution of natural versus anthropogenic contributions to climate change has evolved significantly over time.

The IPCC’s First Assessment Report (FAR, 1990) acknowledged that in the 20th century human activities had begun influencing global climate, but precise quantification of their contribution remained elusive due to uncertainties surrounding natural variability. FAR highlighted the paleoclimatic temperature record of the last millennium by Lamb (1965). This was a proxy temperature reconstruction for England that could more broadly represent the European and North Atlantic climates. This reconstruction identified a pronounced Medieval Warm Period (MWP) (900–1300 AD), which was estimated definitely warmer than the first half of the 20th century, followed by the Little Ice Age (LIA) (1300–1850 AD). On the basis of such evidence, FAR noted that the warming observed since 1900 was “*broadly consistent with predictions of climate models, but it is also of the same magnitude as natural climate variability*”, and suggested that “*the observed increase could be largely due to this natural variability; alternatively this variability and other human factors could have offset a still larger human-induced greenhouse warming*” (FAR Executive Summary, p. xii).

The Second Assessment Report (SAR, 1995) largely corroborated FAR’s findings, estimating that anthropogenic activities could have accounted for approximately 50% of the observed global warming of the 20th century with natural variability contributing the remainder. SAR and FAR also noted a moderate global cooling from the 1940s to the 1970s.

The IPCC's Third Assessment Report (TAR, 2001) posited that human activities likely accounted for around 70% of the observed warming since 1900, emphasizing the role of greenhouse gas emissions (e.g., carbon dioxide, methane, nitrous oxide) from industrial processes, agriculture, and deforestation. TAR introduced a novel reconstruction of the Northern Hemisphere temperatures over the past millennium (Mann et al., 1999), which depicted the controversial “hockey-stick” pattern showing a very modest $\sim 0.2^{\circ}\text{C}$ cooling from MWP to LIA followed by $\sim 1^{\circ}\text{C}$ warming from 1900 to 2000. This graph suggested that the 20th-century warming was unprecedented and that the overall temperature pattern of the last millennium correlated well with historical greenhouse gas concentration records; such a correlation increased confidence in climate models and in their climate attribution assessments (cf. Crowley, 2000). However, the hockey-stick graph contradicted earlier paleoclimate research (e.g. Lamb, 1965) and sparked controversy (e.g. Soon and Baliunas, 2003; Soon et al., 2003; von Storch et al., 2004) due also to methodological concerns (McIntyre and McKittrick, 2003), rapidly becoming even a politically charged debate (e.g.: Deming, 2006; Gore, 2006).

The Fourth Assessment Report (AR4, 2007) proposed again the hockey-stick graph (Mann et al., 1999) and concluded that “*most of the observed increase in global average temperatures since the mid-20th century is ‘very likely’ (i.e., >90% probability) due to the observed increase in anthropogenic greenhouse gas concentrations*”.

Meanwhile, several novel paleoclimatic studies (e.g.: Moberg et al., 2005; Mann et al., 2008) revealed a more pronounced MWP, sometimes comparable to the Current Warm Period (CWP) of the last of the last decades of the 20th century (e.g.: Ljungqvist, 2010; Christiansen and Ljungqvist, 2012). These records were acknowledged in the IPCC Fifth Assessment Report (AR5, 2013, its figure 5.7), where the original hockey-stick temperature graph was abandoned. However, the report maintained that “*It is ‘extremely likely’ (i.e., 95–100% probability) that human influence was the dominant cause of global warming between 1951 and 2010*”.

Finally, AR6 (IPCC, 2021, 2023) attributed $0.8\text{--}1.3^{\circ}\text{C}$ of the observed $0.95\text{--}1.20^{\circ}\text{C}$ warming (from 1850–1900 to 2011–2020) to anthropogenic emissions, and relied on the PAGES-2K Consortium (2019) proxy model, which again attenuated the Medieval Warm Period although more moderately than in the original hockey-stick temperature record proposed by Mann et al. (1999). However, representing the Common Era temperature history through a single paleoclimatic reconstruction has been recently criticized as reductive (Esper et al., 2024), indicating that the debate remains ongoing. Accurate assessments of past climates are necessary to validate the AGWT, as discussed below.

2.2 The crucial role of the “Global Climate Models” (GCMs)

Despite significant uncertainties in paleoclimate temperature reconstructions, the IPCC's understanding of climate change attribution from the pre-industrial period (1850–1900) to the present largely relies on computational experiments conducted with sophisticated numerical climate models. The principal characteristics and findings of these models are extensively summarized in the IPCC's Fourth, Fifth, and Sixth Assessment Reports (IPCC, 2007, 2013, 2021).

Numerical climate models, commonly referred to as “*General Circulation Models*” or “*Global Climate Models*” (GCMs), are advanced computational tools designed to simulate the dynamics of the climate system. These models capture interactions between the ocean, atmosphere, and land, predicting variations in climate parameters based on imposed radiative forcing functions. Radiative forcing functions include alterations driven by greenhouse gas concentrations (e.g., carbon dioxide [CO_2], methane [CH_4]), atmospheric aerosols (e.g., industrial sulphate aerosols, black carbon), land-use changes (e.g., deforestation, urbanization), solar radiation fluctuations, and volcanic activity, which introduces aerosols and gases into the atmosphere: see Figures 1A and 1C. Each of these factors can perturb the energy balance of the climate system, resulting in either warming or cooling effects. GCMs simulate the system's integrated response to the combination of these forcing functions.

The climate system's response to variations in radiative forcing is mediated by mechanisms known as climate feedbacks. These feedbacks may amplify or diminish the initial changes induced by the forcing; they are categorized as positive (leading to enhanced warming) or negative (leading to mitigated warming). Key

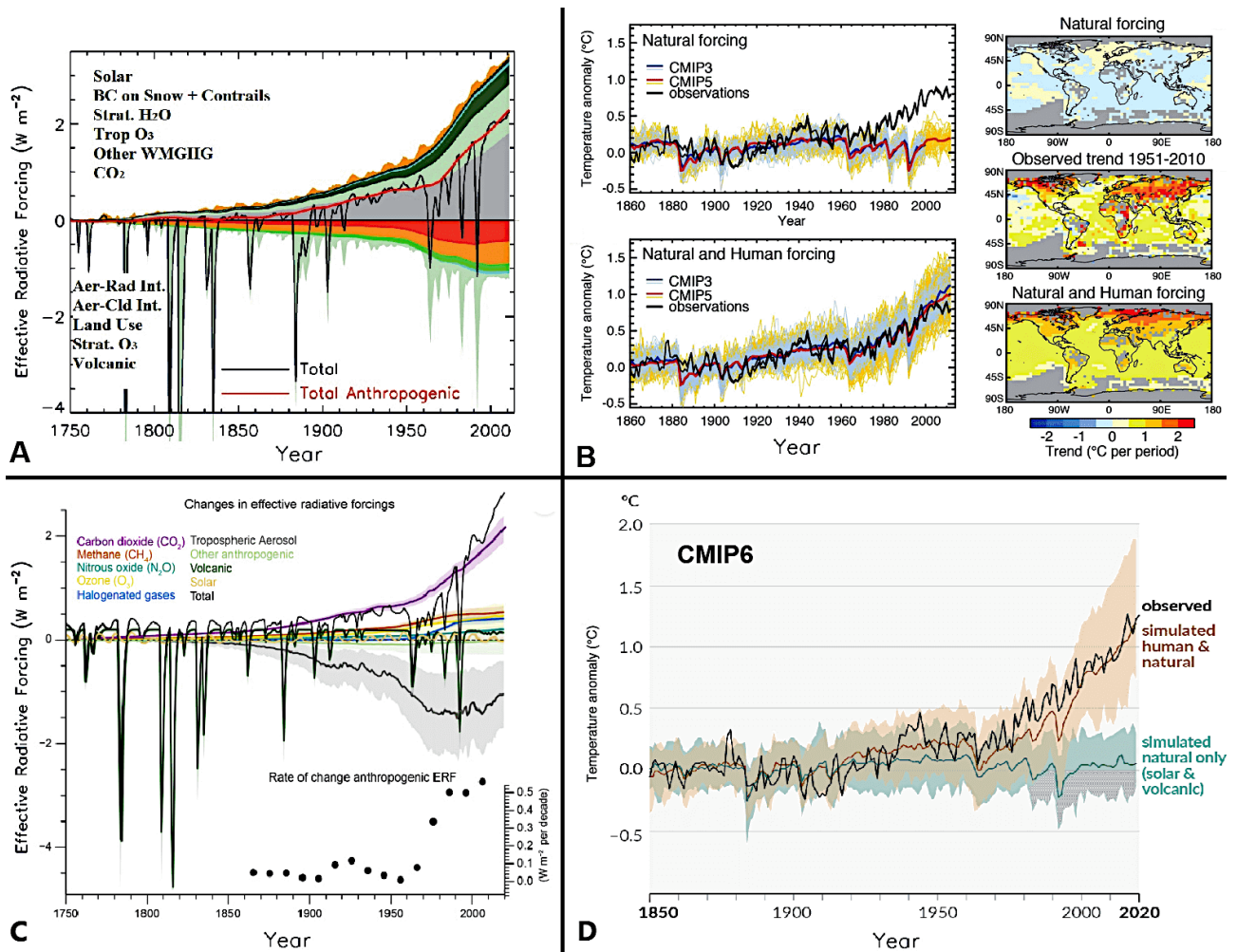


Figure 1: (A) Compilation of the radiative forcing functions utilized in the CMIP5 GCMs (adapted from IPCC, 2013, Figure 8.18). (B) Variations in observed global surface temperature (black) alongside the CMIP3 and CMIP5 model simulations incorporating only natural forcing and combined natural-anthropogenic forcing (adapted from IPCC, 2013, FAQ 10.1, Figure 1). (C) Compilation of the radiative forcing functions utilized in the CMIP6 GCMs (adapted from IPCC, 2021, Figure 2.10). (D) Observed global surface temperature variations (black) alongside the CMIP6 model simulations incorporating only natural forcing and combined natural-anthropogenic forcing (adapted from IPCC, 2021, Figure SPM.1). Notably, in both (B) and (D), the observational data necessary to validate the GCM predictions that consider only natural forcings are not reported because they do not exist.

feedback mechanisms include:

- *Water Vapor Feedback* — A positive feedback governed by the Clausius-Clapeyron law, which links ocean evaporation rates to temperature increases;
- *Albedo Feedback* — A positive feedback arising from changes in surface reflectivity due to ice and snow cover variations;
- *Cloud Feedback* — Particularly challenging to quantify, as cloud formation, type, and distribution are sensitive to warming; certain clouds cool the surface by reflecting solar radiation, while others trap emitted heat, making their net contribution highly uncertain;
- *Lapse Rate Feedback* — A negative feedback involving modifications to atmospheric temperature vertical gradients;
- *Carbon Cycle Feedback* — Activated by warming-induced CO_2 release from soils and oceans (per Henry's law), further increasing atmospheric CO_2 concentrations;

- *Vegetation Feedback* — Temperature and precipitation changes alter vegetation cover, which influences carbon storage and surface albedo.

While all available GCMs indicate that the positive feedbacks surpass the negative ones thus amplifying the effects of radiative forcing, large uncertainties associated with crucial feedback mechanisms — particularly those related to water vapor and cloud formation — remain substantial.

A doubling of atmospheric CO₂ from pre-industrial levels (280 ppm) to 560 ppm is estimated to increase radiative forcing by approximately $\Delta F_{2\times\text{CO}_2} = 3.7 \text{ W/m}^2$ at the Earth's surface. Under idealized assumptions — neglecting feedbacks and treating Earth as a black body governed by the Stefan-Boltzmann law — this forcing would theoretically result in $\sim 1^\circ\text{C}$ warming upon restoration of energy balance: $\Delta T_{2\times\text{CO}_2} = \Delta F_{2\times\text{CO}_2} / 4\sigma T^3 \approx 1^\circ\text{C}$ (Rahmstorf, 2008). However, the Coupled Model Intercomparison Project Phase 6 (CMIP6) GCMs adopted in AR6 (IPCC, 2021) estimate equilibrium climate sensitivity (ECS) — the projected warming at equilibrium due to a CO₂ doubling — ranging from 1.8°C to 5.6°C , reflecting substantial theoretical uncertainty in the net climate feedback amplification (cf. Hausfather et al., 2022; IPCC, 2021; Scafetta, 2024).

The development of GCMs has been organized under the Coupled Model Intercomparison Project (CMIP, <https://wcrp-cmip.org/>, accessed on April 10, 2025), a global collaborative initiative aimed at advancing climate modeling capabilities and understanding climate change processes. Initiated in 1995 by the World Climate Research Programme's (WCRP) Working Group on Coupled Modeling (WGCM), CMIP operates in phases:

- CMIP1 & CMIP2 — Developed during the 1990s, comprising 18 models;
- CMIP3 — Published in the mid-2000s, including 20 models used for AR4 (IPCC, 2007);
- CMIP5 — Conducted between 2010 and 2014, integrating 40 models from over 20 international groups for AR5 (IPCC, 2013);
- CMIP6 — Initiated in 2013 and ongoing, incorporating 55 models that formed the basis for AR6 (IPCC, 2021; Eyring et al., 2016).

Through CMIP, the scientific community continues to refine the GCMs, yet uncertainties in feedback processes and ECS highlight the need for ongoing improvements in climate modeling physical reliability and accuracy.

2.3 Summary of the GCM results supporting the AGWT

Figure 1 summarizes the findings of the GCMs developed during the Coupled Model Intercomparison Project (CMIP) phases 3, 5 and 6. Figures 1A and 1C illustrate the effective radiative forcing functions utilized in the CMIP5 and CMIP6 GCMs, respectively (IPCC, 2013, 2021), while Figures 1B and 1D present the observed global surface temperature record (black) alongside the GCM simulations generated under two scenarios: one including only natural forcings (solar + volcanic) and the other combining both natural and anthropogenic forcings.

Figures 1A and 1C show that the combined contributions of the solar and volcanic effective radiative forcings are substantially smaller relative to the cumulative impact of anthropogenic forcings. Solar forcing exhibits a modest 11-year cycle superimposed on an almost negligible upward trend, while volcanic forcing is characterized by sharp negative spikes resulting from major eruptions. These volcanic spikes induce short-term cooling effects lasting only a few years (Zanchettin et al., 2022).

The GCM simulations depicted in Figures 1B and 1D strongly support the Anthropogenic Global Warming Theory (AGWT). When GCMs are driven solely by solar and volcanic forcing functions — the only two natural components assumed to influence Earth's climate — the numerical simulations fail to produce any substantial warming or cooling trends throughout the 20th century. This indicates that, absent anthropogenic contributions, the models predict a relatively stable climate from the pre-industrial era (1850–1900) to present.

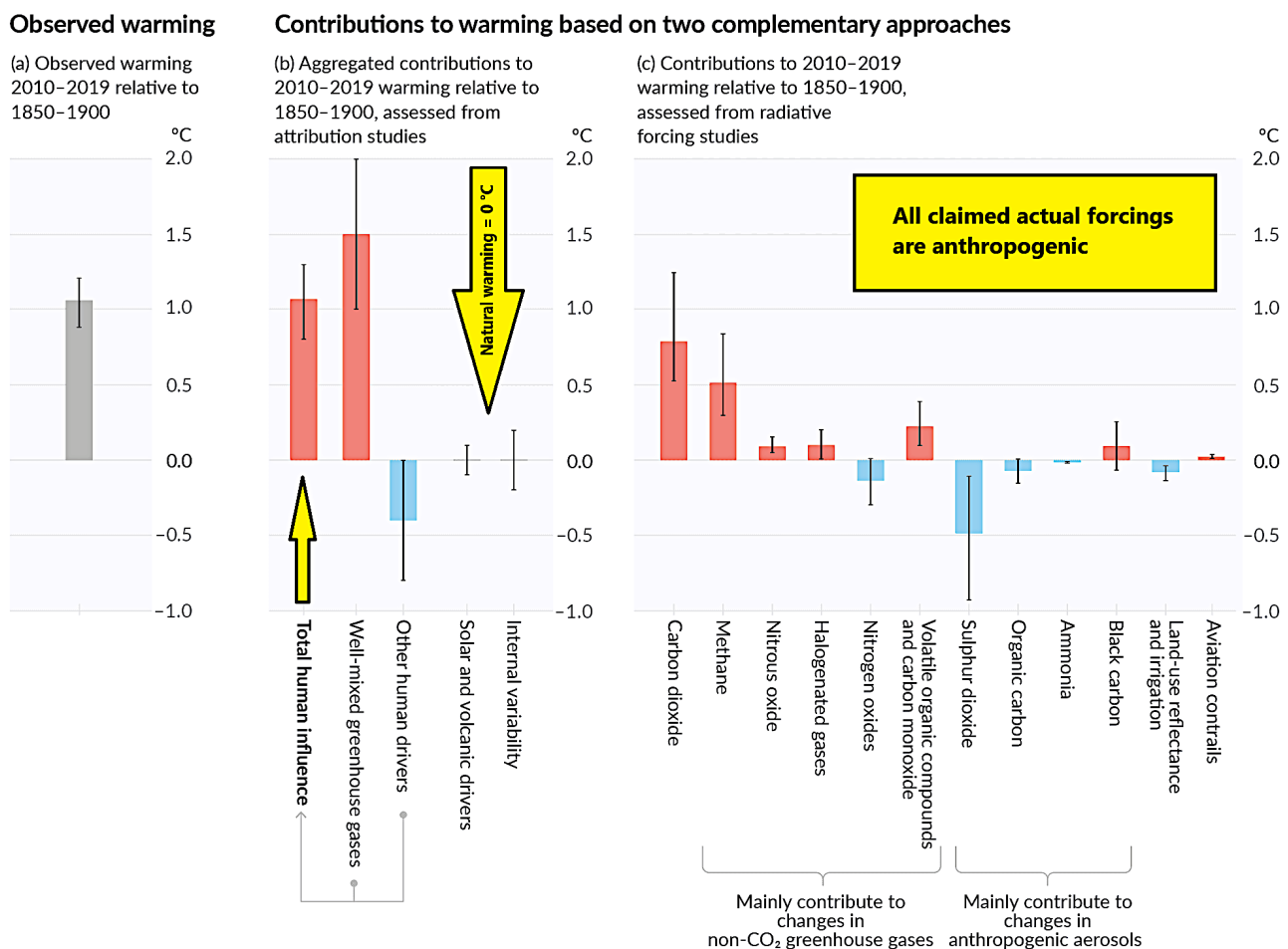


Figure 2: Attributions of warming associated with the radiative forcing functions utilized in the CMIP6 GCMs from 1850–1900 to 2010–2019 (adapted from IPCC, 2021, Figure SPM.2). Notably, natural components — including solar and volcanic drivers, as well as internal variability — are estimated to have contributed an average of 0 °C each. Thus, the observed warming is attributed to anthropogenic drivers alone.

However, by incorporating anthropogenic radiative forcing functions, the GCMs successfully replicate the observed global surface warming trend. This comparison implies that, according to these GCMs, nearly 100% of the warming recorded since the 1850–1900 period is attributable to anthropogenic factors, as explicitly concluded in AR6 (IPCC, 2021).

Figure 2 explicitly illustrates the attribution results derived from the CMIP6 models, showing the average warming contribution of radiative forcing components from 1850–1900 to 2010–2019 (IPCC, 2021, its figure SPM.2). According to these GCMs, both natural (solar + volcanic) forcings and internal climate variability contributed approximately 0°C to the observed warming. Instead, nearly 100% of the observed 1.07°C global surface warming is attributed to anthropogenic forcings, with well-mixed greenhouse gases contributing ~1.5°C and anthropogenic aerosols offsetting ~0.4°C of the warming.

The CMIP6 GCMs are also employed to simulate future climate scenarios based on hypothetical radiative forcing functions derived from Shared Socioeconomic Pathways (SSPs). The ones mainly adopted in the IPCC AR6 are:

- SSP1-2.6 — low greenhouse gas emissions, with robust adaptation and mitigation measures leading to Net-Zero CO₂ emissions between 2050–2075;
- SSP2-4.5 — intermediate emissions, where CO₂ levels remain near current levels until 2050 and subsequently decline without achieving Net-Zero by 2100;
- SSP3-7.0 — high emissions, with CO₂ concentrations doubling by 2100 under minimal policy interven-

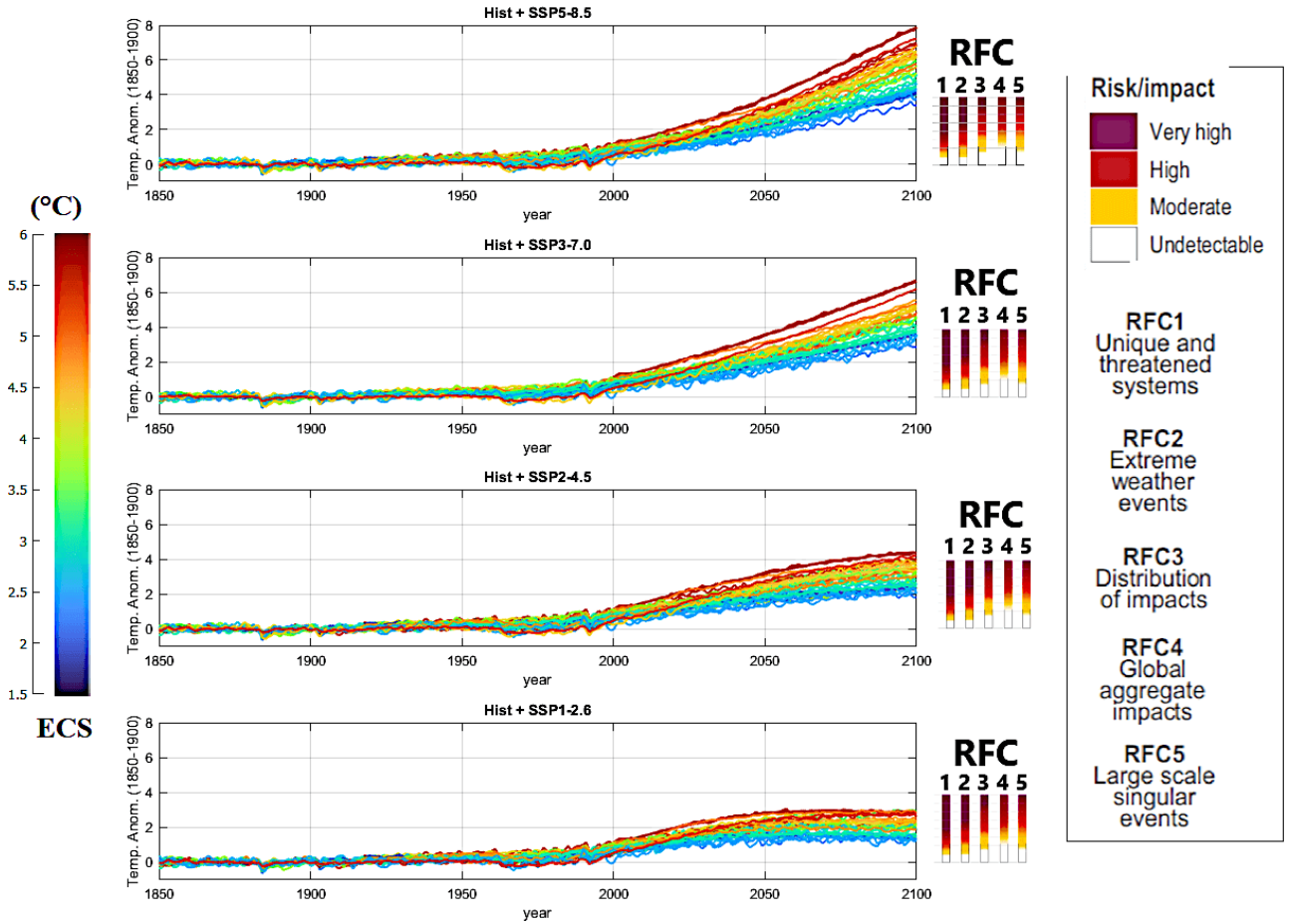


Figure 3: CMIP6 GCM ensemble mean simulations spanning from 1850 to 2100, employing historical effective radiative forcing functions from 1850 to 2014 (see Figure 1C) and the forcing functions based on the SSP scenarios 1-2.6, 2-4.5, 3-7.0, and 5-8.5. Curve colors are scaled according to the equilibrium climate sensitivity (ECS) of the models. The right panels depict the risks and impacts of climate change in relation to various global Reasons for Concern (RFCs) (IPCC, 2023). (Adapted from Scafetta, 2024).

tion;

- SSP5-8.5 — very high emissions, with CO₂ levels tripling by 2075 under a worst-case scenario devoid of mitigation measures.

Figure 3 shows the ensemble mean simulations of the CMIP6 GCMs spanning 1850–2100. These simulations adopt historical radiative forcing functions from 1850–2014 (as illustrated in Figure 1C) and SSP-derived forcing functions for 2015–2100. The color-coded curves correspond to the Equilibrium Climate Sensitivity (ECS) values of the models. Results indicate that the global surface temperature could rise significantly — potentially up to 8°C relative to the 1850–1900 reference period — if SSP5-8.5 is implemented and the ECS value is high (5–6°C).

The right panels of Figure 3 illustrate the projected impacts and risks of climate change associated with various global Reasons for Concern (RFCs). These projections suggest that only SSP1-2.6, which employs aggressive mitigation and Net-Zero policies, can limit the 21st-century warming to below 2°C relative to pre-industrial levels, which is the threshold identified as critical under the Paris Agreement (2016).

2.4 Conclusion

Over the span of approximately three decades, from the publication of the First Assessment Report (FAR, IPCC, 1990) to the Sixth Assessment Report (AR6, IPCC, 2021), the Intergovernmental Panel on Climate Change (IPCC) has significantly advanced its understanding of the role of anthropogenic emissions in driving global

warming. In the 1990s the IPCC posited that both natural mechanisms and human activities could have contributed roughly equally ($\sim 50\%$ each) to the observed warming of the 20th century. However, since the years 2000s the prevailing scientific opinion has shifted, and the IPCC (AR6, 2021) now asserts that human activities are almost exclusively responsible ($\sim 100\%$) for the global warming and climate change observed from 1850–1900 to 2011–2020.

The most recent assessment reports IPCC (2021, 2023) underscore this conclusion with striking clarity. As shown in Figure 2, the average contribution of natural factors — solar and volcanic forcing and internal natural variability — to global warming during the aforementioned period is estimated to be approximately 0°C . Consequently, from the CMIP GCM perspective, concerns about future climate warming due to additional anthropogenic greenhouse gas (GHG) emissions are well-founded. However, this conclusion depends on the reliability of global surface temperature records and the robustness of the physical science underpinning global climate models (GCMs).

Under the worst-case scenario, the SSP5-8.5, which assumes very high and accelerating GHG emissions without mitigation, the GCM projections indicate alarming potential warming of 4°C to 8°C by 2080–2100. Despite these concerning projections, the IPCC (AR6, 2021, its table 12.12, p. 1856) expresses low confidence in attributing changes in the frequency, severity, or extent of several climate impact drivers, such as: river floods, frost, landslides, hydrological drought, drought, agricultural and ecological drought, fire weather, mean wind speed, severe wind storms, tropical cyclones, sand and dust storms, heavy snow and ice storms, hail, snow avalanches, coastal erosion, coastal flooding, marine heat waves, air pollution, and surface radiation. Conversely, AR6 identifies moderate-to-high confidence in climate impact drivers more directly linked to increasing atmospheric CO_2 concentrations and global warming. These include: increases in mean air temperature, extreme heat events, sea level, mean ocean temperature, ocean acidity, and ocean salinity; decreases in cold spells, snow cover, glaciers, ice sheets, permafrost, lake ice, river ice, sea ice, and dissolved oxygen; regional variability in mean precipitation (increasing in some regions and decreasing in others).

This evolution of understanding underscores the complexity of the climate system and the importance of continuously refining projections through improved climate modeling and robust observational datasets.

3 Main challenges to the AGWT

Scientific critiques of the Anthropogenic Global Warming Theory (AGWT) emerge from diverse perspectives, reflecting significant concerns about persistent physical uncertainties and the potential validity of alternative explanations for climate change.

3.1 Erroneous or unsatisfactory critiques

First of all, it is crucial to differentiate scientifically substantiated critiques from various misguided claims often circulating online, which tend to oversimplify the physics of climate change. One such incorrect argument asserts that additional CO_2 emissions cannot affect the climate due to a supposed saturation of the infrared (IR) absorption bands of such gas. This claim is demonstrably inaccurate, as the CO_2 IR absorption bands have not reached their maximum capacity yet. This fact is also acknowledged by van Wijngaarden and Happer (2023, their figure 7) — two noted skeptics of climate change alarmism — who calculated that doubling CO_2 concentrations from 400 to 800 ppm would reduce the upward IR heat flux by approximately 3 W/m^2 at the mesopause altitude (86 km) under standard atmospheric conditions without clouds, assuming a surface temperature of 288.7 K . This result is slightly lower and does not differ significantly from what already reported in the scientific literature and in the IPCC reports, and can be easily verified using the MODTRAN Infrared Light in the Atmosphere model (available online at <https://climatemodels.uchicago.edu/modtran/>, accessed on April 10, 2025), which also estimates a downward IR heat flux at the surface of about 3.6 W/m^2 under identical physical conditions.

In fact, the CO₂ infrared (IR) absorption bands are quasi-saturated, leading to a logarithmic relationship between CO₂ concentration and radiative forcing. For instance, a doubling of atmospheric CO₂ concentration from 400 to 800 ppm results in a typically-estimated increase in radiative forcing of approximately 3.7 W/m², yielding to a theoretical radiative forcing function of the type: $\Delta F_{\text{CO}_2} \approx 3.7 \log_2(P_{\text{CO}_2}/400) \text{ W/m}^2$ with a 10% uncertainty (Myhre, 1998; Etminan et al., 2016); here P_{CO_2} is the CO₂ atmospheric concentration. This evidence directly contradicts the saturation hypothesis that incorrectly infers that any increase in CO₂ levels would result in a radiative forcing increase of 0.0 W/m². As already explained in Section 2.2, the CMIP6 GCMs predict that a radiative forcing of 3.7 W/m² could induce, at equilibrium, a warming from about 1.8 to 5.7°C, depending on the modeled net feedback strength.

It is important to realize that the principal scientific challenge lies not in debating the CO₂ saturation argument but rather in accurately determining the climate sensitivity to radiative forcings that depends on the sign and magnitude of the climate feedback, the actual forcings of the climate system, and the quantitative detection of climate change. Addressing these complex scientific issues requires a detailed understanding of the climate system, of its astronomical environment and of its feedback mechanisms, domains that remain highly uncertain and form a critical focus of ongoing research, as elaborated below.

van Wijngaarden and Happer (2023) expressed skepticism only toward climate change alarmism by arguing that the net climate feedback should predominantly be negative. This is a legitimate physical expectation that the authors supported by citing the findings of Lindzen et al. (2001) and Lindzen and Choi (2011) obtained by comparing high-frequency deseasonalized fluctuations in sea surface temperatures and the concurrent fluctuations in top-of-atmosphere (TOA) outgoing radiation using ERBE and CERES satellite data from 1985 to 2008. However, van Wijngaarden and Happer (2023) specifically invoked also Le Chatelier’s Principle — which states that when a system at equilibrium experiences a disturbance, it will adjust to counteract the disturbance and establish a new equilibrium — to suggest that the climate system should inherently resist radiative perturbations. Citing Le Chatelier’s Principle to conclude that the net climate feedback should be strictly negative appears to oversimplify the complexity of the climate system, which incorporates both negative feedbacks (such as increased cloud cover reflecting sunlight) and positive feedbacks (like ice-albedo effects, where melting ice reduces reflectivity and accelerates warming). It is the interplay between these positive and negative feedbacks that ultimately determines the thermodynamic conditions of the new equilibrium of the climate system. The new equilibrium temperature will depend on the prevailing feedback mechanisms; whether the net feedback is negative or positive just determines whether the resulting temperature deviates downward or upward from the level expected solely due to increased atmospheric CO₂, which is ~1°C for CO₂ doubling (Rahmstorf, 2008). Thus, in this regard, van Wijngaarden and Happer (2023) appear to express only an opinion against the possibility of a catastrophic runaway greenhouse effect scenario where Le Chatelier’s Principle is not satisfied because the new equilibrium is never reached. Such a catastrophic scenario did not occur even during the Cambrian Period (~540–485 million years ago) when the Earth’s temperature was much higher than today and atmospheric CO₂ levels were estimated to be 4,000–5,000 ppm (Royer et al., 2001), that is ten times larger than current levels. In this regard, van Wijngaarden and Happer (2023) do not appear to have actually developed a solid critique of the AGWT advocated by the IPCC, which is perfectly compatible with Le Chatelier’s Principle. Indeed, none of the CMIP GCMs used in IPCC reports predicts a catastrophic runaway greenhouse effect scenario. Only critiques grounded in empirical observations could offer a solid foundation for challenging the AGWT.

In the following, Section 3 provides a summary of the primary scientific critiques of the AGWT outlined in Section 2. It further sets the stage for the exploration of alternative interpretations of climate change, discussed in Sections 4 and 5. Together, these critiques underscore the complexity of the debates surrounding the causes and consequences of climate change and highlight the range of scientific opinions in this evolving research field.

Appendix B.

In relation to Section 3.1, the figure below illustrates the infrared light spectra obtained using MODTRAN (available at the web page: <https://climatemodels.uchicago.edu/modtran/>) in a standard atmosphere under the physical conditions shown in the right-hand inset. The MODTRAN model simulates the emission and absorption of infrared radiation in the atmosphere.

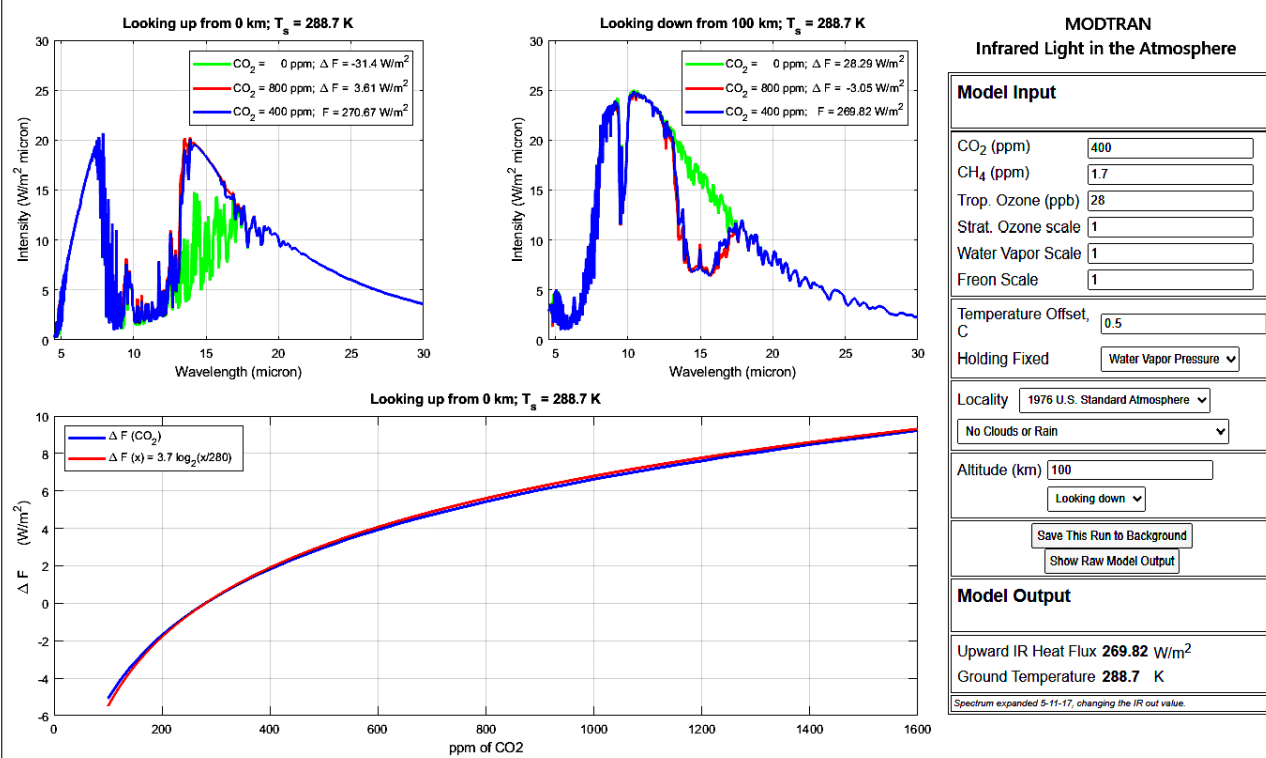
The curves represent theoretical emission spectra at different atmospheric CO₂ concentrations: (green) 0 ppm, (blue) 400 ppm, and (red) 800 ppm.

The top-left panel displays the infrared light spectra observed at the surface of the atmosphere (0 km) looking upward. The top-right panel shows the spectra at the top of the atmosphere (100 km) looking downward; this figure closely aligns with the results obtained by van Wijngaarden and Happer (2023).

The total energy flux from all infrared light is labeled as Upward IR Heat Flux, F , measured in units of W/m^2 . The quantities ΔF in the upper inserts indicate the variation in radiative forcing relative to the baseline value at 400 ppm.

The bottom panel illustrates how radiative forcing changes as a function of CO₂ concentration relative to the pre-industrial level of 280 ppm. The blue curve represents ΔF values obtained with MODTRAN, while the red curve corresponds to the traditionally used approximation function $\Delta F(CO_2) = 3.7 \log_2(CO_2/280)$.

The model effectively demonstrates the influence of wavelength-selective greenhouse gases on Earth's outgoing infrared energy flux, indicating that the spectral bands of the CO₂ present in the atmosphere are not fully saturated yet.



3.2 The concept of “consensus” in the climate change debate

The concept of “consensus” holds political significance but is less meaningful within scientific discourse, where the core principle is the verifiability of results through empirical evidence. Yet, in the realm of climate change, an appeal to consensus is often employed to bolster the validity of the Anthropogenic Global Warming Theory (AGWT), its associated alarmist claims and Net-Zero policies.

For instance, assumptions that climate change science is settled have led editors of Earth science and health journals to advocate for urgent global action on climate change (McNutt, 2015), assessing that “our planet is

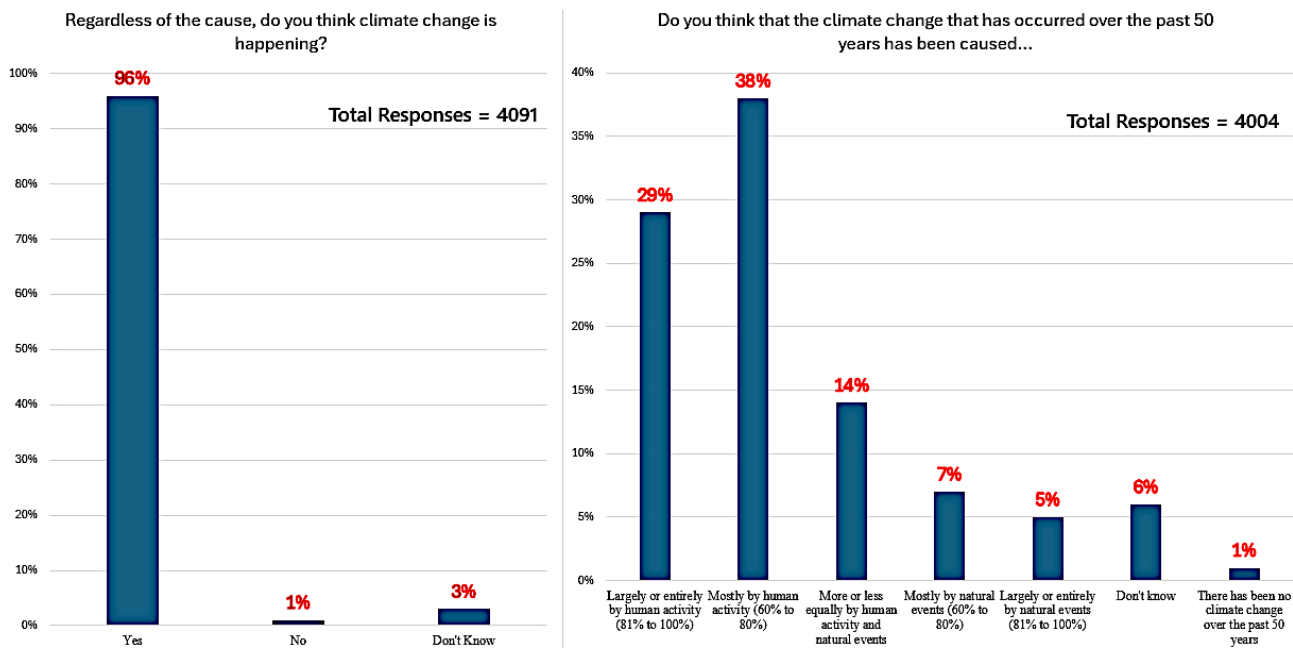


Figure 4: Survey conducted by the American Meteorological Society among its members revealing a wide range of opinions on the causes of climate change (adapted from Maibach et al., 2016, pp. 5 and 8). Only 29% of respondents agreed that global warming was predominantly or entirely (81% to 100%) attributable to human activity — a stance even more moderate than the definitive 100% attribution claimed by the IPCC (AR6, 2021, 2023), as shown in Figures 1 and 2.

in crisis" (Filippelli et al., 2021) and warning that unmitigated climate change poses the 21st-century "*greatest threat to global public health*" (Atwoli et al., 2021). These appeals align with the commitments under the Paris Agreement adopted at the United Nations Conference of the Parties (COP21) in 2015 (Paris Agreement, 2016).

Despite claims of scientific consensus, skepticism persists among scientists and the public due to unresolved uncertainties and concerns surrounding these assertions. Studies suggesting overwhelming agreement among climate scientists — often citing figures such as 97% or even 99% (Cook et al., 2013; Lynas et al., 2021) — are frequently interpreted as evidence of consensus on AGWT. However, critics (e.g.: Montford, 2013; Legates et al., 2015) challenge such conclusions, pointing to statistical flaws and misleading interpretations, which rely on selective datasets and imprecise survey methodologies.

A case in point is the ambiguous nature of the statement "*humans are causing global warming*" (Cook et al., 2013). This statement can be interpreted to mean that nearly all observed warming (~100%) is due to anthropogenic activities, as asserted by the AGWT and explicitly claimed by the IPCC (AR6, 2021). However, the same statement could also mean that only a portion (~50%) of the warming is attributable to human influence, reflecting earlier IPCC reports such as FAR and SAR (1990; 1995). Reliable surveys must, therefore, distinguish between these divergent attribution scenarios, as their implications for climate science and assessments of future risks differ significantly.

When surveys adopt clearer attribution distinctions, the diversity of scientific opinions on climate change becomes evident. Broadly, there is general agreement among scientists on qualitative aspects such as that global warming has occurred since 1850–1900, the greenhouse effect is real, anthropogenic emissions have exacerbated it, and this has contributed to warming over the past century. However, there is no consensus on the precise quantitative attribution of natural versus anthropogenic factors to the observed warming.

For example, Figure 4 summarizes a national survey by the American Meteorological Society revealing a wide range of opinions among respondents about the causes of climate change (Maibach et al., 2016, pp. 5 and 8). While 96% agreed that climate change is occurring, only 29% attributed it mainly or entirely to human activities (81% to 100%), while 38% attributed it mostly to human activities (60% to 80%). Fourteen percent attributed climate change equally to human and natural causes (40% to 60%), and smaller percentages

leaned toward predominantly natural drivers or expressed uncertainty. This means that at least 71% of the respondents disagree with the IPCC AR6's claim that humans are responsible for 100% of the observed global warming. Additionally, two-thirds of respondents believed that aggressive mitigation policies would only moderately or slightly reduce future warming (Maibach et al., 2016, p. 9). This diversity of opinions is not unexpected because it well aligns with the range of views documented in the IPCC assessment reports from FAR (1990) to AR6 (2021).

Indeed, although the IPCC findings have evolved to assert in AR6 that anthropogenic factors are the sole cause of climate change since 1850–1900, shifts in scientific conclusions do not necessarily reflect genuine progress, which requires reducing underlying uncertainties. In science, new findings that appear to challenge earlier results must rigorously justify the invalidation of previous conclusions, not just propose an alternative viewpoint. However, in geosciences, conflicting studies often coexist, with earlier findings persisting despite newer apparently contradictory research.

One prominent example of persistent uncertainty in climate science is the assessment of the equilibrium climate sensitivity (ECS), a crucial metric for gauging the response of the climate system to radiative forcing. From Charney et al. (1979) to AR6 (IPCC, 2021), the ECS uncertainty range has remained relatively unchanged — if not broadened (Undorf et al., 2022) — as illustrated in Figure 5A. This persistent uncertainty underscores unresolved methodological and scientific challenges.

Consensus-based arguments also risk logical fallacies, such as appeals to popularity or authority. In fact, many individuals, including researchers in climate-related fields, may accept the IPCC conclusions without critically engaging with the uncertainties highlighted within the IPCC's own reports. Consequently, reliance on such forms of “*consensus*” does little to resolve the crux of the climate debate regarding whether human activity accounts for 100% of observed warming between 1850–1900 and 2011–2020, as asserted by AR6 (IPCC, 2021), or whether a more moderate contribution (~50%) might better align with actual scientific findings. If the latter opinion holds, the projected 21st-century warming based on the CMIP5 and CMIP6 GCMs would be substantially lower, mitigating assessments of future climate change risks and hazards (Scafetta, 2013a, 2024).

The following subsections delve into key scientific open issues that question the reliability of the GCMs and directly challenge the AGWT. These open key issues continue to be debated in the scientific literature.

3.3 The impossibility of testing the main prediction of the GCMs

The scientific method necessitates that the hypotheses, including physical models, are rigorously tested to ensure that their predictions align with empirical evidence. When evidence supports a hypothesis, the model may be retained; however, when results challenge it, the model must be discarded or revised, requiring the formulation of a new hypothesis or model.

As discussed in Section 2 and illustrated in Figures 1B and 1D, the claim that human activity accounts for approximately 100% of the observed warming from 1850–1900 to 2011–2020 is derived solely from the climate simulations of the existing GCMs. These simulations rely on specific radiative forcing functions, which are assumed to be complete and accurate. However, the only tangible evidence is that there is no data fully confirming the main GCM prediction. More specifically, no data exists to demonstrate that, absent anthropogenic forcing, the Earth's climate would have remained stable from 1850–1900 to the present. Thus, such critical prediction of the GCMs cannot be empirically validated, as there is no “*twin Earth*” devoid of human influence from which to obtain the necessary data. Consequently, the absence of such data — as also reflected in Figures 1B and 1D — highlights the key limitation in the validation of these models.

Therefore, the AGWT remains a hypothesis contingent upon the reliability of the current GCMs, which can only be “assumed” but not “proven” correct. The fact that the primary prediction of these models has neither been experimentally validated nor is it likely to be so in the future, leaves open the possibility that the present GCMs and their climate attribution assessments (as depicted in Figures 1 and 2) may be fundamentally flawed.

While certain qualitative arguments, supported by paleoclimatic evidence (e.g., the hockey-stick temperature reconstruction by Mann et al., 1999) suggest that the current warm period surpasses past warm peri-

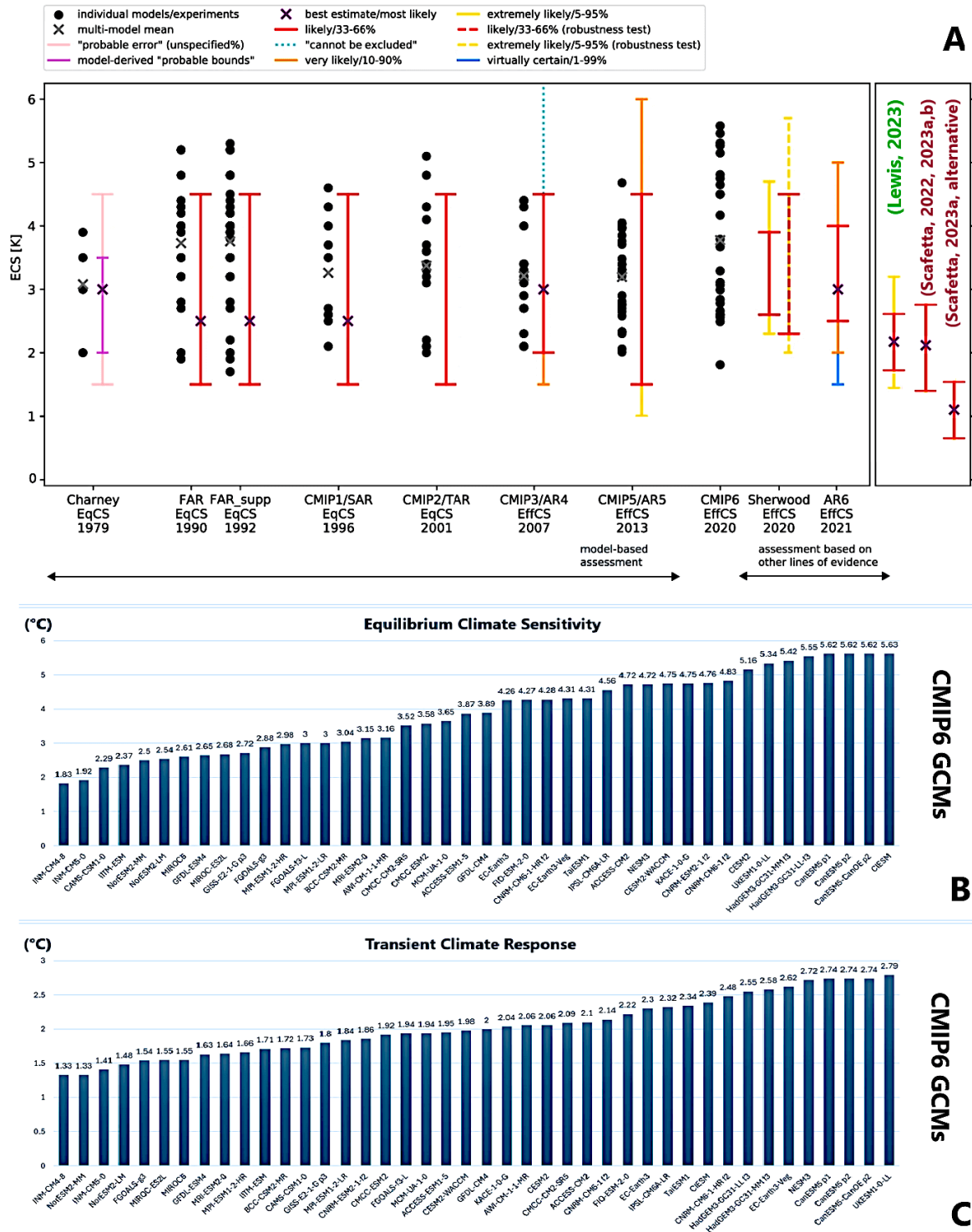


Figure 5: [A] Historical progression of the equilibrium climate sensitivity (ECS) estimates from Charney et al. (1979) to AR6 (IPCC, 2021) (adapted from Undorf et al., 2022), with the addition of the recent estimates from Lewis (2023) and Scafetta (2022, 2023a,b). The lowest estimate — $ECS = 1.1 \pm 0.4$ °C — assumes that the climate system is hypersensitive to solar activity variations; see Sections 4.2.3 and 4.3.2. [B] The equilibrium climate sensitivity (ECS) and [C] the transient climate response (TCR) of the CMIP6 GCMs (IPCC, 2021; Hausfather et al., 2022; Scafetta, 2024).

ods such as the Medieval Warm Period on a global scale, such evidence does not confirm the validity of the AGWT's climate attribution assessments proposed in the latest IPCC assessment report (AR6, 2021). Hockey-stick reconstructions, as Crowley (2000) posited, may “*enhance confidence*” that anthropogenic forcings significantly contributed to current warming but cannot definitively prove they are its sole (~100%) cause. Crowley

(2000), for example, used hockey-stick temperature records and still estimated that “*about 25% of the 20th-century temperature increase can be attributed to natural variability*”, which was primarily due to increased solar activity during the 19th and 20th centuries.

Importantly, the GCMs themselves may be based on assumptions, mechanisms, and specific forcings that could inadequately capture the complexity of the Earth’s climate system. Such limitations can result in over-estimated projections of anthropogenic warming and its impacts. For instance, natural processes like solar forcing and internal climate variability may not be accurately represented in the GCMs, a fact that could have yielded to potentially underestimate their contributions to observed climate variability. Indeed, natural processes may have had a larger influence on climate variability than the 0°C warming predicted by the CMIP6 models (Figure 2).

Additionally, many GCM mechanisms depend on parameterization, calibration, and tuning of free parameters. These parameters are adjusted to enable the GCMs to approximate the observed climate system as closely as possible (McSweeney and Hausfather, 2018). Tuning involves iterative tests to identify parameter values that produce optimal agreement between model outputs and observational data. However, such tuning does not guarantee that the models are physically accurate. Parameter values can vary significantly when model mechanisms and forcings are altered, as demonstrated in various studies (e.g.: Golaz et al., 2019; Ma et al., 2022; Mauritsen et al., 2019). Thus, the apparent agreement between the GCM predictions and observed warming from 1850–1900 to 2011–2020 under specific radiative forcing functions, as shown in Figure 1, may stem more from tuning methodologies rather than from intrinsic physical accuracy.

3.4 The GCMs’ failure in capturing natural climate variability

In scientific literature and in the same IPCC assessment reports there is growing evidence of physical uncertainty that raises significant questions about the reliability of the GCMs. A key challenge lies in the inherent difficulty of rigorously validating these models as also argued above. This section explores some of the most pressing open questions currently under debate, including the pervasive issue of the GCMs’ inability to reconstruct major patterns in natural climate variability.

3.4.1 The “hot model” problem

As shown in Figure 5, the CMIP6 GCMs predict a wide and inconsistent range of equilibrium climate sensitivity (ECS) and transient climate response (TCR) values, spanning from 1.8°C to 5.6 °C and from 1.33°C to 2.79°C, respectively (cf. Hausfather et al., 2022; IPCC, 2021, Figure 7.18). This large uncertainty range presents significant challenges to accurately evaluating the risks and potential hazards of future climate change, as suggested in Figure 3 (cf. Scafetta, 2024).

The ECS uncertainty is attributed to variations in the mechanisms, parameterizations, and free parameter settings employed by different GCMs. These differences significantly influence the modeling of key climate feedbacks, such as water vapor and cloud formation (Lutsko et al., 2022). The discrepancies among GCM projections become especially pronounced outside the historical period, where internal free parameter tuning is not possible. For instance, under the same Shared Socioeconomic Pathways (SSPs), the GCMs display divergent climate projections for the 21st century, as illustrated in Figure 3 with curves color-coded by ECS values ranging from low [blue] to high [red] values.

A major unresolved question in climate science is how to constrain the ECS and TCR values to better approximate the true sensitivity and response times of the climate system. While the GCMs estimate ECS to fall within 1.8°C to 5.6°C, broader literature reports ranges as wide as 0.5°C to 10°C (Knutti et al., 2017). IPCC (AR6, 2021) proposed a likely ECS range from 2.5°C to 4.0°C (17–83% probability) and a very likely range from 2.0°C to 5.0°C (5–95% probability), based on the assessment by Sherwood et al. (2020), who used multiple lines of evidence by emerging constraints and paleoclimate data.

However, such assessment remains contentious. For example, the reanalysis of the same line of evidences proposed by Lewis (2023) directly challenged the assessment by Sherwood et al. (2020) by highlighting a num-

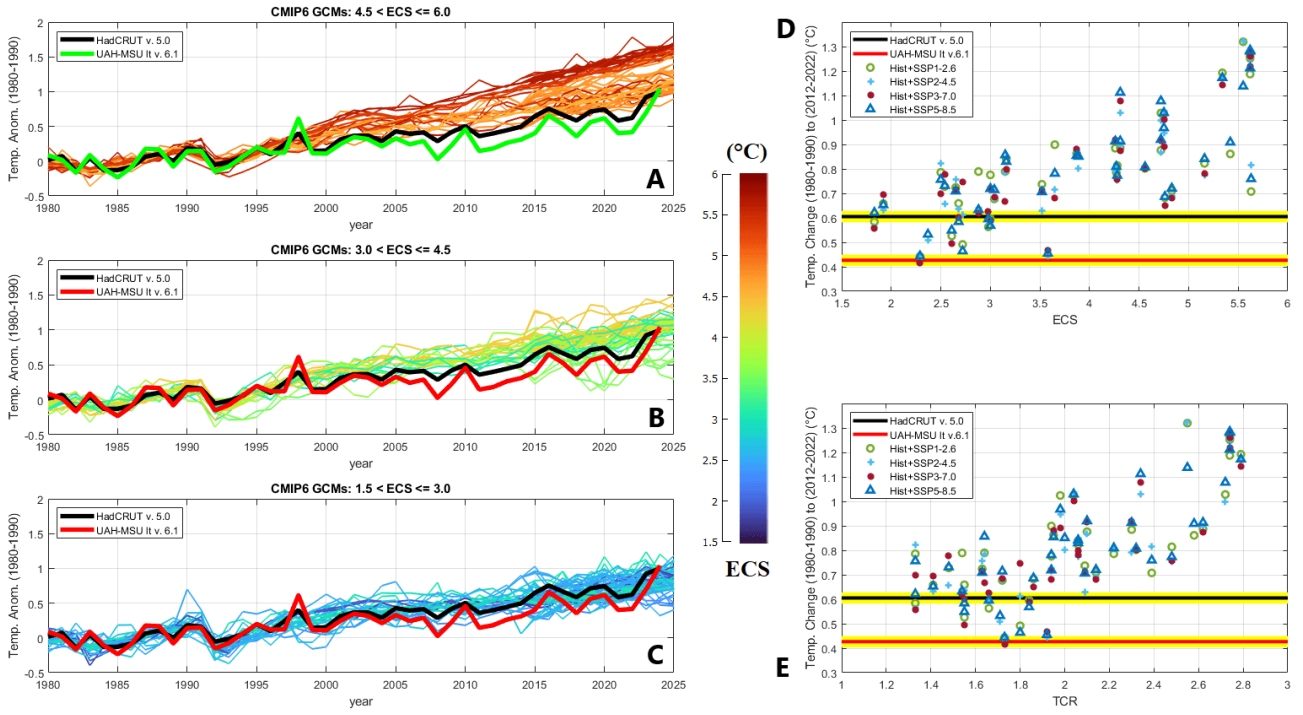


Figure 6: [A, B, C] The CMIP6 GCM simulations separated into three macro-GCM ensembles based on their ECS values, as represented by a colored scale. The synthetic temperature records are compared with the HadCRUT v5.0 (infilled data) global surface temperatures (Morice et al., 2021) and the UAH-MSU It v6.1 satellite-based temperature dataset (Spencer et al., 2017). [D, E] Temperature changes from 1980–1990 to 2012–2022, as simulated by the 42 adopted GCMs, are evaluated against the warming observed in the HadCRUT v5.0 ($0.605\text{ °C} \pm 0.02\text{ °C}$) and UAH-MSU It v. 6.1 ($0.427\text{ °C} \pm 0.03\text{ °C}$) records, against the ECS and TCR values of the GCMs. (Adapted from Scafetta, 2024).

ber of possible statistical errors and other shortcomings. Lewis (2023) estimated that the same evidence could suggest a significantly lower ECS range, with a median of 2.16 °C (17–83% range: $1.75\text{--}2.7\text{ °C}$; 5–95% range: $1.55\text{--}3.2\text{ °C}$). Other studies propose even lower values centered between 0.5 °C to 2 °C (Forster and Gregory, 2006; Lindzen and Choi, 2011; Harde, 2014; Monckton et al., 2015). Similar low ECS estimates ($\text{ECS} < 3.0\text{ °C}$) have been reported by Scafetta (2013a, 2022, 2023a,b,c). See Figure 5A. In general, Gervais (2016), Knutti et al. (2017) and Rugenstein et al. (2023) highlighted that already in the early 2010s, several authors noted that climate sensitivity estimates from climate models differed significantly from those based on observed warming and radiative balance studies, with the latter suggesting much lower values. Attempts to solve this conundrum — for example by assessing whether ECS may be variable under different time-scales and/or physical conditions (Rugenstein et al., 2023) — are under investigation.

ECS and TCR values are critical for understanding the climate’s sensitivity to radiative forcing and for estimating expected future warming under different SSP scenarios (as shown in Figure 3). Notably, the GCM-derived ECS and TCR estimates cannot be treated as repeated measurements of a single observable but rather as diverse theoretical estimates. Consequently, the true ECS and TCR values may fall either within or outside the ranges reported by the GCMs. For example, the actual ECS and TCR values could potentially be lower than those predicted by any GCM, as suggested in multiple studies (cf.: Knutti et al., 2017; Harde, 2014; Lewis, 2023; Lindzen and Choi, 2011; Monckton et al., 2015; Scafetta, 2023a,b, 2024).

Several lines of evidence indicate that the GCMs may inadequately represent key aspects of climate change. For example, the CMIP6 GCMs — particularly those with ECS values exceeding 3 °C — tend to overestimate the warming observed from 1980 to 2022 (Scafetta, 2022, 2023b, 2024). This persistent bias, which is undisputed for high-ECS GCMs, is widely referred to as the “hot model” problem (Hausfather et al., 2022). Furthermore, the GCMs significantly overestimate warming trends between 1979 and 2014 across the vertical atmospheric profile, particularly in the upper tropical troposphere (Mitchell et al., 2020; McKittrick and Christy, 2018, 2020;

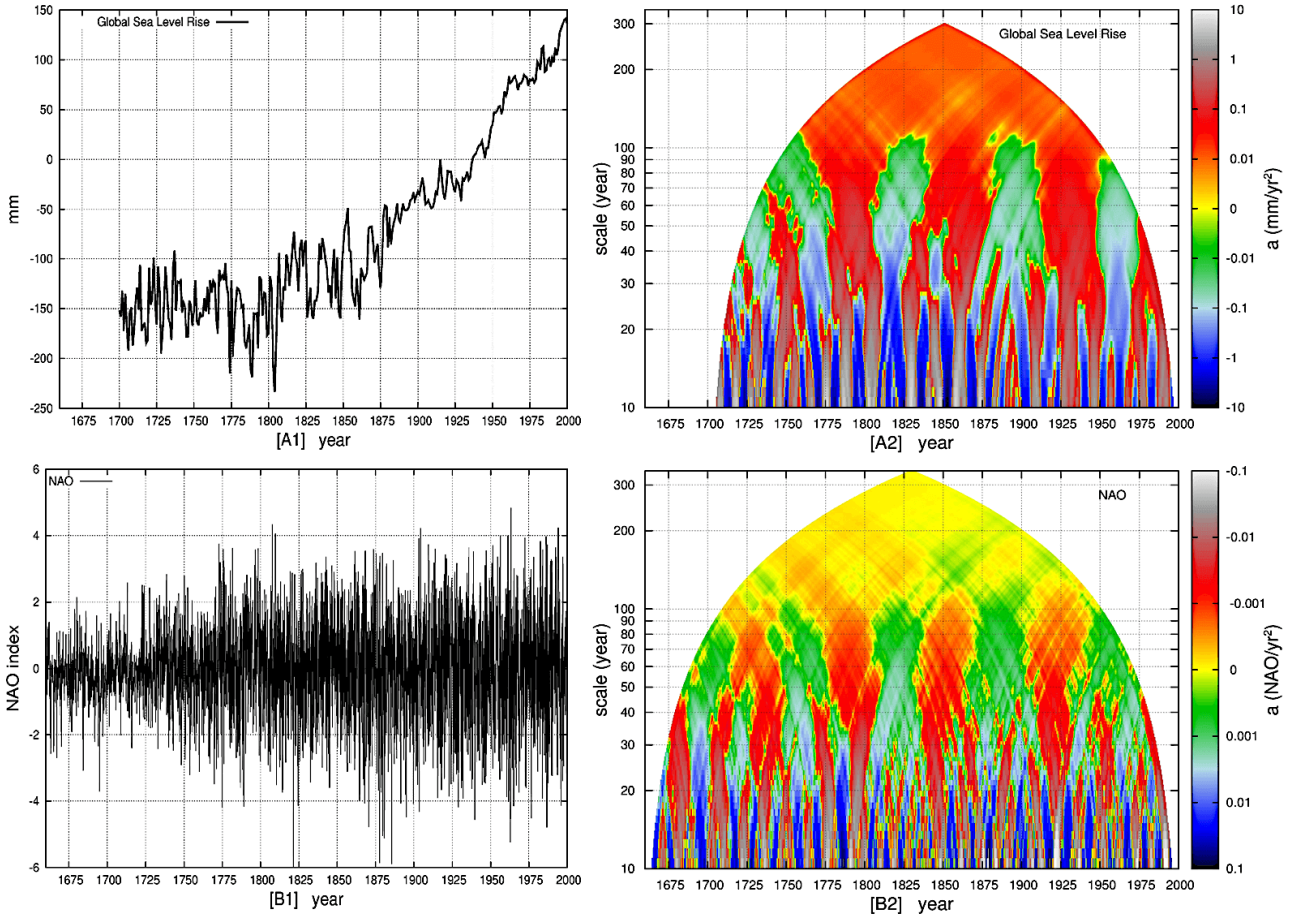


Figure 7: [A1] Global sea level record from Jevrejeva et al (2008) (left), alongside its multi-scale acceleration analysis (MSAA) colored diagram (right). [B1] North Atlantic Oscillation (NAO) from Luterbacher et al. (2002) (left), alongside its MSAA colored diagram (right). The diagrams highlight a consistent 55–70-year oscillation since 1700, represented by alternating green and red regions within the 30–110-year scale. (Adapted from Scafetta, 2014a).

Hudson, 2023). This problem is documented by the IPCC (AR6, 2021, its figure 3.10) and, in the literature, it is referred to as the “missing hot-spot” conundrum. In fact, while models predict a strong warming in the upper tropical troposphere, several observations suggest a weaker or absent warming in that region. Potential reasons for the missing hot-spot include data errors, natural variability, but, of course, also climate model limitations.

Figures 6A–C compare the CMIP6 GCM simulations (grouped by low [1.5–3.0°C], medium [3.1–4.5°C], and high [4.6–6.0°C] ECS values) against the HadCRUT5 global surface temperature record (Morice et al., 2021) and satellite-based UAH-MSU v. 6.1 record (Spencer et al., 2017). The warm bias of the medium- and high-ECS models is statistically significant. Figures 6D–E further highlight these biases, showing that the GCM-predicted warming from 1980–1990 to 2012–2022 exceeds observed warming by the HadCRUT5 (0.605 ± 0.02 °C) and UAH-MSU v6.1 (0.427 ± 0.03 °C). Figure 6 updates Scafetta (2023b, 2024), where this issue is discussed in more details.

The analysis shown in Figure 6 does not consider the years 2023–2024, which were marked by a sudden temperature spike possibly linked to the Hunga Tonga-Hunga Ha’apai eruption in 2022. This submarine volcanic eruption significantly increased stratospheric water vapor by ~10%, potentially exerting a positive radiative forcing effect (Jenkins et al., 2023; Schoeberl et al., 2024). However, even accounting for this anomaly, the warming estimates for 2014–2024 (~ 0.70 °C for HadCRUT5 and ~ 0.54 °C for UAH-MSU) remain below most of the GCM projections. In the future, the rapid cooling that has been observing since the mid-2024 peak could further exacerbate the “hot model” problem rather than mitigate it.

3.4.2 The 50–70-year cycle and its implications

The CMIP3 and CMIP5 GCMs have been identified as failing to adequately reconstruct observed climate oscillations on decadal to multidecadal timescales (Scafetta, 2012a, 2013a). Specifically, the climate system exhibits a distinct quasi-60-year oscillation that these models fail to replicate. This natural oscillation has resulted in alternating warming (w) and cooling (c) phases superimposed on a long-term secular trend: 1850–1880 (w), 1880–1910 (c), 1910–1940 (w), 1940–1970 (c), 1970–2000 (w), and possibly 2000–2030? (c) (e.g.: Scafetta, 2014a; Wyatt and Curry, 2014). Evidence of this oscillation has also been recently observed in sunshine hours over central Europe (Lüdecke et al., 2024), suggesting a direct link between surface temperatures and cloud cover.

A prominent manifestation of a quasi-60-year oscillation can be seen in the Atlantic Multidecadal Oscillation (AMO) index, which tracks the variability of the North Atlantic sea surface temperatures (SSTs) (Schlesinger and Ramankutty, 1994). The AMO index is calculated by removing the linear trend from the SSTs observed within the region [0°N–70°N, 80°W–20°E], thereby isolating the oscillation from the broader secular warming trend that may still have both natural and anthropogenic origins. This oscillation has been documented in climate data since 1700 (e.g. Scafetta, 2014a), it is recognized as a defining feature of the North Atlantic ocean-atmosphere variability over the past 8,000 years (Knudsen et al., 2011), and it is found also in the paleoclimatic reconstruction of the Northern Hemisphere by Mann et al. (1999) during the last millennium, as well as in other long-term climate records (Black et al., 1999; Davis and Bohling, 2001; Neff, 2001; Agnihotri and Dutta, 2003; Patterson et al., 2004; Klyashtorin et al., 2008; Camuffo, 2010.; Chambers et al., 2012; Mazzarella and Scafetta, 2012; Scafetta, 2012c; Wyatt and Curry, 2014).

For instance, Figure 7 compares the global sea level record (Jevrejeva et al, 2008) and the North Atlantic Oscillation (NAO) record (Luterbacher et al., 2002) since 1700. The right panels feature their multi-scale acceleration analysis (MSAA) plot introduced by Scafetta (2014a). The analyses highlight the 50–70-year oscillation evident in both datasets. Such spectral coherence between two independent yet physically coupled indices — AMO and NAO — underscores the assertion that this quasi-60-year oscillation is a genuine dynamical feature of the climate system, rather than an artifact.

The warming observed from the 1910s to the 1940s, followed by the cooling from the 1940s to the 1970s, clearly appeared in some figures published in the IPCC FAR (1995, its figure 8.4). Notably, this oscillatory pattern shows no correlation with the anthropogenic forcing functions, which have monotonically accelerated since 1750 (Figure 1A and 1C).

Figure 8 provides further evidence by comparing observed oceanic surface temperatures in the region [0°N–70°N, 80°W–20°E], as captured by: (a) CMIP6 GCM ensemble simulations; (b) HadSST4 records (Kennedy et al., 2019) and NOAA/CIRES/DOE 20th Century Reanalysis V3; and (c) the AMO index from NOAA. The data reveal that the GCMs fail to replicate the amplitude of the natural oscillation observed in the historical record. For instance, while GCMs predict a monotonic warming trend ($\sim 0.2^{\circ}\text{C}$) from 1880 to 1960 — with occasional interruptions from volcanic events — the data show a distinct oscillatory pattern, alternating between warming and cooling phases with amplitudes up to $0.4\text{--}0.5^{\circ}\text{C}$.

The existence of a natural 50–70-year cycle not modeled by the CMIP6 GCMs challenges the AGWT (cf. Gervais, 2016; Scafetta, 2013a), particularly because the observed warming from the 1970s to 2000s is strikingly similar to the warming from the 1910s to 1940s. This suggests that natural variability, such as the quasi-60-year oscillation, may have contributed to the recent warming trends (cf.: Scafetta, 2012a, 2013a), contrary to the finding of the GCMs attributing all 1970–2000 warming solely to anthropogenic forces. Figures 8A–B estimate the warming from 1940 to 2020 as $+0.8^{\circ}\text{C}$ for the GCMs and $+0.4^{\circ}\text{C}$ for the observed data, which further demonstrates the discrepancy between the GCM simulations and the empirical records.

Discrepancies between model predictions and observations spanning decadal and longer timescales are significant. Indeed, climate models are expected to reproduce changes occurring over periods exceeding ~ 15 years, whether driven by external forcings or internal variability. For example, Knight et al. (2009) remarked that “simulations rule out (at the 95% level) zero trends for intervals of 15 year or more” implying that observing such prolonged data inconsistencies with the GCM expected warming rates signals physical flaws in the models.

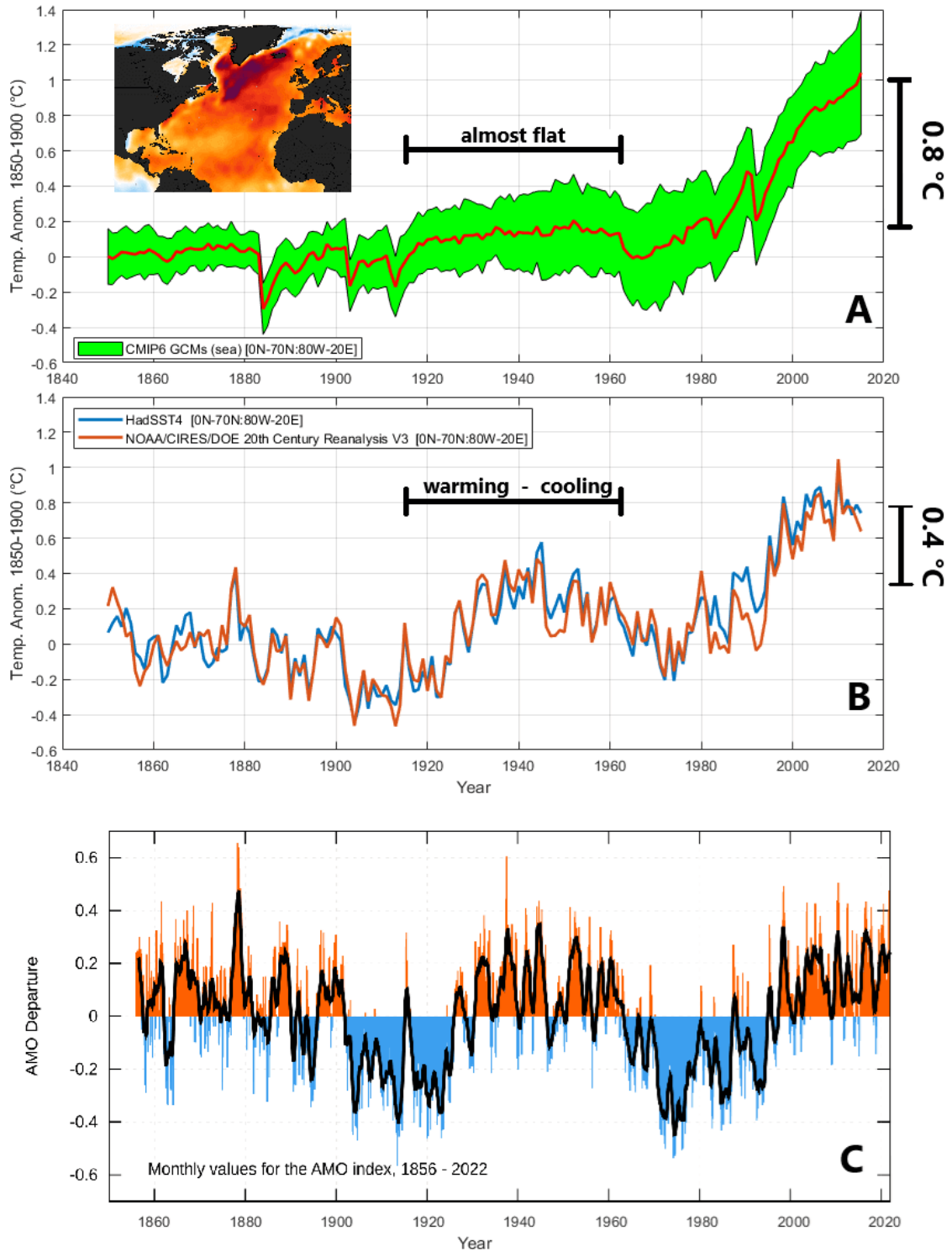


Figure 8: [A] CMIP6 GCM ensemble temperature simulation for the North Atlantic Ocean surface ([0°N–70°N : 80°W–20°E]). [B] Sea surface temperature records for the same North Atlantic region ([0°N–70°N : 80°W–20°E]) derived from HadSST4 (Kennedy et al., 2019) and the NOAA/CIRES/DOE 20th Century Reanalysis V3. The side panel shows the approximate warming from 1940 to 2020: +0.8 °C based on GCM simulations; and +0.4 °C based on observational data. [C] Atlantic Multidecadal Oscillation (AMO) index, calculated as the linearly detrended North Atlantic Ocean surface temperature anomalies from 1856 to 2022. The insert in [A] depicts the approximate North Atlantic region used to define the AMO index.

Similar multi-decadal discrepancies are evident in precipitation patterns and trends. Both CMIP5 and CMIP6 GCMs struggle to model also such climatic patterns accurately, as demonstrated by various studies (e.g.: Connolly et al., 2019; Li et al., 2022; Zhang et al., 2025; Hellmuth et al., 2025; Plavcová et al., 2025).

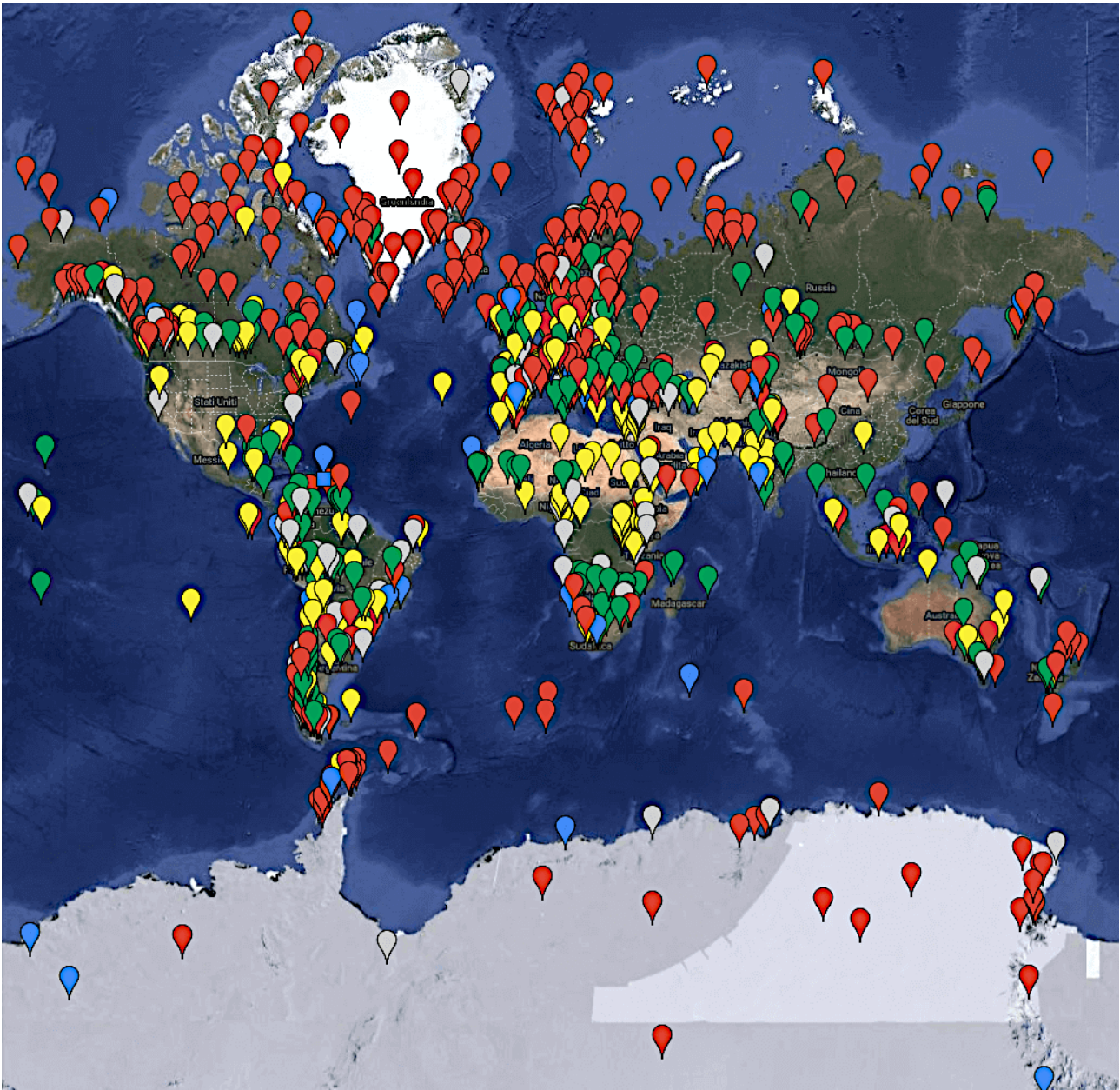


Figure 9: Climate reconstructions derived from 1,272 scientific studies on the “Medieval Warm Period” (MWP) spanning from 1000–1200 AD (Lüning, 2022). Each point represents the location of a specific study where the color represents the observed climate: warm (red), cool (blue), dry (yellow), wet (green), and no trend or unclear (grey). The interactive map is accessible at <http://t1p.de/mwp> (accessed on April 10, 2025).

3.4.3 The Medieval Warm Period

Global climate records from the past 1500 years reveal two prominent periods of anomalous temperatures predating the 20th century: the Medieval Warm Period (MWP), spanning approximately 900–1300 AD, and the Little Ice Age (LIA), occurring roughly from 1400 to 1850 AD (Lamb, 1965). The magnitude and spatial patterns of the MWP have been a focal point of scientific debate, particularly following the introduction of the hockey-stick temperature graph by Mann et al. (1999), which minimized its significance. A wealth of evidence, however, supports the existence of a distinct MWP and LIA (Soon and Baliunas, 2003; Soon et al., 2003; von Storch et al., 2004), with regions such as Europe, the North Atlantic (Lasher and Axford, 2019) and China (Ge et al., 2017) having potentially experienced temperatures comparable to or exceeding those of the modern warm period.

While discussions continue on whether the MWP was a global or predominantly regional phenomenon

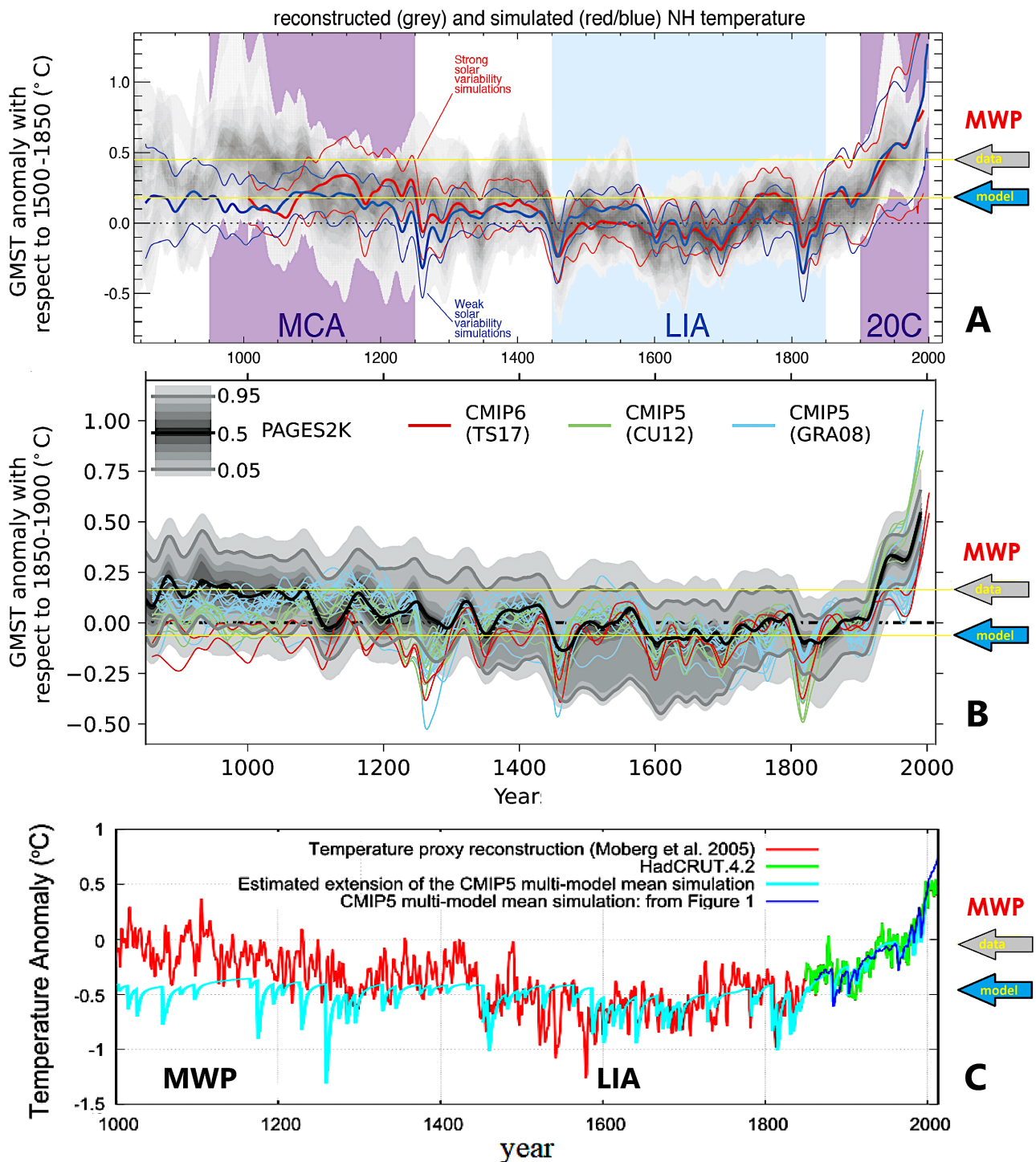


Figure 10: The Medieval Warm Period (MWP) temperature conundrum. [A] Comparison of simulated versus reconstructed Northern Hemisphere temperature anomalies over the last millennium, including the Medieval Climate Anomaly (MCA), Little Ice Age (LIA), and 20th century (20C) (adapted from IPCC, 2013, its Figure 5.8). [B] Time series of global mean surface temperature anomalies from the PAGES2K multi-proxy model relative to 1850–1900, incorporating the simulations from the CMIP5 and CMIP6 GCMs (adapted from IPCC, 2021, its Figure 3.2). [C] Comparison of the multi-model mean simulation (cyan) for the CMIP GCMs against the temperature proxy reconstruction by Moberg et al. (2005) (red), which is calibrated and extended with the HadCRUT temperature record (green) beginning in 1850 (cf.: Scafetta, 2013a, 2021b). Blue and gray arrows to the side indicate the approximate average temperature during the MWP estimated by the proxy models and simulated by the GCMs, spanning approximately from 900 to 1100 AD.

(Mann et al., 2009), numerous studies — including the IPCC Assessment Reports — acknowledge a Medieval Warm anomaly relative to the subsequent LIA. For instance, the “Medieval Warm Period 1000–1200 AD” project

(Lüning, 2022) summarizes approximately 1300 studies, which predominantly support a warm MWP. The resulting map is shown in Figure 9, which highlights that the number of studies and sites supporting a warm MWP (red points) far outnumber those supporting a medieval cool period (blue points).

Climate reconstructions often rely on multi-proxy models, which are inherently accompanied by considerable uncertainties (AR5, IPCC, 2013, its figure 5.7). However, when the GCM predictions are compared to the available paleoclimatic temperature records, significant discrepancies emerge during historically warm periods including the MWP.

This issue is evident in Figure 10A, which compares reconstructed and simulated Northern Hemisphere (NH) temperature changes over the past millennium (AR5, IPCC, 2013, its figure 5.8), and Figure 10B, which plots global mean surface temperature anomalies from PAGES-2K Consortium (2019) against the CMIP5 and CMIP6 GCM simulations (AR6, IPCC, 2021, its figure 3.2). These comparisons consistently show that the GCMs fail to adequately reconstruct the MWP, as highlighted by the colored and black arrows indicating the divergence between the GCM ensemble simulations and the proxy-based temperature reconstructions.

This failure is particularly apparent in the CMIP6 models (Figure 10B), where simulations exhibit a climatic near-stationarity between 850 and 1900 AD, apart from brief cooling periods triggered by volcanic eruptions. Figure 10C reinforces this point by comparing an empirical simulation of the multi-model mean (cyan curve) with the Moberg et al. (2005) reconstruction (red curve), calibrated with the HadCRUT dataset (green curve) since 1850, as proposed by Scafetta (2013a, 2021b), who attributed this modeling failure to inadequate representation of solar forcing in the CMIP5 and CMIP6 GCMs. The GCMs assume minimal secular solar variability as Section 4.2 discusses in more detail.

The IPCC (AR6, 2021, pp. 433) explicitly acknowledges “*larger disagreements between models and temperature reconstructions*” before the year 1300. Notably, AR6 emphasized the PAGES-2K Consortium (2019) temperature reconstruction, which dampens the MWP anomaly compared to alternative reconstructions (e.g. IPCC, 2013, its figure 5.7). This decision to exclusively utilize the PAGES-2K Consortium (2019) paleoclimatic proxy reconstruction has been recently criticized as reductive (Esper et al., 2024) because it oversimplifies the physical complexity of the Common Era climate variability as highlighted in the scientific literature.

In conclusion, the CMIP6 GCMs predict an approximately stable natural climate extending from 800 AD to the present when only natural (solar + volcanic) radiative forcings are applied (Figure 1D). However, this prediction conflicts with extensive paleoclimatic evidence and historical records documenting pronounced cooling from the MWP to the LIA. All recent multi-proxy reconstructions (e.g., IPCC, 2013, its figure 5.8; Esper et al., 2024; PAGES-2K Consortium, 2019) consistently capture a significant temperature decline over this interval, although the extent of this cooling depends on the adopted paleoclimatic record. The failure of the GCMs to replicate such natural variability underscores severe limitations in their ability to accurately reconstruct past climate dynamics. Reconstructing the warm periods of the pre-industrial era is an essential condition in ensuring the reliability of the GCM assessments (Figure 2) regarding the attribution of the global surface warming reported from 1850–1900 to 2010–2019. This is because the recent global surface warming may have been partially driven by the same natural mechanisms (e.g. solar forcing) that caused other warm periods over the past millennia.

3.4.4 The Holocene temperature conundrum

The limitations of the GCMs in simulating natural climate change become increasingly apparent when the entirety of the Holocene epoch is analyzed. The mismatch between data and model predictions over this prolonged period, termed the “*Holocene temperature conundrum*” (Liu et al., 2014), raises further substantial concerns about the reliability of the existing global climate models (Figure 11).

The core of this conundrum lies in the gradual and near-monotonic increase in atmospheric greenhouse gases — carbon dioxide (CO₂) and methane (CH₄) — likely driven by processes such as oceanic degassing and permafrost melting (Figure 11, green dots). Over this epoch, the climate models predict a quasi-monotonic warming due to the rise in the greenhouse gas concentrations (Figure 11, red curve). However, paleoclimatic

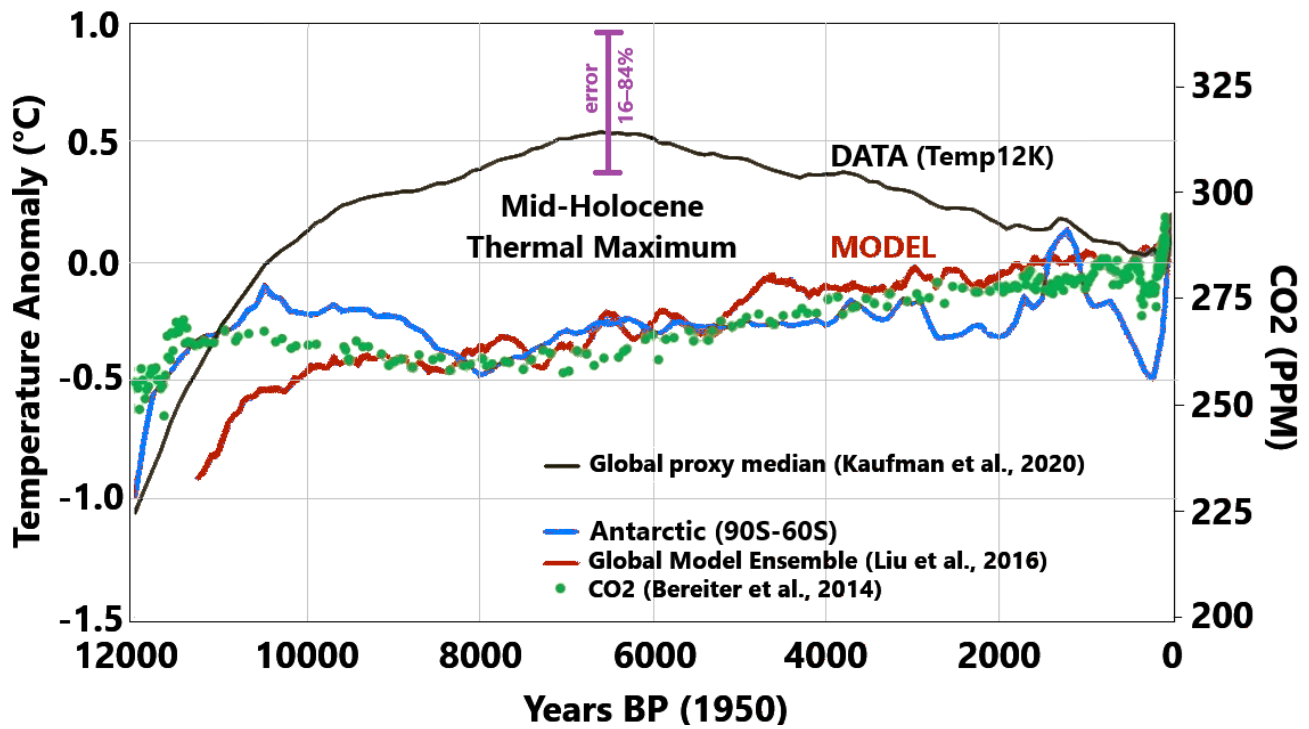


Figure 11: The Holocene temperature conundrum: (black line) global median temperature proxy from Kaufman et al. (2020); (red line) global climate model ensemble from Liu et al. (2014); (green dots) EPICA Dome-C CO₂ record from Bereiter et al. (2015); (blue line) Antarctic temperature proxy from Kaufman et al. (2020).

proxies derived from natural archives — including ice cores, sediment layers, and biological indicators — consistently suggest the occurrence of an early-to-mid Holocene Thermal Maximum (HTM), which is also known as the “*Holocene Optimum*”. The HTM contradicts the models’ predictions.

Empirical evidence supports a significantly warm HTM, with summer temperatures in East Greenland during the early Holocene estimated to be at least 3°C higher than present (Westhoff et al., 2022). Similar warming trends were documented in central Europe (Zander et al., 2024; Melo et al., 2022), the eastern Mediterranean (Cruz-Silva et al., 2023), in Japan (Murata et al., 2025), and in numerous other regions. Antarctica appears to be the notable exception, showing a gradual warming rather than an HTM (Figure 11, blue curve). Nevertheless, even this claim is debated, with alternative studies suggesting the existence of the HTM in Antarctica as well (Jones et al., 2023). On a global scale, several paleoclimatic reconstructions suggest that the HTM was warmer than present-day temperatures, although some estimates, such as those in Figure 11 (Kaufman et al., 2020), appear to mitigate its intensity.

Additional support for a warm HTM comes from other studies showing that global mean sea levels were higher than today during the mid-Holocene (Creel et al., 2024), and showing evidence of the African Humid Period (also known as the “*Green Sahara*”), which occurred between approximately 14,800 and 5,500 years ago (deMenocal and Tierney, 2012; Kaufman et al., 2020). After the HTM, the surface temperatures declined throughout the late Holocene, culminating in the minimum recorded during the Little Ice Age. This dynamics correlates strongly with the changes in mean daily insolation at 65°N on summer solstices due to variations in the orbital parameters of the Earth (Laskar et al., 2011; see also the Milankovitch orbital data viewer at <https://biocycle.atmos.colostate.edu/shiny/Milankovitch/>, accessed April 10, 2025).

Efforts to address the Holocene temperature conundrum have included investigating seasonal temperature variations since many paleoclimatic proxies actually represent summer temperatures, as suggested by Bova et al. (2021). However, such interpretations have been challenged by other researchers confirming the HTM also in annual temperature proxies (Cartapanis et al., 2022; Dong et al., 2022; Kaufman and Broadman, 2023).

The Holocene temperature conundrum ultimately casts doubt on the accuracy of either paleoclimatic reconstructions or the climate models, or both. However, the large body of empirical evidence supporting a

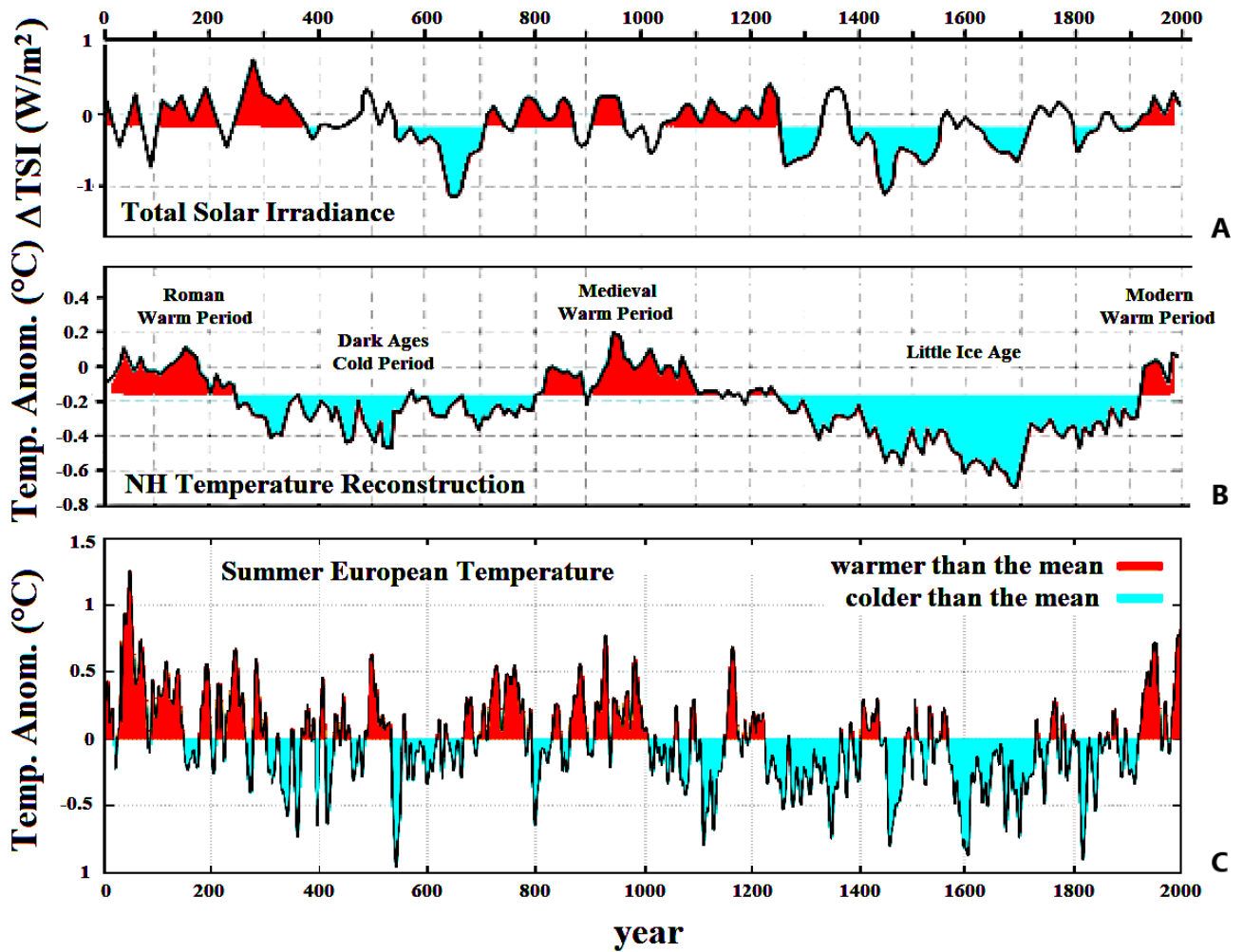


Figure 12: Synchronous quasi-millennial cycles observed in: [A] a reconstruction of total solar irradiance (Steinhilber et al., 2012); [B] a reconstruction of the Northern Hemisphere surface temperatures (Ljungqvist, 2010); [C] a reconstruction of the summer European temperatures (Luterbacher, 2016).

prominent HTM implies that even the latest climate models significantly overestimate the impact of greenhouse gases relative to other factors, such as the climatic impact of variations in solar radiation input.

Additionally, the Holocene epoch appears marked by pronounced quasi-millennial oscillations (Alley, 2000; Bond et al., 2001; Kerr, 2001; Kutschera et al., 2020). Current climate models lack the capability to reconstruct these quasi-periodic warm and cool periods, as evidenced by their failure to accurately simulate the latest past warm and cool periods such as the cooling from the Medieval Warm Period (MWP) to the Little Ice Age (LIA).

3.5 Conclusion: assessing the CMIP GCMs versus natural climate variability

The evidence presented above highlights critical limitations in the Global Climate Models (GCMs), casting doubts on the robustness of the Anthropogenic Global Warming Theory (AGWT). AGWT is heavily reliant on the climate attribution analyses derived from the GCMs, yet substantial empirical data challenges the validity of these models. Specifically, the GCMs have consistently failed to reproduce natural climate variability across multiple timescales throughout the Holocene, particularly during key historical warm periods. Furthermore, their central prediction — that Earth's climate would have remained stable from 1850–1900 to 2011–2020 in the absence of anthropogenic forcing — cannot be validated because of lack of data. The notion that the discrepancies between models and observational data may arise solely from data uncertainties does not resolve the presented challenges, as scientific models must ultimately be validated through empirical evidence. Conse-

quently, the AGWT promoted by the IPCC (2021) cannot be considered supported by empirical evidence.

The inability of the CMIP3, CMIP5 and CMIP6 GCMs to accurately reconstruct natural climate variability — including the Medieval Warm Period (MWP), and other extended warm periods of the past such as the Holocene Thermal Maximum (HTM) — raises fundamental questions. Specifically, concerns arise regarding whether these models employ appropriate natural radiative forcings and incorporate essential physical mechanisms necessary to accurately simulate past warm periods. This shortcoming suggests that the observed warming from 1850–1900 to 2011–2020 may not be exclusively attributable to anthropogenic activities because it cannot be ruled out that it was partly induced by the same mechanisms responsible for the other natural warm periods observed throughout the Holocene; mechanisms that are absent or remain insufficiently implemented in the current GCMs because of the models' failure in reconstructing the warm periods of the past.

For example, a significant quasi-millennial oscillation has been documented in the climate system over the past ~9,000 years (e.g.: Bond et al., 2001; Kerr, 2001; Neff, 2001; Kutschera et al., 2020). This oscillation is evident in records such as the Greenland GISP2 ice core (Alley, 2000) and many others. Notably, the Medieval Warm Period (MWP) was preceded by the Roman Warm Period (RWP), which occurred roughly 900–1000 years earlier (Ljungqvist, 2010; Christiansen and Ljungqvist, 2012; Klimentko et al., 2014; Luterbacher, 2016; Kutschera et al., 2020; Li et al., 2023). The existence of this quasi-millennial cycle — expected to peak again in the second half of the 21st century for solar and astronomical reasons (Scafetta, 2012b; Scafetta and Bianchini, 2023) — contrasts sharply with the AGWT's assertion that the warming observed since 1850–1900 is solely (~100%) due to human emissions.

Figure 12 illustrates this quasi-millennial cycle by comparing two paleoclimatic temperature reconstructions of the Northern Hemisphere and summer temperatures in Europe (Ljungqvist, 2010; Luterbacher, 2016) with a reconstruction of total solar irradiance based on the ¹⁴C record (Steinhilber et al., 2012). The analysis highlights three warm periods — the Roman (0–300 AD), the Medieval (800–1300 AD), and the contemporary (1900–2100 AD) warm periods — which appear equally warm, along with two cold periods: one during the Dark Ages (DACP) (400–800 AD) and one, even colder, during the Little Ice Age (LIA) (1300–1850 AD). This evidence suggests that the warming observed in the 20th century was partly driven by the warm phase of a quasi-millennial natural cycle driven by solar activity, which itself exhibits a similar cyclical variation. Further discussion on this issue is provided in Section 4.2.

4 Alternative approaches to the detection, attribution, and modeling of climate change

This section explores several critical and unresolved challenges concerning the reliability of global surface temperature records used for detecting climate change, as well as how the solar effect on the climate is addressed in modeling frameworks.

4.1 Challenges in assessing the reliability of global surface temperature records

The Intergovernmental Panel on Climate Change (IPCC) Sixth Assessment Report (AR6, 2023) states that the *“Global surface temperature was 1.09 [0.95 to 1.20] °C higher in 2011–2020 than 1850–1900, with larger increases over land (1.59 [1.34 to 1.83] °C) than over the ocean (0.88 [0.68 to 1.01] °C)”*. Despite this, determining the precise magnitude of the global warming between 1850–1900 and 2011–2020 remains contentious due to the sensitivity of the outcomes to methodological decisions, which has led to notable discrepancies among alternative temperature datasets.

Global surface temperature anomalies are constructed from observational records collected at meteorological stations distributed worldwide and from sea surface temperature data obtained from buoys, ships, and ocean reference stations. The processing methodology involves calculating monthly mean temperatures at each station from daily maximum and minimum values, from which annual averages are derived. These av-

erages are then normalized relative to a chosen baseline period (e.g., 1961–1990) and aggregated to produce yearly global temperature anomalies. However, significant methodological issues persist throughout these stages.

A prominent concern is the uneven geographical distribution of the observational networks, such as weather stations and shipping routes. This issue is typically addressed through gridded averaging, wherein the Earth’s surface is divided into cells (e.g. $0.25^{\circ} \times 0.25^{\circ}$) based on latitude and longitude, and temperature anomalies for each cell are averaged to produce global estimates. Nonetheless, historical underrepresentation of vast areas — such as the Southern Hemisphere and sparsely inhabited regions like deserts, polar regions, forests, and expansive oceanic zones — introduces substantial uncertainties. For instance, prior to 1950, the majority of the temperature records originated from North America, Europe, and East Asia, complicating efforts to accurately reconstruct global temperature anomalies during earlier historical periods (cf.: Lawrimore, 2011; Menne et al., 2018). Furthermore, gaps in station operation, changes in instrumentation, and station relocations lead to missing data and biases, undermining temperature trend analyses. Collectively, spatial and temporal inconsistencies in local temperature records pose significant obstacles to accurately assessing global temperature trends.

Another fundamental issue pertains to the suitability of local temperature records for analyzing long-term climate trends. Weather stations are primarily designed to monitor short-term meteorological variations rather than long-term climatic changes. Over extended periods, environmental transformations surrounding stations — such as urbanization, deforestation, or afforestation — alongside station replacements and relocations, can introduce systematic non-climatic biases into the data. These biases, if predominantly aligned in one direction, could significantly distort ensemble averages and, consequently, affect global temperature anomaly computations (D’Aleo, 2016; Watts, 2022). As a result, the integrity of the temperature records as indicators of long-term climatic trends demands critical evaluation.

4.1.1 The urban heat island effect

Urban areas are consistently warmer than their rural counterparts due to several contributing factors. In cities, natural soil is frequently replaced by heat-absorbing artificial materials, while high-rise buildings disrupt air-flow and create heat-trapping canyon effects. Additionally, in urban landscapes rainwater drains, unlike in rural areas where water moistens the soil and facilitates cooling via evaporation. Vegetation, which is more prevalent in rural areas, utilizes sunlight for photosynthesis rather than converting it into heat. Furthermore, anthropogenic activities, including vehicular emissions, building heating and the use of air conditioning systems, intensify urban heating. This cumulative phenomenon is widely recognized as the “urban heat island” (UHI) effect (McKittrick and Michaels, 2007; Mohajerani, 2017; Stewart and Oke, 2012).

As urbanization progresses, the temperature recorded by proximate weather stations tends to increase, reflecting enhanced UHI effects. This issue is particularly significant given that urban areas account for less than 4% of the Earth’s land surface, yet a substantial proportion of weather stations within the Global Historical Climatology Network (GHCN) are situated in urban settings (see Figure 13). Additionally, the ongoing shift of weather stations from rural to urban environments exacerbates the problem. The global marked increase in urbanization since 1900 and, in particular, after 1950 underscores the growing relevance of this issue (cf. Scafetta, 2021a).

The IPCC Sixth Assessment Report (AR6, 2021, Chapter 2) asserts that global surface temperature records are minimally affected by UHI bias, estimating its contribution to global warming to be less than 10%, thereby suggesting it can be disregarded for first-order analyses. However, a study by Helbling and Meierrieks (2023), which analyzed data from 118 countries spanning from 1960 to 2016, identified a strong correlation between rising temperatures and urbanization rates. This is just one of the recent evidence that has led some researchers to argue that UHI contamination of climate records may have been underestimated, advocating for a comprehensive reevaluation of global temperature datasets and climate change mitigation strategies.

For example, Soon et al. (2023) examined the Northern Hemisphere land surface temperatures from 1850

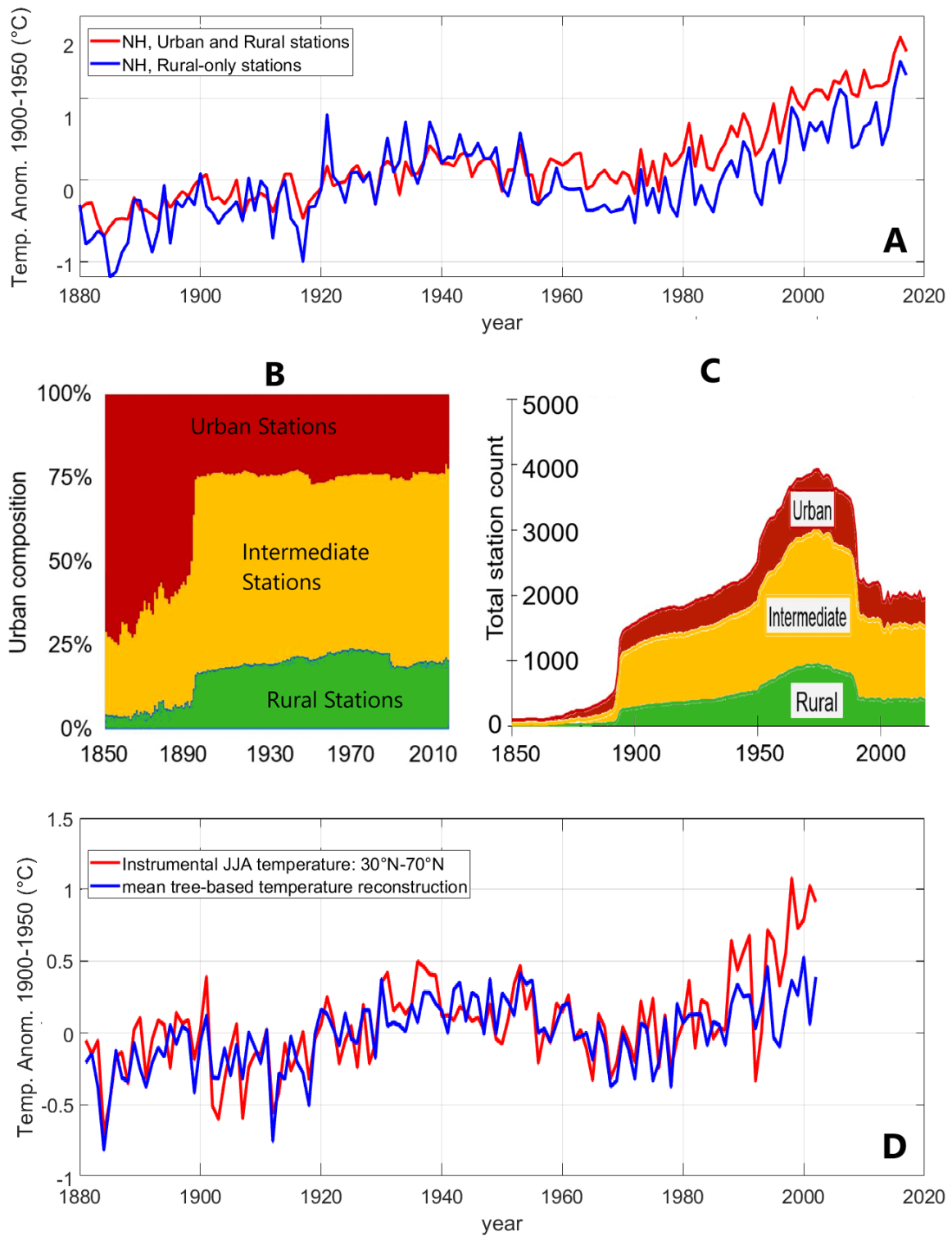


Figure 13: [A] Divergence observed in the Northern Hemisphere land surface air temperature estimates between a reconstruction based on rural-and-urban stations versus a reconstruction based exclusively on rural stations. [B, C] Percentage and total count of stations categorized into urban, intermediate, and rural subsets (adapted from Soon et al., 2023). [D] Divergence between summer (JJA) instrumental temperature averages across land areas (30°N–70°N; red) and tree-ring-based mean temperature reconstructions (blue), relative to the 1930–1960 baseline period (adapted from Esper et al., 2018).

to 2018 using two distinct datasets: one encompassing both rural and urban stations and another based exclusively on verified rural stations. Their analysis revealed significant differences in the long-term warming trends. Specifically, the combined rural-urban dataset indicated a warming rate of 0.89°C per century since 1850, whereas the rural-only dataset showed a markedly lower rate of 0.55°C per century. This divergence,

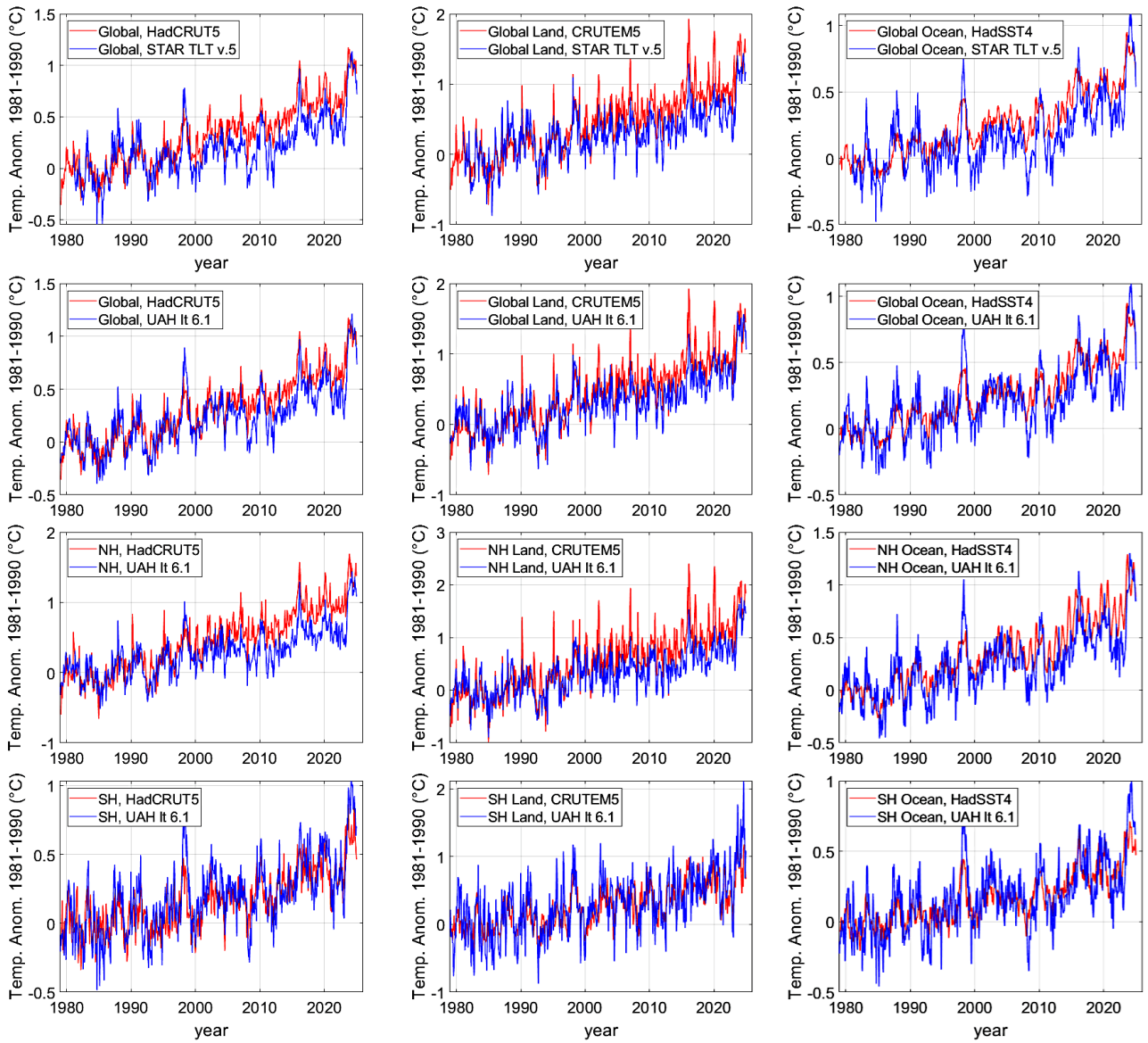


Figure 14: Comparison of surface temperature records — HadCRUT5 (global), CRUTEM5 (land), and HadSST4 (ocean) (red) (Morice et al., 2021; Osborn et al., 2021; Kennedy et al., 2019) — with the satellite-based lower troposphere temperature records NOAA-STAR v5.0 (Zou et al., 2023) and UAH MSU v6.1 (blue) (Spencer et al., 2017).

illustrated in Figure 13A, underscores the influence of urbanization on the global temperature records used to assess climate change. Figures 13B and 13C provide details on the composition and total number of stations employed in the study.

4.1.2 The divergence problems with the dendrochronological proxies and the satellite records

A similar pattern is observed in Figure 13D, which compares instrumental summer (June–August) temperatures averaged over land areas between 30°N and 70°N latitude (red) with tree-ring-based mean temperature reconstructions within the same latitudes (blue) (Esper et al., 2018). Instrumental records exhibit a pronounced warming trend post-1980, a phenomenon referred to as the “*divergence problem*”, where instrumental temperatures and dendrochronological proxies show conflicting trends. This discrepancy raises questions about the reliability of both global surface temperature records and dendrochronological proxies as tools for reconstructing past climate variations (Büntgen et al., 2021; Cai and Lu, 2023). For instance, Moberg et al. (2005) argued that tree-ring records are more effective at capturing the high-frequency components of climate signals while attenuating the secular and millennial low-frequency modulation, potentially due to biological adaptations of

region	Had-CRU (°C) (± 95%)	UAH 6.1 (°C) (± 95%)	Had-CRU – UAH (°C) (± 95%)	% % (± 95%)	STAR5 (°C) (± 95%)	Had-CRU – STAR (°C) (± 95%)	% % (± 95%)
Global (Land+Ocean)	0.73 ± 0.02	0.58 ± 0.02	0.15 ± 0.03	-21% ± 04%	0.53 ± 0.02	+0.20 ± 0.03	-27% ± 04%
Global (Land)	1.03 ± 0.15	0.79 ± 0.02	0.24 ± 0.15	-23% ± 14%	0.68 ± 0.02	+0.35 ± 0.15	-34% ± 14%
Global (Ocean)	0.58 ± 0.02	0.49 ± 0.02	0.09 ± 0.03	-16% ± 05%	0.46 ± 0.02	+0.12 ± 0.03	-21% ± 05%
NH (Land+Ocean)	1.03 ± 0.03	0.69 ± 0.02	0.34 ± 0.04	-33% ± 04%	0.72 ± 0.02	+0.31 ± 0.04	-30% ± 04%
NH (Land)	1.24 ± 0.15	0.83 ± 0.02	0.41 ± 0.15	-33% ± 12%			
NH (Ocean)	0.77 ± 0.02	0.59 ± 0.02	0.18 ± 0.03	-23% ± 04%			
SH (Land+Ocean)	0.42 ± 0.05	0.46 ± 0.02	-0.04 ± 0.06	+10% ± 14%	0.34 ± 0.02	+0.08 ± 0.06	-19% ± 14%
SH (Land)	0.62 ± 0.31	0.70 ± 0.02	-0.08 ± 0.31	+12% ± 49%			
SH (Ocean)	0.40 ± 0.02	0.42 ± 0.02	-0.02 ± 0.03	+5% ± 07%			

Table 1: Temperature increase from January 2014 to December 2024 relative to the baseline period of January 1981 to December 1990, as determined from surface temperature records (HadCRUT5-global, CRUTEM5-land, and HadSST-ocean) compared to the satellite UAH-MSU v6.1 (Spencer et al., 2017) and NOAA-STAR v5.0 (Zou et al., 2023) lower troposphere temperature record. These records are illustrated in Figure 14. Error bars represent approximately the 95% confidence interval. For UAH-MSU and NOAA-STAR v5.0, the error bars are not explicitly reported but assumed here to match the global surface temperature error (± 0.02 °C) across all regions.

the trees to changing climatic conditions. Nevertheless, the substantial and anomalous divergence observed after 1980 (as depicted in Figure 13D) together with the divergence observed with the record from the rural-only stations (depicted in Figure 13A), casts doubt on the accuracy of the adopted climatic temperature records.

Figure 14 highlights critical concerns regarding the reliability of the current global surface temperature records. It presents a comparative analysis of the HadCRUT5 (global), CRUTEM5 (land), and HadSST (ocean) surface temperature datasets (Morice et al., 2021; Osborn et al., 2021; Kennedy et al., 2019) with the satellite-based UAH MSU v6.1 lower troposphere temperature records (Spencer et al., 2017), which is available since December 1978. Additionally, the figure delineates results by hemisphere, distinguishing the Northern Hemisphere (39% land, 61% ocean, encompassing 90% of the global population) from the Southern Hemisphere (19% land, 81% ocean, hosting 10% of the global population).

The warming of the lower troposphere should approximate the expected surface warming across sufficiently large spatial scales. However, the GCMs predict that the troposphere — particularly at its top — should exhibit greater warming than at the surface (Mitchell et al., 2020; McKittrick and Christy, 2020; Hudson, 2023), as illustrated in the IPCC (AR6, 2021, its figure 3.10). Contrary to these predictions, Figure 14 reveals that satellite observations report a markedly lower warming rate relative to global surface temperature records. Specifically, the surface records exhibit a excess warming of approximately 21%, which equates to a global excess warming of roughly $+0.15^{\circ}\text{C}$ from 1981–1990 to 2014–2024, a significant discrepancy. Furthermore, the figure indicates pronounced surface excess warming in the Northern Hemisphere: approximately 33% over land and 23% over ocean. In contrast, the surface and satellite temperature trends in the Southern Hemisphere — across both land and ocean — align well within their uncertainties (see Table 1). Similarly, at the upper tropical troposphere the GCMs predict a “*hot-spot*” that is not observed in the data (McKittrick and Christy, 2018, 2020; Mitchell et al., 2020).

The compatibility of surface and satellite temperature records in the Southern Hemisphere, as evidenced in Figure 14, supports the assumption that the warming trend in the two records should be comparable, implying that the substantial warming bias observed in Northern Hemisphere land surface temperatures implies the influence of non-climatic factors, notably urban heat island (UHI) effects. Similarly, Northern Hemisphere sea surface temperatures display a slight warming bias relative to the satellite measurements, potentially attributable to inadequate monitoring of the extensive polar regions. In such areas, missing data are reconstructed using models, which may inadvertently introduce additional warming biases, as discussed by Scafetta (2021c). The reduced land area and the lower population density in the Southern Hemisphere likely mitigate the impact of non-climatic warming biases unrelated to climate change. If the warming trend indicated by the lower troposphere satellite temperature record offers a more reliable estimate of the actual global surface temperature trend, the above findings further question the accuracy of the CMIP6 GCMs, as they would all appear to overestimate the actual warming, as noted in Section 3.3.1 and in Figure 6.

The UAH-MSU lower troposphere temperature record (Spencer et al., 2017) has been subject to debate, particularly following adjustments to the Remote Sensing System (RSS) dataset in 2014. These revisions led to the development of an alternative satellite-based temperature record by Mears and Wentz (2016), aligning more closely with the accepted surface-based global temperature records. The NOAA-STAR v. 4.0 dataset also reflected similar trends (Santer et al., 2017), seemingly in contradiction to the UAH-MSU findings. However, the UAH-MSU-It dataset has demonstrated consistency with global warming trends derived from the Integrated Global Radiosonde Archive (IGRA) and reanalysis datasets (Christy et al., 2018). Additionally, recent updates to the NOAA-STAR records (Zou et al., 2023) have acknowledged prior errors, culminating in the NOAA-STAR v. 5.0 dataset. This latest dataset exhibits slightly lower warming from 1981–1990 to 2014–2024 relative to UAH-MSU (refer to Table 1 and Figure 14, top panels). Collectively, these observations suggest that the global surface temperature records may be significantly warm-biased due to improper data processing and non-climatic influences at the surface, particularly over land.

4.1.3 The excessive Tmin warming relative to the Tmax warming

An alternative method for identifying non-climatic warming biases in surface temperature records has been explored by Scafetta and Ouyang (2019) and Scafetta (2021a). Their analysis revealed substantial regions within global land surface temperature datasets that exhibit anomalously high nighttime warming (T_{min}) relative to daytime temperatures (T_{max}). This finding diverges from the predictions of the GCMs, which typically suggest only moderate additional nighttime warming in comparison to daytime warming.

Daytime surface warming is effectively mitigated by convective vertical air movements, facilitated by a relatively elevated boundary inversion layer. In contrast, nighttime warming forces a horizontal dispersion of warm air near the surface due to the typically lower position of the boundary inversion layer (cf. Figure 15, top). In urban environments, this meteorological behavior expands urban heat island (UHI) effects during night, resulting in a stronger influence on nearby thermometers at night compared to during day. Consequently, as urban areas continue to grow, urbanization amplifies the warming trend in T_{min} compared to T_{max} (cf. Kim and Christy, 2022).

Figure 15 illustrates the global spatial divergence between T_{min} and T_{max} across the periods 1945–1955 and 2013–2023, utilizing the CRU-TS4.08 land temperature data (Harris et al., 2020). Prominent orange-red regions in the Northern Hemisphere, often forming localized warm clusters, indicate intense nighttime warming, which are often near urban centers. Conversely, the Southern Hemisphere exhibits a lower variability. Interestingly, even small urban centers can produce significant UHI effects (Cardoso et al., 2017; Pinho and Orgaz, 2000). The darkest wide areas may reflect anomalies in the dataset, which could be potentially linked to regions exhibiting minimal warming in T_{min} or influenced by phenomena such as urban cool island (UCI) effects as in arid areas, in deforestation zones, or in regions where permafrost may be melting (cf.: Scafetta and Ouyang, 2019; Scafetta, 2021a).

4.1.4 Urban blending and homogenization uncertainties

The above findings appear to underscore critical failures of the adopted “*homogenization*” processes. These are designed to correct biases in meteorological records caused by environmental, instrumental, or methodological changes (Menne et al., 2018). Homogenization algorithms aim to enhance the accuracy of temperature datasets by identifying and rectifying such inconsistencies, thus enabling accurate assessment of true climate trends. For instance, the Global Historical Climatology Network (GHCN) provides temperature datasets in both non-homogenized and homogenized formats, with the latter used for constructing global climate records. Despite their intended function, these algorithms exhibit limitations. Studies have highlighted inconsistencies in detecting breakpoints within temperature records (Squintu, 2020). For example, O’Neill et al. (2022) found that the homogenized temperature records can change each time the raw temperature records are reprocessed by such homogenization algorithms.

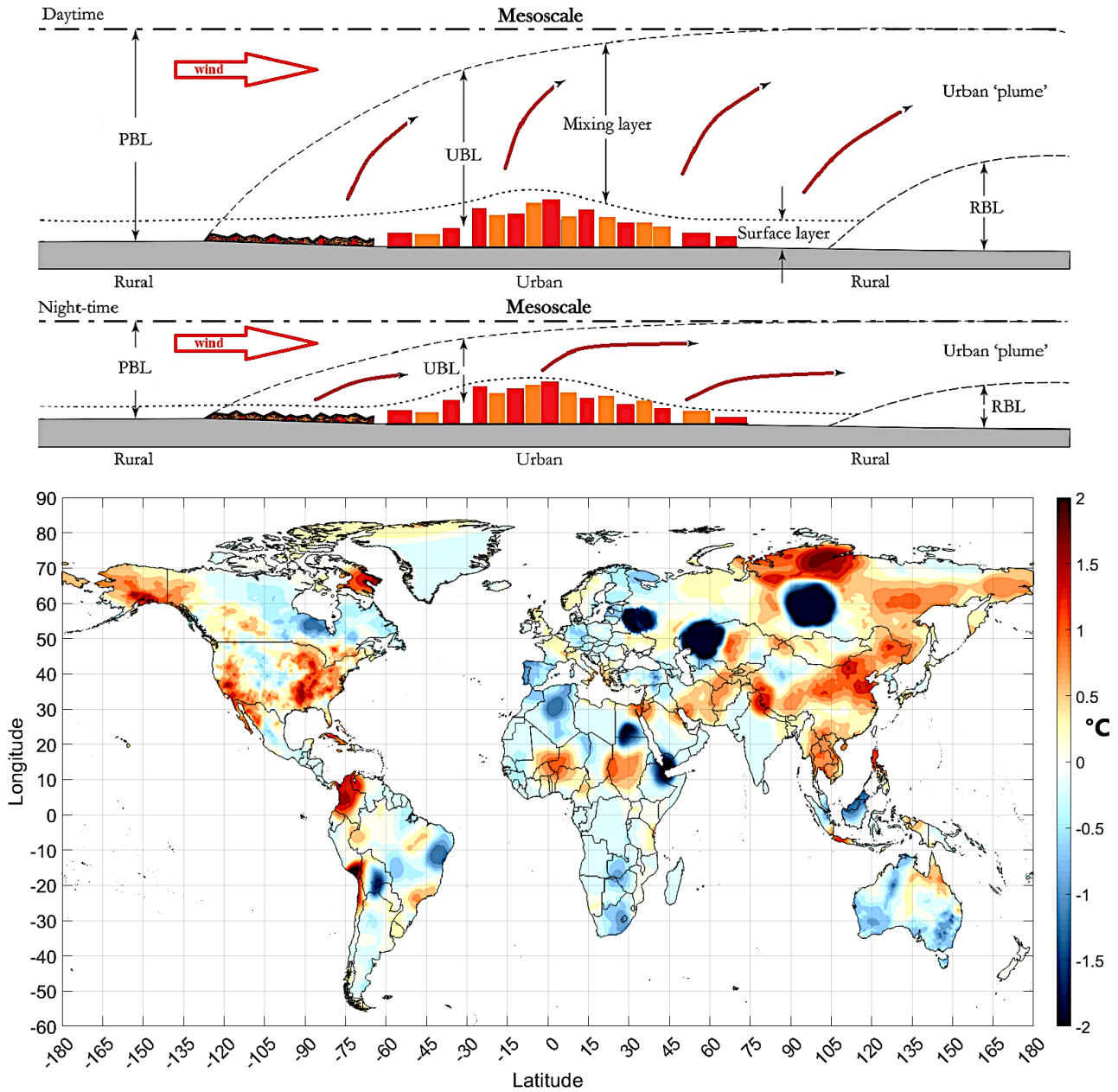


Figure 15: [Top] Diagram illustrating boundary layer structure over a city and its surrounding areas: a high daytime boundary layer facilitates heat dispersion, while a low nocturnal boundary layer retains hot air near the surface. [Bottom] Global map of the divergence between T_{\min} and T_{\max} comparing the periods 1945–1955 and 2013–2023, based on the CRU-TS4.08 land temperature data (Harris et al., 2020). (cf.: Scafetta and Ouyang, 2019; Scafetta, 2021a).

Moreover, Katata et al. (2023) identified evidence of “urban blending” or aliasing of trend biases within homogenized records. The blending artifact occurs when homogenization algorithms inadvertently transfer portions of the warm bias from heavily affected urban stations to less affected nearby stations, thereby distorting temperature records. As urbanization expands globally, these blending effects may have contributed to artificial warming biases in global surface temperature datasets. This phenomenon could explain the above observed discrepancies when comparing surface temperature records against rural-only datasets, satellite-based records, tree-ring chronologies, or the observed excessive divergence between daytime and nighttime temperature trends (Figures 13, 14, and 15).

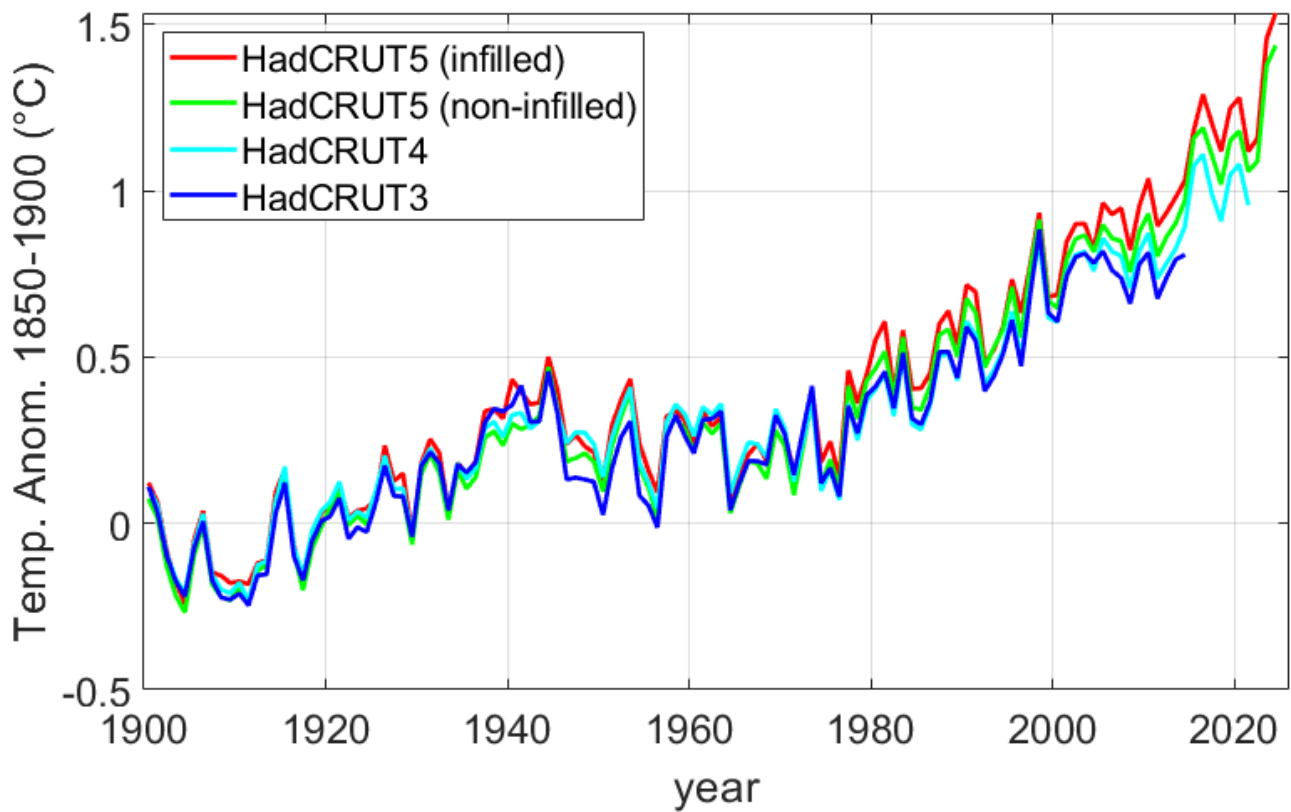


Figure 16: Comparison of global temperature records: HadCRUT3 (discontinued in 2014; Brohan et al., 2006), HadCRUT4 (discontinued in 2021; Morice et al., 2012), and HadCRUT5, including both the infilled and non-infilled versions (Morice et al., 2021).

4.1.5 The “disappearance” of the 2000–2014 temperature “pause” or “hiatus”

Global temperature datasets used for climate change analyses are subject to continuous updates, often reflecting substantial changes between successive versions. For example, the transition from HadCRUT3 (discontinued in 2014) (Brohan et al., 2006) to HadCRUT4 (discontinued in 2021) (Morice et al., 2012) and subsequently to HadCRUT5 (Morice et al., 2021) resulted in notable temperature alterations during the overlapping periods. In particular, Figure 16 highlights increasingly larger warming trends in these updated records after 2000, with increases up to 20% by 2014 (cf. Scafetta, 2023c). These modifications are likely to be attributable to the incorporation of additional input data, adjustments in homogenization algorithms, and the inclusion of model-based synthetic data to fill uncovered regions. Such changes may have been also influenced by efforts to mitigate the discrepancies observed between the GCM predictions and earlier datasets like HadCRUT3, where the data-model divergences had become increasingly apparent (Scafetta, 2012a; Fyfe et al., 2013). In fact, the latest revisions of the global surface temperature records effectively removed the well documented temperature “pause” or “hiatus” observed from 2000 to 2014 in several records, whose existence was acknowledged also by the IPCC (AR5, 2013). However, this 2000–2014 hiatus is still well visible in the latest ocean and satellite-based temperature records (Figure 14), raising further questions about the reliability of the latest global surface temperature records, in particular, over land.

In summary, while substantial evidence supports a global surface warming between 1850–1900 and 2011–2020, several factors — including comparisons of sea and land records with model projections (Scafetta, 2021a) — indicate that the actual global surface temperature warming may be 15–25% lower than what reported by the IPCC (2021). The concerns surrounding the reliability of current temperature records merit further investigation and scrutiny.

lished by Eddy (1977), which demonstrates that the Holocene ^{14}C cosmogenic record — a widely used proxy for variations in solar activity — is significantly correlated with multiple climatic indices. These include: (1) the timing of Alpine and global glacier advances and retreats (Le Roy Ladurie, 1967; Denton and Karlén, 1973); (2) an estimated mean annual temperature in England; and (3) reconstructed winter severity indices for the Paris-London region, dating back to the Medieval Warm Period (Lamb, 1965, 1972). Notably, historical records extensively document similar alternating warm and cold periods, which are closely linked to the rise and decline of civilizations (Diamond, 2005; Fagan, 2008). For instance, the Viking settlements in Greenland thrived during the Medieval Warm Period — a time of prolonged high solar activity — but were abandoned with the onset of the Little Ice Age, which was characterized by long periods of low solar activity (Eddy, 1976; Lasher and Axford, 2019).

Recent studies have further substantiated the presence of a significant correlation between solar and climate variability throughout the Holocene, including in the last century (e.g.: Hoyt and Schatten, 1997; Kerr, 2001; Bond et al., 2001; Neff, 2001; Scafetta et al., 2004; Kirkby, 2007; Steinhilber et al., 2012; Scafetta, 2012b; Soon and Legate, 2013; Czymzik et al., 2016; Connolly et al., 2023; Scafetta and Bianchini, 2023; Scafetta, 2023a; Xiao et al., 2024, and numerous others). Figures 17D–F provide examples of this connection. However, as discussed in Section 2, the IPCC (AR6, 2021) aligns with the CMIP6 GCMs’ prediction that the solar influence on climate change is negligible, particularly from 1850–1900 to the present (Figures 2 and 3). This raises a fundamental question: how can the IPCC’s claim be reconciled with the paleoclimate evidence that indicates a robust correlation between solar activity and climatic records throughout the Holocene?

This apparent paradox has been addressed in numerous recent studies (Scafetta et al., 2019; Scafetta, 2023a; Connolly et al., 2024, 2023). One key finding suggests that the CMIP6 GCMs underestimate the solar contribution to climate change by a large factor because these models rely only on a specific TSI forcing function characterized by a very low secular variability (Matthes et al., 2017), which, however, may be fundamentally flawed. Additionally, these models may likely exclude significant solar-climate physical mechanisms simply because they are still poorly understood.

The CMIP6 GCMs primarily attribute the Sun’s influence on climate to variations in its luminosity, as reported in the total solar irradiance (TSI) and solar spectral irradiance (SSI) forcings. While orbital changes also affect solar irradiance reaching Earth, these factors are categorized as orbital forcings and are predominantly relevant on multi-millennial or longer timescales. The issues related to these topics warrant further examination, as outlined below.

4.2.1 The TSI satellite composites (1978 to date)

Decadal and long-term variations in solar activity remain largely uncertain due to the limitations in the available data, as solar irradiance can only be accurately measured by satellites since 1978 (Hoyt and Schatten, 1997; Willson and Mordvinov, 2003).

Satellite-based total solar irradiance (TSI) records have been the subject of considerable debate, as their composites are not unique; for a detailed discussion, see Scafetta et al. (2019) and Connolly et al. (2024). Scientific studies highlight that, in addition to the well-documented 11-year solar cycle, various TSI composites are possible, and they exhibit distinct multidecadal trends. Such differences depend on the specific TSI satellite records utilized, the adjustments applied to the officially published data, and the selection of the overlapping periods. For example, while some TSI composites indicate a slight decrease or negligible trend from 1980 to 2023, others suggest a modest positive trend, and others even suggest a pronounced increase from 1980 to 2000 followed by a stabilization or slight decline from 2000 to 2023. Figure 18A illustrates examples of these TSI satellite composites; additional details are provided in Connolly et al. (2024).

Notably, the TSI composites constructed using the 1979–2013 ACRIM TSI satellite composite (Willson and Mordvinov, 2003) depict an increase from 1980 to 2000, followed by either a slight decrease or a near-stationary trend depending on the dataset used. The NASA-JPL ACRIM-based TSI composites show a strong correlation with the global surface temperature changes from 1980 to 2014, including a rapid warming trend from 1980 to

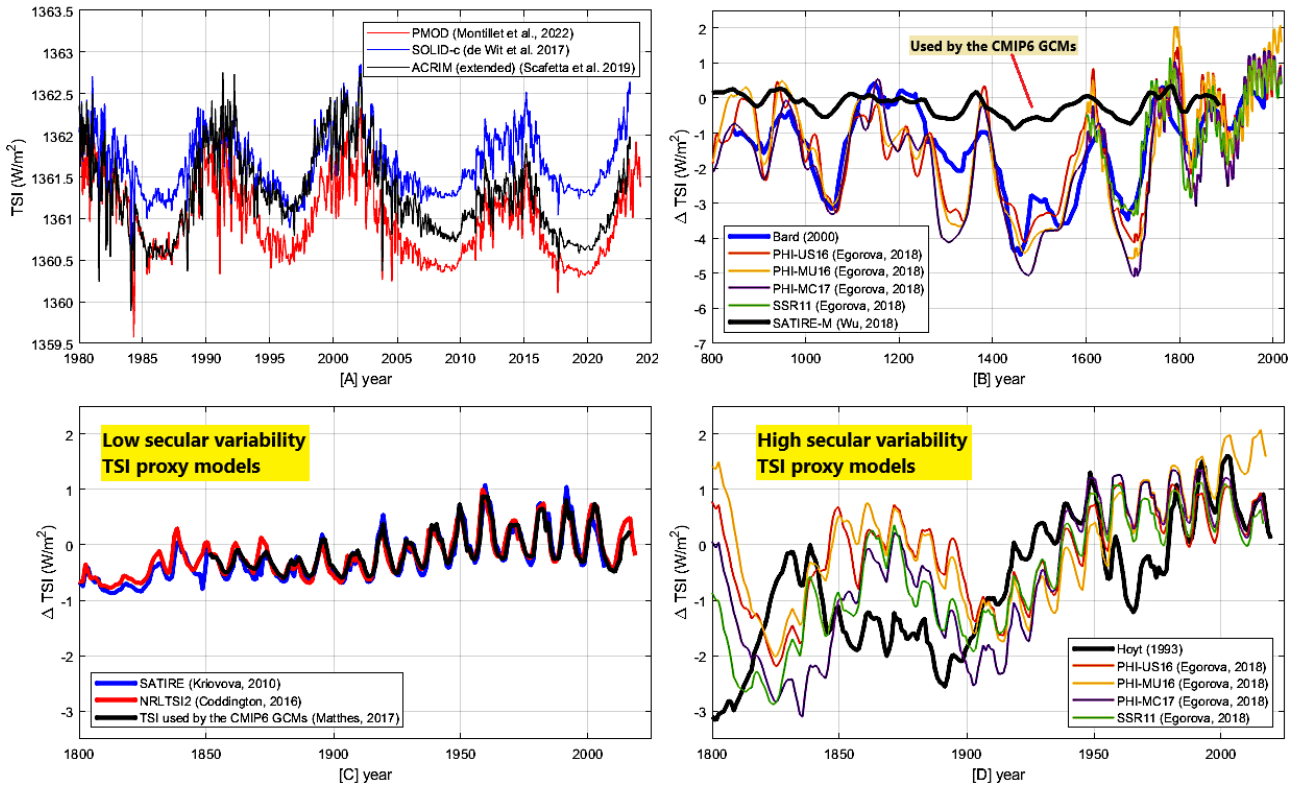


Figure 18: [A] Compilation sample of available total solar irradiance (TSI) satellite composites. [B, C, D] Compilation of alternative TSI proxy records. Data sources are found in Soon et al. (2023), Connolly et al. (2024) and Wu et al. (2018).

2000, and a subsequent plateau from 2000 to 2014. These observations suggest a significant solar contribution to climate change (Scafetta and West, 2008).

By contrast, the CMIP6 GCMs adopted the solar forcing model proposed by Matthes et al. (2017), which averages two distinct TSI models: NRLTSI2 (an empirical model proposed by Kopp et al., 2016, and Coddington, 2016) and SATIRE (a semi-empirical model proposed by Yeo et al., 2014). The TSI forcing proposed by Matthes et al. (2017) posits a slight decline in TSI from 1980 to 2020, which explains why the CMIP6 GCMs attribute no significant warming to solar influence during this period.

A critical scientific question arises regarding the accuracy of the TSI forcing proposed by Matthes et al. (2017), as its declining trend from 1980 to the present conflicts with the ACRIM-based TSI satellite composites, which is a composite constructed directly from the published TSI satellite data. The ACRIM-based composites contradict the NRLTSI2 and SATIRE TSI models. Among the few TSI composites compatible with NRLTSI2 are those that make use of the satellite TSI records modified by PMOD (Fröhlich, 2012). However, even the PMOD-adjusted composites fail to align with the substantial downward trends in successive solar minima predicted by the SATIRE model, as highlighted also by de Wit et al. (2017).

The modifications applied by PMOD to the published TSI satellite records rely on subjective decisions by Dr. Fröhlich, who adopted TSI proxy models and hypothetical sensor degradation corrections, which were revised multiple times. This methodology has been criticized, as it departs from the standard scientific approach, which typically involves adjusting models to fit experimental published data rather than altering published data based on model assumptions. In general, published experimental data can be further adjusted only based on strict experimental considerations alone. For a comprehensive discussion, see Scafetta et al. (2019) and Connolly et al. (2024). The PMOD adjustments of the published TSI satellite records remain contentious and were never endorsed by the TSI satellite experimental teams led by other researchers such as Drs. Richard C. Willson for ACRIM and Douglass V. Hoyt for Nimbus7 (Scafetta et al., 2019). Consequently, the unresolved ACRIM-PMOD controversy continues to carry significant implications for both solar and climate science (Con-

nolly et al., 2024). Despite this, the IPCC (AR6, 2021) has recently chosen to disregard this debate, even though it was acknowledged in the earlier IPCC assessment reports.

4.2.2 The long-scale TSI proxy models

To investigate long-term variations in solar activity, researchers employ proxies such as sunspot numbers and cosmogenic isotope records of ^{14}C and ^{10}Be . In the absence of direct Total Solar Irradiance (TSI) measurements prior to 1978 and due to uncertainties in the TSI satellite composites after 1980, modeling TSI changes over centuries and millennia remains highly challenging. While sunspot numbers and cosmogenic records can identify alternating periods of high and low solar activity, the precise magnitude of solar luminosity variations remains unknown, rendering rigorous validation of solar models unfeasible. Consequently, various TSI proxy models have been proposed in recent decades. Selected examples of these models are illustrated in Figures 18B, 18C, and 18D.

Notably, the TSI model developed by Matthes et al. (2017), which underpins the TSI forcing for the CMIP6 GCMs, shows minimal secular variability, as it remains nearly constant from 1850 to 2020 (Figure 18C). For millennial-scale simulations, the CMIP6 GCMs use the TSI forcing derived from the SATIRE-M model (Wu et al., 2018), which similarly shows a modest secular modulation (Figure 18B). Consequently, it is unsurprising that the CMIP6 GCMs attribute negligible climate effects to solar forcing (Figures 1, 2, and 10).

In contrast, other TSI proxy models documented in the literature display significantly larger secular variability (Figures 18B and 18D) (e.g.: Hoyt and Schatten, 1993; Bard et al., 2000; Egorova et al., 2018; Penza et al., 2022). These models suggest a marked increase in solar activity since the 17th century and continuing during the 20th century, which correlates well with the observed global warming since the Little Ice Age. An increase of solar activity during the 19th and 20th century is also supported by records of the solar coronal magnetic field (Lockwood et al., 1999). This solar-climate correlation is evident over centuries and millennia and is particularly robust when specific TSI models are chosen (Scafetta and West, 2007; Scafetta, 2023a; Soon et al., 2023).

Given the absence of direct measurements of TSI secular variability, the proposed TSI proxy models derived also from assumptions that changed over time. For instance, Lean et al (1995) estimated that at the Maunder Minimum (1645–1715) TSI could have been 0.25% (approximately 3.5 W/m^2) lower than the contemporary TSI satellite baseline, currently estimated at approximately 1361 W/m^2 . However, this same estimate was later reduced by Lean et al. (2005) to 0.1% (approximately 1.3 W/m^2). More recently, Yeo et al. (2020) asserted that the Sun's darkest possible state could not exceed a reduction of $2.0 \pm 0.7 \text{ W/m}^2$ relative to the modern baseline. These revised claims, supported partly by the low multi-decadal variability of the TSI composites constructed using the modified PMOD TSI satellite records underlie, the modest secular variability presented by TSI models such as NRLTSI2 and SATIRE (Figure 18C). However, indirect evidence from luminosity changes in Sun-like stars (Judge et al., 2020) and the direct correlation between climate records and the TSI models with large secular variability suggest a much larger TSI variability over multi-centennial timescales (Schmutz, 2021).

In fact, Schmutz (2021) presented a compelling argument: the strong correlation between climate and solar activity records over secular and millennial scales (Figure 18B) convincingly challenges the assumption that solar activity has been characterized by a minimal multidecadal and secular variability, as those manifested by the NRLTSI2 and SATIRE TSI models. As illustrated in Figure 10, when the GCMs are driven by TSI proxy models with low multidecadal and secular variability, they just fail to capture the cooling transition from the Medieval Warm Period to the Little Ice Age, casting doubt on both the validity of these GCMs and their underlying solar forcing assumptions.

4.2.3 A solar-induced corpuscular forcing of the climate

Schmutz (2021) estimated that the emergence of the Maunder Minimum-type cold climate excursions characteristic of the Little Ice Age necessitates a total solar irradiance (TSI) reduction of approximately 10 W/m^2 from present. This magnitude of TSI change exceeds by more than a factor of 10 the variability of the TSI

functions employed in the CMIP6 GCMs, but it also is two to three times greater than TSI variability of the high-variability TSI proxy models (Figure 18B). Consequently, the climate system appears to exhibit an amplified sensitivity to TSI variations (Soon et al., 2000; Ziskin and Shaviv, 2012). This over-sensitivity is observed also in analyses of the climate response to the 11-year solar cycle, whose amplitude is more reliably constrained than the TSI long-term secular modulation (e.g.: Shaviv, 2008; Scafetta, 2023a). This raises a critical question: what accounts for the observed amplification of the solar signal within the climate system? The resolution of this puzzle may require acknowledging the existence of additional mechanisms through which solar activity influences climate beyond direct TSI forcing. In particular, a still poorly understood form of solar corpuscular forcing has been hypothesized as a potential major contributor.

More specifically, cosmogenic isotope records (^{14}C and ^{10}Be), which serve as proxies for reconstructing past solar activity, are generated by cosmic rays interacting with the Earth's atmosphere. Solar magnetic activity modulates the cosmic ray flux, which increases during periods of low solar activity and decreases when solar activity is high. Additionally, cosmic ray flux may experience episodic enhancements due to supernova events. Several studies have proposed that atmospheric ionization induced by cosmic rays plays a significant role in the formation of cloud condensation nuclei, thereby exerting a direct influence on the cloud formation processes (Shaviv and Veizer, 2003; Svensmark and Friis-Christensen, 1997; Kirkby, 2007). A comprehensive review of these findings is available in Svensmark (2019).

A decline in solar activity is associated with increased cosmic ray flux, which in turn leads to a greater atmosphere ionization and, therefore, a more extended cloud cover, which increases the Earth's albedo by reflecting more incoming shortwave radiation back into space. This mechanism could result in a notable surface cooling since also a very small increase in cloud cover may reduce the solar forcing at the surface by several watts per square meter (van Wijngaarden and Happer, 2025). Conversely, higher solar activity reduces cosmic ray flux, diminishing cloud cover and thereby lowering the albedo of the Earth, leading to a surface warming.

The cosmic ray hypothesis posits that variations in solar magnetic activity may be even more significant than changes in solar luminosity in driving climate changes via direct corpuscular forcing of the cloud system (Easterbrook, 2019). Empirical evidence supporting this hypothesis includes findings by Czymzik et al. (2016), who identified a robust correlation between cosmogenic records and flood frequency across Europe during the Holocene, suggesting a direct link to cloud formation (17F).

Despite its potential explanatory power, the cosmic ray hypothesis remains controversial. The CLOUD experiment at CERN, designed to investigate this mechanism, concluded that cosmic rays are insufficient to induce significant nucleation of cloud condensation nuclei (Kirkby et al., 2011). However, observations of strong correlations between cosmic ray flux and cloud cover during Forbush decreases — which are sudden drops in cosmic ray flux typically caused by solar coronal mass ejections — suggest that the conclusions of the CLOUD experiment may require re-evaluation (Svensmark et al., 2016; Svensmark, 2019; Matsumoto et al., 2022). Additional recent evidence for a pronounced 11-year solar cycle signature in cloud records has been documented by Miyahara et al. (2023). Moreover, Svensmark (2022) showed that the correlation between the cosmic ray flux record and climatic data extend over the last 3.5 billion years, where ocean nutrient proxy data were found to covary with supernova frequency. These latest results further reinforce the hypothesis that cosmic rays can significantly drive climate changes.

Another potential corpuscular forcing mechanism involves interplanetary dust falling on Earth, which remains an area requiring further investigation. Ionized interplanetary dust may exert direct influence on cloud nucleation and contribute to climate variability. For instance, Scafetta et al. (2020) identified a 60-year cycle in meteorite fall frequency that exhibits strong coherence with the 60-year climatic oscillation (Figures 7 and 8). This cycle, which has persisted for centuries, appears to be linked to the 60-year modulation of Jupiter's orbital eccentricity, primarily governed by its gravitational interaction with Saturn.

The prospect that solar activity could indirectly influence the climate through corpuscular forcings and space weather dynamics — processes which are not accounted for in the current GCMs — merits further scrutiny. Variability in cloud cover has been proposed as a primary driver of climate change, as illustrated

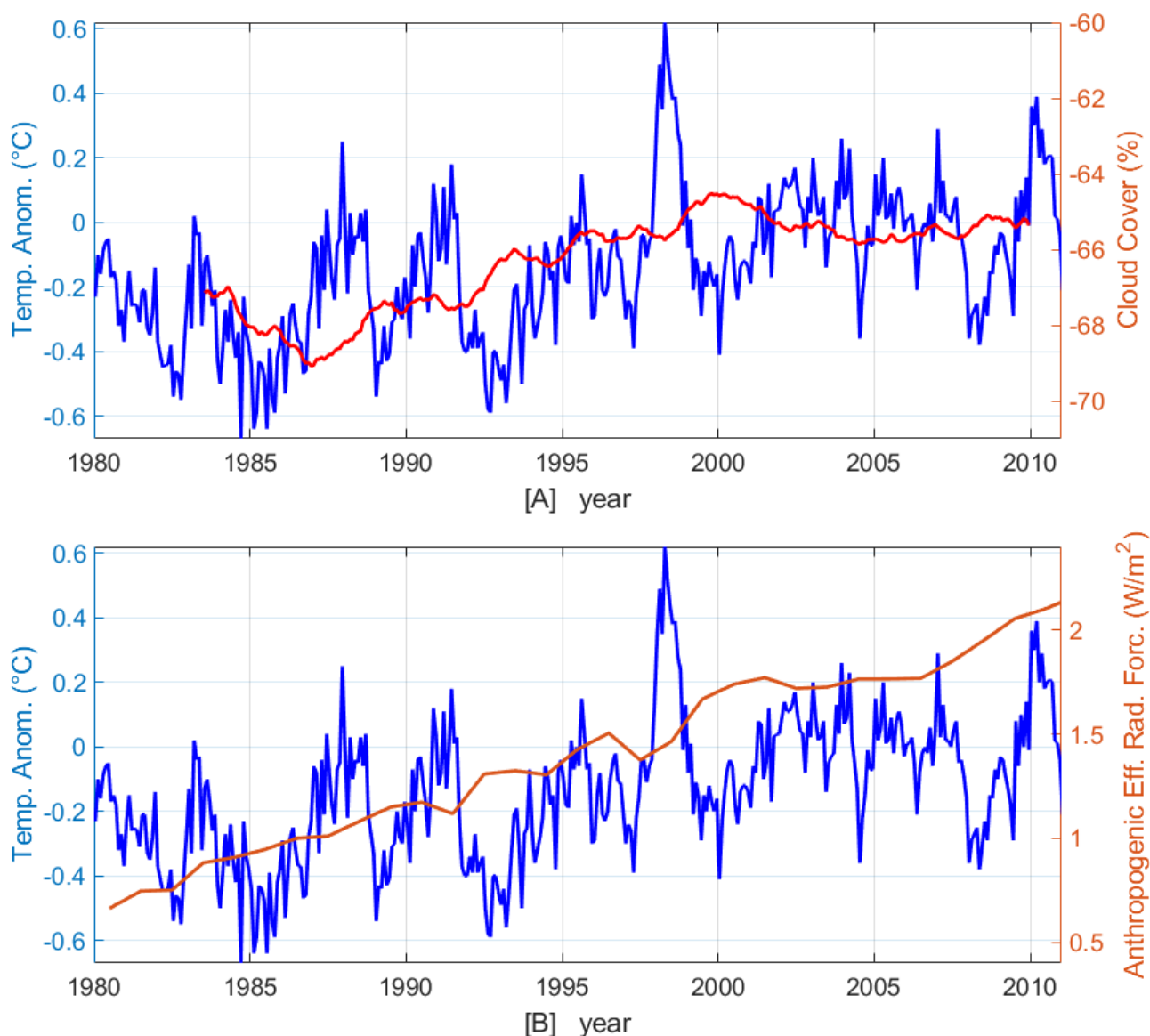


Figure 19: Comparison of the UAH-MSU It v6.1 global satellite temperature record (blue) with: [A] the global cloud cover percentage data from the International Satellite Cloud Climatology Project (ISCCP); [B] the total anthropogenic effective radiative forcing employed in the CMIP6 GCMs.

by Scafetta (2013a, its figure 19), who demonstrated a strong negative correlation between the ISCCP global monthly cloud cover and the global temperature records from 1983 to 2010.

Figure 19A highlights this negative correlation by plotting the UAH MSU It v 6.1 global satellite temperature record (blue) against the ISCCP global cloud cover percentage record from July 1983 to December 2009 (inverted scale). Both curves exhibit a well-correlated increase from 1980 to 2000 followed by a more constant level from 2000 to 2010. In contrast, Figure 19B juxtaposes the same temperature record with the total anthropogenic effective radiative forcing function adopted by the CMIP6 GCMs (Figure 1C), which exhibits a continuous linear increase from 1980 to 2010. This comparison underscores that global temperature records align more closely with variations in cloud cover than with the anthropogenic forcing record.

5 Modeling climate change using empirical and semi-empirical models

As discussed above, several fundamental challenges complicate the detection, attribution, and modeling of climate change. Global surface temperature records may exhibit significant warming biases, while numerical climate models may contain unresolved physical uncertainties. Additionally, the actual solar forcing — recog-

nized as the dominant natural driver of climate change on millennial timescales — remains highly uncertain because the long-term solar activity variability is not well known and the mechanisms through which solar phenomena influence climate may include both radiative forcing and a poorly understood corpuscular forcing. In response to these concerns, various proposals advocate for the use of empirical and semi-empirical models to enhance climate change modeling.

5.1 From reductionist to holistic approaches in climate modeling

The Intergovernmental Panel on Climate Change Assessment Reports (2007; 2013; 2021) have relied predominantly on computer-based global climate models (GCMs). These models exemplify a reductionist scientific approach, which seeks to simplify complex systems by focusing on individual components. While reductionism can offer valuable insights, it also presents several limitations such as:

1. *loss of context* — by isolating individual components, reductionist methodologies may overlook critical interactions, leading to an incomplete understanding of the climate system.
2. *oversimplification* — certain essential processes, such as cloud formation, remain poorly represented in the GCMs, affecting their accuracy in climate simulation and projections;
3. *emergent properties* — some systemic properties only manifest when the climate system is analyzed holistically and cannot be discerned by examining isolated components;
4. *interconnected systems* — complex climate feedback mechanisms and relationships may be inadequately captured by reductionist models, leading to misleading conclusions;
5. *application limits* — insights derived from reductionist models may not be readily transferable to real-world applications where a broader, integrative understanding is required.

Given these constraints, a more comprehensive approach incorporating holistic methodologies is necessary to achieve an improved understanding of complex climate dynamics. Holistic models, particularly empirical and semi-empirical frameworks, offer several advantages such as:

1. *reliance on observational data* — these models emphasize empirical data, enabling a direct modeling of real-world climate patterns, thereby addressing limitations present in numerical climate models such as the CMIP6 GCMs;
2. *simplicity and transparency* — compared to complex GCMs, empirical models tend to be more accessible and interpretable;
3. *robust statistical frameworks* — these models apply rigorous statistical techniques to quantify the influence of both anthropogenic and natural climate drivers;
4. *direct attribution of climate signals* — by comparing observed trends with historical records, empirical models help to link specific climate variations to their underlying physical drivers;
5. *policy and adaptation applications* — empirical models provide clear evidence that can inform climate policy and adaptation strategies more effectively than complex numerical models.

However, empirical models also have inherent limitations:

1. *data dependence* — the reliability of empirical models is contingent on the quality and completeness of the available data, which can sometimes lead to inaccuracies;
2. *simplification assumptions* — while useful, empirical models may overlook complex climate interactions, leading to potential misrepresentations;

3. *nonlinearity and complexity* — the inherently nonlinear behavior of the climate system poses challenges for empirical modeling, sometimes resulting in oversimplifications;
4. *regional specificity* — findings based on one geographic region may not be universally applicable, complicating broader climate assessments.
5. *attribution uncertainty* — while empirical models provide valuable insights into climate change attribution, they may be less robust than physically based models for quantifying the contributions of individual factors.

Thus, the study of complex natural systems necessitates the integration of both holistic and reductionist methodologies. Since each approach has inherent strengths and limitations, comparing numerical and empiric models should allow for a more accurate representation of climate processes. Let us now discuss some of the empirical modeling of the climate system proposed in scientific literature.

5.2 Empirical and semi-empirical approaches in climate science

Several types of empirical and semi-empirical models are commonly employed in climate science such as:

1. *Empirical Climate Models* (ECMs) — ECMs use statistical techniques such as multiple linear regression and spectral analysis to identify relationships between climate change and external drivers. Examples include models assessing El Niño-Southern Oscillation dynamics, volcanic aerosol contributions, solar radiation, and anthropogenic influences. These models provide preliminary attribution of observed temperature changes.
2. *Energy Balance Models* (EBMs) — EBMs represent climate dynamics by balancing incoming solar radiation with outgoing thermal emissions. They range from simple zero-dimensional (0-D) models, which treat the Earth as a single thermal unit, to more complex one-dimensional (1-D) and multi-dimensional formulations that account for latitudinal and spatial variations.
3. *Statistical Downscaling Models* (SDMs) — SDMs refine broad-scale climate projections from the GCMs to more localized resolutions, enabling assessments of regional climate impacts.
4. *Machine Learning Models* (MLMs) — Machine learning methodologies have recently been introduced in climate research, offering promising capabilities for identifying nonlinear relationships and predicting climate patterns from large datasets. While MLMs have notable potential, challenges related to interpretability and data requirements remain.

Each of these modeling approaches possesses unique strengths and limitations, and they are frequently utilized in combination to provide a more comprehensive understanding of climate change.

The following subsections provide an overview of empirical models presented in the literature that attribute climate change to both anthropogenic and natural drivers by directly analyzing the climatic records. This discussion will primarily focus on studies published after the release of the IPCC's Sixth Assessment Report (2021). These models employ diverse mathematical methodologies and underscore the significant role of solar influences in climate change, though the extent of this contribution varies depending on underlying assumptions and the specific methodologies used by model developers. For further technical details and statistical validation, readers are encouraged to consult the cited references.

5.3 A simple linear regression model

Regression models are widely regarded as the simplest and most used analytical tools in climate change attribution studies. They rely on statistical techniques such as multi-linear regression analysis to explore relationships between climate variables and a set of predictors. For instance, Chylek et al. (2014) utilized this

approach to model the global surface temperature record by incorporating known radiative forcing functions of greenhouse gases (GHG), aerosols (AER), solar irradiance (SOL), volcanic activity (VOLC), as well as indices for the El Niño Southern Oscillation (ENSO) and the Atlantic Multidecadal Oscillation (AMO) as explanatory variables. They proposed the following multi-linear regression model:

$$T(t) = a_0 + a_1 \cdot F_{GHG}(t) + a_2 \cdot F_{AER}(t) + a_3 \cdot F_{SOL}(t) + a_4 \cdot F_{VOLC}(t) + a_5 \cdot I_{ENSO}(t) + a_6 \cdot I_{AMO}(t) \quad (1)$$

where the free parameters $a_{0...6}$ represent six regression coefficients. In their analysis, Chylek et al. (2014) adopted the climate forcin

g functions derived from the GISS ModelE (Hansen et al., 2007), which utilizes an earlier version of the NRLTSI TSI model based on the PMOD-modified TSI satellite composite (Lean, 2000). They concluded that anthropogenic forcing and the positive phase of the AMO collectively accounted for approximately two-thirds and one-third, respectively, of the global warming observed since 1975.

Despite its apparent utility, the proposed model has several potential limitations. First, its reliance on a potentially inaccurate solar forcing function likely skewed the results because as the post-1975 warming, which the model attributed to AMO, could have also be partially attributed to solar activity variations if TSI records compatible with the ACRIM TSI satellite composite were used (Scafetta and West, 2008; Scafetta, 2009; Connolly et al., 2023). Second, the climate system processes the radiative forcing functions through inherently non-linear mechanisms, and thus the assumed linear relationships between $T(t)$ and its radiative forcing components may oversimplify reality. Furthermore, ENSO and AMO are subsystems of the climate system and, therefore, they cannot necessarily be considered physically independent of the forcing functions.

Multi-linear regression analysis can also produce ambiguous or erroneous results when significant collinearity exists among predictors or when non-linear effects are neglected. For example, Benestad and Schmidt (2009) applied a multilinear regression model to global surface temperatures incorporating the ten radiative forcing functions used by the GISS model. Their result suggested that solar forcing may have contributed approximately 0.1°C to the 0.65°C warming observed from 1900 to 2000, but they acknowledged the lack of robustness for such finding.

In fact, Scafetta (2013b) demonstrated that multilinear regression models using GISS forcing functions could effectively reproduce global temperature records even if the well-mixed GHG forcing function were ignored because of its collinearity with the other predictors. Additional analyses by Scafetta and West (2006a,b, 2007) and later Scafetta (2009) indicated that the solar influences may have contributed to 50% or more of the warming between 1900 and 2000. These findings were derived using analytical methods such as wavelet frequency decomposition and simplified zero-dimensional energy balance models, which account for some non-linear effects. Models such as the one proposed in Eq. 1 may underestimate solar contributions due to the climate system's tendency to attenuate high-frequency signals while amplifying low-frequency components, a consequence of its thermal inertia. In this context, Benestad and Schmidt (2009) identified a significant solar signature, though it was attenuated relative to the finding of Scafetta and West (2006a,b, 2007) largely due to methodological errors in wavelet analysis, as later highlighted by Scafetta (2013b).

5.4 A simple ECM based on a zero-dimensional EBM

Empirical regression models are most effective when they balance simplicity and complexity. They should incorporate the minimum number of physically relevant predictors, chosen carefully to avoid collinearity. Additionally, these models should simulate some non-linearity. For example, radiative forcing functions are not inherently linear predictors of climate behavior, as the climate system processes them by attenuating the high-frequency components relative to the low-frequency ones due to its thermal capacity.

Taking into account the above considerations, Scafetta (2023a) proposed modeling the global surface tem-

perature record, $T(t)$, using the following equation:

$$T(t) = T_A(t) + T_V(t) + T_S(t) + \xi(t) = T_{AVS}(t) + \xi(t), \quad (2)$$

where $T(t)$ is derived from four components: anthropogenic, $T_A(t)$; volcano, $T_V(t)$; solar, $T_S(t)$; plus a fast-fluctuating component, $\xi(t)$, simulating fast fluctuations such as the ENSO signal. The three main contributors can be estimated using a 0-D energy balance equation with a given time response, which can be generally modeled as:

$$C \frac{dT(t)}{dt} = \frac{1-a}{4} S - \sigma \epsilon T(t)^4 + G. \quad (3)$$

On the left side, $T(t)$ is the mean global temperature in Kelvin, C represents the effective heat capacity of the Earth's surface and atmosphere. On the right side, in the first term a denotes the albedo, S is the incoming solar radiation adjusted for the planetary sphericity (the denominator "4"); the second term represents the outgoing longwave radiation, which depends on the temperature itself; finally, G incorporates the effect of the greenhouse gases.

By redefining the constants and simplifying the formulation, the above equation can be approximated for each forcing component using differential equations based on the temperature anomalies, $\Delta T(t) = T(t) - T_0$, which are relative to a given mean temperature T_0 :

$$\frac{\Delta T_A(t) - \Delta T_A(t - \Delta t)}{\Delta t} = \frac{k_A F_A(t) - \Delta T_A(t - \Delta t)}{\tau} = \alpha_A \cdot F_A(t) - \beta \cdot \Delta T_A(t - \Delta t) \quad (4)$$

$$\frac{\Delta T_V(t) - \Delta T_V(t - \Delta t)}{\Delta t} = \frac{k_V F_V(t) - \Delta T_V(t - \Delta t)}{\tau} = \alpha_V \cdot F_V(t) - \beta \cdot \Delta T_V(t - \Delta t) \quad (5)$$

$$\frac{\Delta T_S(t) - \Delta T_S(t - \Delta t)}{\Delta t} = \frac{k_S F_S(t) - \Delta T_S(t - \Delta t)}{\tau} = \alpha_S \cdot F_S(t) - \beta \cdot \Delta T_S(t - \Delta t) \quad (6)$$

Here, $F_A(t)$, $F_V(t)$, and $F_S(t)$ represent the anthropogenic, volcanic, and solar effective forcings, respectively. The coefficients $\alpha_A = k_A/\tau$, $\alpha_V = k_V/\tau$, $\alpha_S = k_S/\tau$, and $\beta = 1/\tau$ depend on the sensitivity parameters k_A , k_V and k_S and the characteristic time response τ , which is directly related to the Earth's effective heat capacity. For simplicity, τ is assumed constant for all forcings.

Under equilibrium conditions, the temperature change $\Delta T_{2 \times \text{CO}_2}$, which corresponds to doubling atmospheric CO_2 concentration (for example, from 280 ppm to 560 ppm), is the equilibrium climate sensitivity

$$ECS = \Delta T_{2 \times \text{CO}_2} = k_A \Delta F_{2 \times \text{CO}_2} = 3.7 k_A. \quad (7)$$

For the transient climate response (TCR), which is defined as the temperature average over 20 years around the time of CO_2 doubling under a linear increase scenario (1% annually over 70 years), the calculation gives:

$$TCR = 3.7 k_A - \frac{3.7}{70} k_A \tau \left(1 - e^{-70/\tau}\right) = ECS \left[1 - \frac{\tau}{70} \left(1 - e^{-70/\tau}\right)\right]. \quad (8)$$

By iterating, these equations can be reformulated as:

$$\frac{\Delta T(t) - \Delta T(t - \Delta t)}{\Delta t} = \alpha_A \cdot F_A(t) + \alpha_V \cdot F_V(t) + \alpha_S \cdot F_S(t) - \beta \cdot \Delta T(t - \Delta t), \quad (9)$$

where Δt is set to 1 year. Using multilinear regression analysis, the regression coefficients (α_A , α_V , α_S and β) can be evaluated, and can be used to reconstruct the climatic signatures of each forcing and compute $\Delta T_{AVS}(t)$, the deterministic component of $T(t)$. Unlike Eq. 1, the model expressed by Eq. 9 accounts for the climate system's non-linear processing of the forcing functions due to its heat capacity, which leads to a timescale-dependent amplitude and time-lag in the response of the climate system to the input forcing function.

Scafetta (2023a) demonstrated that if the climate sensitivity is set to be equal for all forcings ($\alpha_A = \alpha_V = \alpha_S$) — indicating that the climate is equally sensitive to all types of forcings — the solar contribution to the global

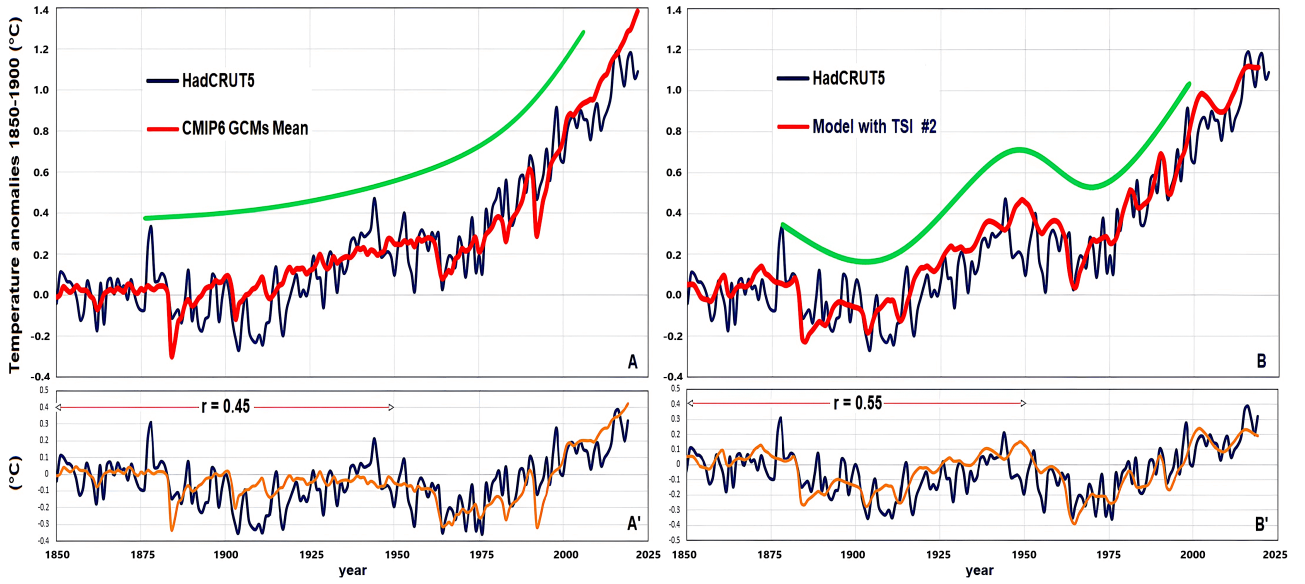


Figure 20: [A] Comparison of the HadCRUT5 global surface temperature record with the CMIP6 GCM ensemble average. [A'] Both records are detrended using the function $f(t) = a(x - 1850)^2$, correlation coefficient of $r = 0.45$ for the period 1850–1950. [B] Comparison of the HadCRUT5 global surface temperature record with the ECM derived from Eq. 2 utilizing a medium-high variability Total Solar Irradiance (TSI) proxy model and assuming the condition $\alpha_A = \alpha_V \neq \alpha_S$. [B'] The same detrending analysis as in [A'] is applied, yielding an improved correlation coefficient of $r = 0.55$. Adapted from Scafetta (2024).

warming from 1850–1900 to 2011–2022 is minimal, particularly when it is adopted the low-secular-variability TSI model used by the CMIP6 GCMs. Under this scenario, the ECS was estimated to be 2.1 ± 0.7 °C (17–83% range), which is consistent with the low ECS range proposed by the IPCC (2021). In this circumstance, the result suggests that most of the observed warming could be attributable to the anthropogenic forcing, although the ECS was estimated to be lower than 3.0°C. This empirically derived ECS range optimally fits the findings of Lewis (2023) and (Scafetta, 2021c, 2022, 2023b).

Alternatively, assuming $\alpha_A = \alpha_V \neq \alpha_S$, which means that the climate sensitivity to solar variations can be different from that to the other radiative forcings, Scafetta (2023a) found that the climate could be also 4 to 6 times more responsive to TSI forcing than to anthropogenic or volcanic forcing. In this circumstance, the result implies an ECS that could be as low as 1.1 ± 0.4 °C (17–83% range), suggesting that solar activity may directly influence the Earth's albedo by physical mechanisms currently absent in the GCMs. Under this scenario, if high-secular-variability TSI models are adopted, solar activity changes could explain ~50% or more of the observed warming from 1850–1900 to 2011–2022.

Figures 20A and 20B, respectively, compare the HadCRUT5 global surface temperature record (black) against the CMIP6 GCM ensemble mean simulation and the ECM output (red) curves. The latter was obtained using high-secular-variability TSI models under the condition $\alpha_A = \alpha_V \neq \alpha_S$. The green curves in both panels A and B highlight the distinct multi-decadal modulation pattern evident in the red curves of the two types of models. In panel A, the red curve demonstrates a steadily increasing trend, reflecting the anthropogenic forcing function. In contrast, the red curve in panel B exhibits a quasi 60-year oscillatory behavior that closely resembles the observed climate temperature record. This distinction becomes more evident in panels A' and B', which display the detrended curves. In Figure 20A', the correlation coefficient for the period 1850 to 1950 is $r = 0.45$, whereas in Figure 20B', the correlation coefficient is notably higher at $r = 0.55$. More specifically, the CMIP6 GCM ensemble average simulation inadequately captures the warming observed from the 1900s to the 1940s and the subsequent cooling from the 1940s to the 1970s. In contrast, these patterns are more accurately reproduced by the ECM derived from Eq. 2 under the outlined assumptions.

5.5 Astronomically-based empirical harmonic models of natural climate variability

There is another widely utilized empirical approach to model climate change, which again considers three primary components: anthropogenic, volcanic, and other natural factors. However, the latter component is conceptualized as made of a complex harmonic signal. The modeling is based on the hypothesis that these other natural climatic components derive from astronomical, solar and lunar forcings that could exhibit approximate harmonic behavior. This empirical methodology involves analyzing the periodogram of the climate records, identifying relevant frequencies, and generating constituent harmonic functions using multiple linear regression analysis. The harmonics are subsequently combined to empirically reconstruct the hypothesized harmonic natural patterns of the climate system.

One notable advantage of this approach lies in its ability to extend harmonics for forecasting purposes. For example, it is well known that seasonal variations can be approximately modeled using annual and semi-annual cycles. However, issues arise when the selected frequencies lack physical justification. Misinterpretation of artifacts in the periodogram as genuine physical frequencies may lead to harmonic models that perform well within the calibration interval, and yet they could diverge substantially from reality outside the regression period. Furthermore, periodograms of climatic records may only approximate true physical frequencies, particularly in the low-frequency domain where error margins are larger.

To mitigate the possibility of using non-physical frequencies, Scafetta (2010, 2013a, 2021b) proposed selecting only those frequencies that can be theoretically derived from astronomical considerations, which is a methodology analogous to that employed in ocean tidal modeling since the seminal work of Sir William Thomson (Lord Kelvin) in 1879 (for a recent application of this methodology see Ardalan and Hashemi-Farahani, 2007). This approach appears justified, because temperature records present periodograms spectrally coherent with planetary, solar, and lunar harmonics (Scafetta, 2010, 2014b, 2021b). Solar records themselves exhibit planetary harmonics across annual to multi-millennial scales (Scafetta, 2012b, 2014b; Scafetta et al., 2016; Scafetta, 2020; Scafetta and Bianchini, 2023). These harmonics include the 11-year solar cycle, the Eddy quasi-millennial cycle, and the Bray-Hallstatt oscillation (~2318 years) identified in radiocarbon and climate records spanning the Holocene. In general, it appears that the natural harmonics of the solar system synchronize both solar and climate oscillations, although the mechanisms underlying such planetary synchronization phenomenon remain under investigation (e.g.: Scafetta, 2012d; Scafetta and Bianchini, 2022; Stefani et al., 2024).

Scafetta (2021b) extended the model first proposed in Scafetta (2010) by hypothesizing that the climate system incorporates 13 major harmonics with periods spanning approximately 3 to 1000 years. Anthropogenic and volcanic contributions were derived from the ensemble mean of the CMIP6 GCM simulations, utilizing half the climate sensitivity estimated by these models, which means that the ECS was estimated to be about 1.5-2.0°C, to incorporate a natural variability described by the adopted harmonic constituent model. The proposed equation is as follows

$$T(t) = T_0 + \sum_{i=1}^{13} A_i \sin [2\pi (f_i \cdot (t - 2000) + \alpha_i)] + 0.5 \cdot GCM(t), \quad (10)$$

where A_i , f_i and α_i per $i = 1, \dots, 13$ are coefficients discussed in detail by Scafetta (2021b, 2024).

Figure 21A shows the output of the above model extended to 2100 using the SSP2-4.5 scenario, which is considered to be the most realistic one (Hausfather and Peters, 2020; Pielke et al., 2022). Figure 21B presents burning ember plots for the top five global reasons for concern (RFCs), based on the IPCC (AR6, 2023) findings under minimal adaptation assumptions. The comparison of panels A and B indicates that the projected temperatures throughout the 21st century are likely to remain within the safe adaptation threshold indicated by the Paris Agreement (2016) limiting global warming to less than 2°C relative to the 1850–1900 pre-industrial period. By contrast, the CMIP6 GCM projections forecast significantly higher, and potentially hazardous, warming levels (Figure 3). Similar conclusions were reached by Connolly et al. (2020) using an alternative and more simple empirical model with low climate sensitivity to radiative forcing under business-as-usual scenarios.

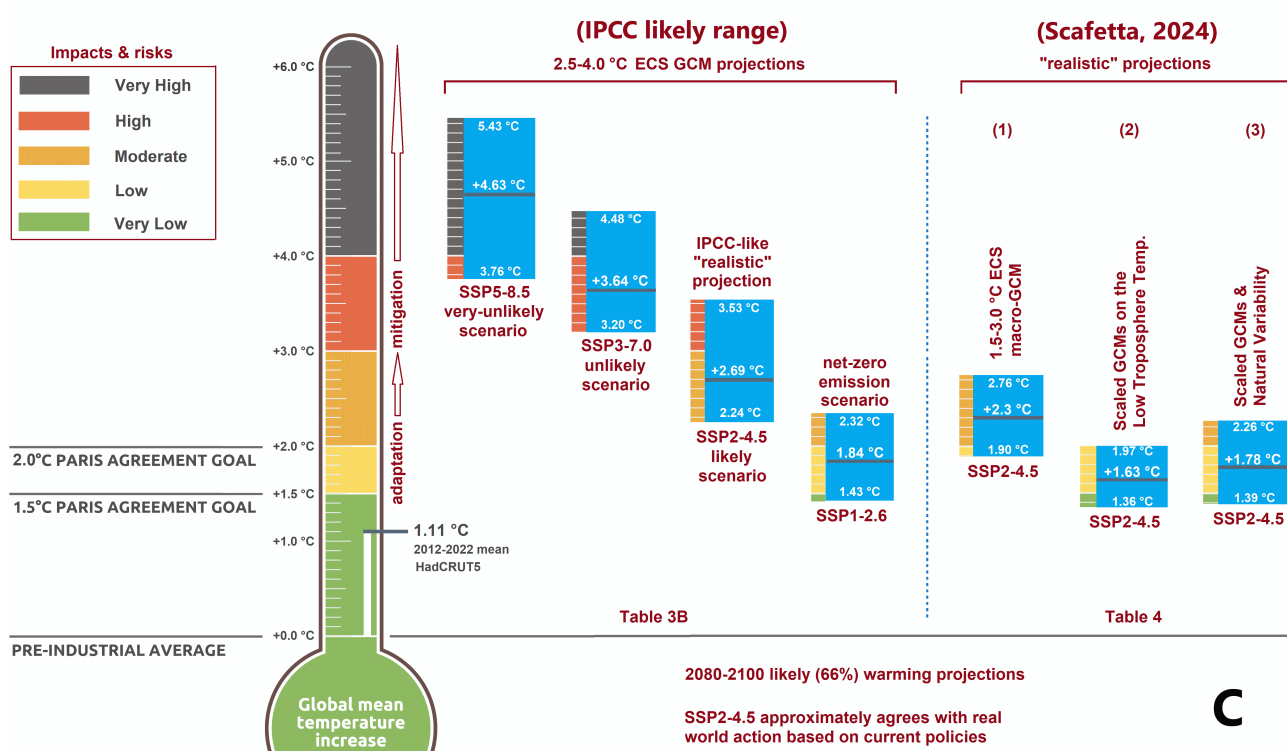
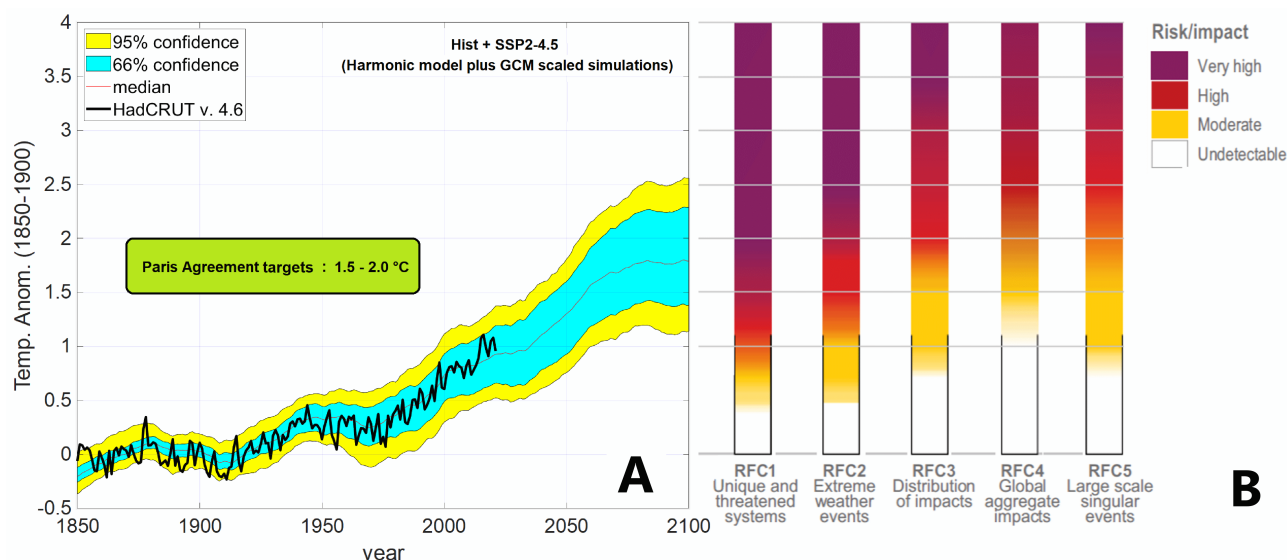


Figure 21: [Top] Comparison of the harmonic empirical global climate model under the SSP2-4.5 scenario with the HadCRUT4.6 record (1850-2021) (Morice et al., 2012) alongside the burning ember diagrams representing the five primary global Reasons for Concern (RFCs) under low-to-no adaptation scenarios, as reported by the IPCC (2023) AR6. [Bottom] Summary and analysis of the projected impacts and risks of global warming for the 2080-2100 period compared to the climate "thermometer" projections from Climate Action Tracker (2024). Adapted from Scafetta (2024).

Figure 21C compares the IPCC predictions with the outputs of alternative empirical climate modeling under three different assumptions based on the considerations discussed in the above sections:

1. using only the CMIP6 GCMs with ECS < 3°C;
2. rescaling the GCMs to fit the satellite low troposphere temperature record;
3. using the empirical model expressed by Eq. 11.

Detailed explanations are found in Scafetta (2024).

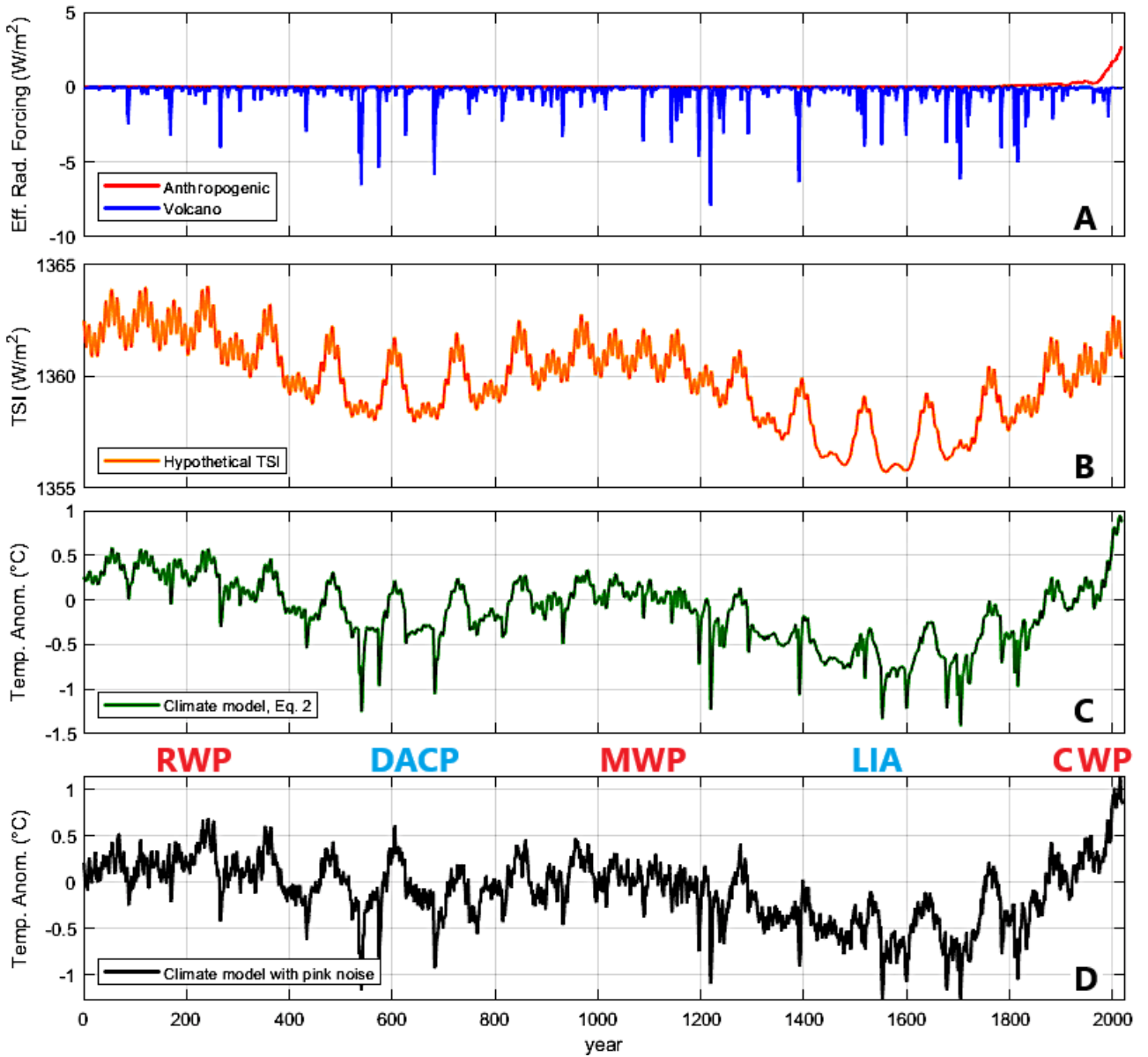


Figure 22: [A] Extended effective anthropogenic and volcanic forcings utilized by CMIP6 GCMs, backdated from 1 to 1750 AD. [B] Synthetic model of total solar irradiance constructed using specific identified climatic harmonics (Scafetta, 2012b, 2020). [C] Climate output generated using the ECM based on Eq. 2, incorporating the parameters obtained by processing the TSI-2 and HadSST4 records from Scafetta (2023a). [D] Same as [C], but with pink noise added to simulate the internal variability of the climate system.

The empirical approaches exhibit more robust alignment with the historical data and project a moderate climate warming throughout the 21st century under realistic development scenarios, such as the SSP2-4.5. These projections suggest that adaptation policies may be sufficient to address future climate challenges without the necessity of adopting economically disruptive Net-Zero mitigation strategies to meet the climate targets of the Paris Agreement (2016).

5.6 A synthetic solar-based empirical climate model from 1 to 2017 AD

Let us finally discuss a synthetic empirical climate model spanning from 1 to 2017 AD that may provide relevant insights into climate patterns over the past two millennia. Figure 22 illustrates an ideal application of the empirical climate model (ECM) formulated in Eq. 2, which integrates the following components:

- *anthropogenic effective radiative forcing* (Figure 22A) — zero anthropogenic forcing is applied from 1 to 1749 AD, while the forcing values adopted by the CMIP6 GCMs are utilized for the period from 1750 to 2017;

- *volcanic effective radiative forcing* (Figure 22A) — the volcanic forcing values used in the CMIP6 GCMs for the period 1750–2017 are extended back from 1 to 1749 AD using the volcanic aerosol optical depth records provided by Toohey and Sigl (2017);
- *solar effective radiative forcing* (Figure 22B) — this forcing is derived from a synthetic total solar irradiance (TSI) model that simulates the major features of the proxy solar records (Figure 18B). The function is calculated by subtracting 1361 W/m^2 and dividing by 8 to align with the TSI effective forcing scale used in the CMIP6 GCMs.

The synthetic TSI model serves as an idealized representation of solar activity variations by reproducing five long harmonics whose frequencies and phases are strictly based on astronomical considerations (Scafetta, 2012b, 2014b, 2020; Scafetta and Bianchini, 2023; Scafetta and Milani, 2025). Additionally, the model incorporates a simulated 11-year solar cycle, with amplitude variations linked to solar activity, that is it diminishes during grand solar minima such as the Maunder Minimum of the 17th century. The periods of the five harmonics are: $P_1 = 60.95$ years, $P_2 = 114.78$ years, $P_3 = 129.95$ years, $P_4 = 983.40$ years, and $P_5 = 2318$ years. The chosen secular harmonics — P_1 , P_2 , and P_3 — account for alternating solar maxima and minima, such as the Maunder and Dalton minima, while the longer millennial oscillations — P_4 and P_5 — correspond to the Eddy and the Bray-Hallstatt cycles observed in both solar and climate records (McCracken et al., 2014; Scafetta et al., 2016). The amplitude of these harmonics approximates the variability found in high-secular-variability TSI models, as those shown in Figure 18 (Bard et al., 2000; Egorova et al., 2018).

The ECM model (Eq. 2) used the following parameters, estimated by Scafetta (2023a) using a solar variability model and the HadSST4 record: $\alpha_A = \alpha_V = 0.083 \text{ }^\circ\text{Cm}^2/\text{yW}$, $\alpha_S = 0.427 \text{ }^\circ\text{Cm}^2/\text{yW}$, and $\beta = 0.303 \text{ 1/y}$. These values imply an ECS equal to $1 \pm 0.3 \text{ }^\circ\text{C}$, and an enhanced sensitivity to TSI forcing by a factor of 5.1 ± 1.5 .

Figures 22C and 22D depict the outputs of Eq. 2, with Figure 22D incorporating pink noise to simulate the internal variability of the climate system. The climate simulation exhibits qualitative similarity to the proxy temperature records depicted in Figures 10 and 12, and with those reported in Esper et al. (2024).

A quasi-millennial cycle is evident, with amplitudes smaller during the first millennium compared to the second. This asymmetry, observed in many paleoclimatic reconstructions, is attributable to the Bray-Hallstatt cycle (~ 2318 years), which is characterized by grand solar minima occurring around ~ 370 and ~ 1530 AD, respectively. The maxima of the quasi-millennial cycle occur around 95, 1175, and 2060 AD, producing warm and cold periods such as the Roman Warm Period (RWP), the Little Ice Age (LIA), and the Current Warm Period (CWP), as shown in the TSI model depicted in Figure 12A and in the climate record plotted in Figure 12B and 12C. The model suggests that approximately 50% of the warming between 1850–1900 and 2011–2020 could be attributed to solar activity, which is consistent with other studies (e.g.: Scafetta and West, 2006b; Scafetta, 2009; Scafetta and West, 2007).

This numerical experiment highlights the importance of utilizing solar records with a substantial multi-secular variability and, in addition, including mechanisms that render the climate hypersensitive to solar activity changes when this is represented by TSI changes alone. The proposed toy-model suggests that TSI alone is unlikely to represent the primary solar forcing agent of the climate system and suggests the involvement of alternative mechanisms, which are still poorly understood, such as a direct solar modulation of the cloud/albedo system. Consequently, the actual ECS values may be relatively low, also ranging approximately from 1.0°C to 1.5°C .

The interpretation of the climate system derived from the above empirical evidences significantly differs from that derived from the CMIP6 GCMs and promoted by the IPCC (2001, 2007, 2013, 2023), and suggest that climate science is still unsettled in many key issues.

6 Conclusion

The findings outlined above underscore significant uncertainties in climate modeling, climate data, solar records, and solar-climate interactions, leaving unresolved the key question of whether observed warming is primarily driven by anthropogenic factors, natural processes, or their interplay. Empirical methodologies, such as those utilized by Scafetta (2023a, 2024) and Connolly et al. (2023), highlight this ongoing ambiguity.

Concerns are mounting regarding the limitations of the CMIP GCMs employed by the IPCC in its assessment reports from 2007, 2013, and 2021. These models appear unable to accurately replicate natural climate variability across different timescales, highlighting critical unresolved issues in fundamental climate dynamics. Also the magnitude of solar variability across temporal scales requires further investigation, particularly given the strong correlations identified between solar proxy records and climate patterns throughout the Holocene. Schmutz (2021) argued that such strong correlations challenge the validity of the low-variability TSI models, such as those proposed by Matthes et al. (2017), Kopp et al., 2016 and Wu et al. (2018). Since these models serve as solar forcing inputs for the CMIP6 GCMs, their choice needs to be reconsidered.

Additionally, the climate system's apparent oversensitivity to solar activity, as observed by various researchers (Soon et al., 2000; Shaviv, 2008; Scafetta, 2009, and many others), complicates the physical issue. Empirical estimates indicate that the climate's sensitivity to solar activity fluctuations may be four to six times greater than its sensitivity to radiative forcings (Scafetta, 2023a), raising important questions about the physical mechanisms underlying the solar-climate interactions. The climate system's oversensitivity to changes in TSI implies that radiative solar forcing alone may not be the primary mechanism driving climate dynamics. Alternative processes, including solar-based corpuscular forcing mechanisms, warrant further exploration. Such mechanisms may significantly influence cloud formation via cosmic ray flux (cf. Svensmark, 2019) or other interplanetary particle interactions with the Earth's atmosphere (Scafetta et al., 2016, 2020).

Cloud-climate interactions introduce additional complexities to attribution analyses, emphasizing the need for precise modeling of cloud processes. Several key observations highlight their critical role:

1. *cloud feedback uncertainty* — variability among climate models in representing cloud feedback significantly contributes to the wide range of ECS estimates derived from the GCMs. The (IPCC, 2021) acknowledges “medium” to “low” confidence in GCM representations of cloud dynamics;
2. *impact of cloudiness on heat transfer* — even minor changes in cloud cover can drastically affect atmospheric heat transfer for a much greater extent than significant shifts in CO₂ concentrations. For example, on heavily overcast days, surface irradiance can drop from 1,000 W/m² to 200 W/m² (van Wijngaarden and Happer, 2025);
3. *trends in global cloud cover* — satellite observations from 1983 to 2010 reveal a decline in global cloud cover from approximately 68% to 65%, corresponding with a ~0.4°C increase in global surface temperatures over the same period (Figure 19A);
4. *regional correlations with cloud dynamics* — Lüdecke et al. (2024) identified strong correlations between central European sunshine durations and the Atlantic Multidecadal Oscillation (AMO) over the period from 1880 to 2020;
5. *flood frequencies and solar proxy records* — Holocene flood frequency records, likely influenced by variations in cloud cover, exhibit significant correlations with solar proxies (Figure 17).

The high equilibrium climate sensitivity (ECS) estimates of the GCMs primarily stem from assumptions about a strong water vapor positive feedback mechanism, initially hypothesized by Manabe and Wetherald (1975). This hypothesis suggests that warming leads to increased evaporation, further amplifying warming. However, uncertainties surrounding water vapor and cloud feedbacks have been acknowledged since the 1960s (Möller, 1963) and are still unresolved (Figure 5). Recent analyses indicate that numerical climate models may overestimate evaporation rates (Ma et al., 2025; Simpson et al., 2024). Additionally, top-of-atmosphere (TOA)

radiative flux measurements suggest that long-wave feedbacks — such as those associated with cirrus cloud formations — may be negative rather than positive (Lindzen and Choi, 2011). Schildknecht (2020) also argues that a proper accounting of cloud-cover dynamics brings ECS estimates closer to or below 1°C.

A number of empirical analyses suggest a moderate climate sensitivity to radiative forcing, with ECS estimates varying depending on the data and assumptions considered. Realistic ECS values could be approximated at least at 2.1 ± 0.7 °C (17–83% range) by combining several lines of climate sensitivity evidence (e.g.: Lewis, 2023; Scafetta, 2022, 2023b). However, significantly lower ECS estimates — even as low as 1.1 ± 0.4 °C (17–83% range) — are also possible if solar variability plays a dominant role through mechanisms alternative to the TSI forcing (cf. Scafetta, 2013a). Such low ECS estimates indicate the existence of balanced positive and negative feedback mechanisms, and have been supported by several researchers (Rasool and Schneider, 1971; Lindzen and Choi, 2011; Harde, 2014; Monckton et al., 2015; Bates, 2016; Knutti et al., 2017; Schildknecht, 2020; Stefani, 2021).

In any case, it is also possible that feedback mechanisms could exhibit scale-dependent behavior. Over short and decadal timescales, they may tend to show slightly negative responses, primarily due to rapid cloud-related adjustments. Over longer timescales, however, feedback responses may become increasingly positive as surface albedo effects linked to glacial melting and vegetation expansion gain influence. Consequently, ECS values around 1.1 ± 0.4 °C or slightly larger may be realistic when climate change is assessed over interannual to millennial timescales.

Biases in global surface temperature records, particularly over land areas, raise concerns about the reported global and regional warming trends. The urban heat island effect, exacerbated by increasing urbanization, likely contributes to these biases (Scafetta, 2021a; Soon et al., 2023). Temperature homogenization algorithms, designed to correct non-climatic warm biases in the meteorological records, appear to blend them into surrounding rural and suburban stations rather than fully removing urban-induced thermal anomalies (D'Aleo, 2016; O'Neill et al., 2022; Katata et al., 2023). Consequently, land surface temperature records — particularly those from the Northern Hemisphere — tend to show exaggerated warming trends compared to alternative datasets (Figure 13), including the satellite-based lower troposphere temperature measurements and sea surface temperature records (Figure 14).

The IPCC (2023), unequivocally attributes the observed global surface warming from 1850–1900 to 2011–2020 almost entirely ($\sim 100\%$) to anthropogenic drivers; such assessment supports the climate alarmist frameworks that dominate European policymaking that yielded to policies such as the EU Green Deal and Net-Zero by 2050. However, the CMIP GCM prediction that without anthropogenic drivers the climate would have remained nearly stable from 1850–1900 to 2011–2020 cannot be validated because of missing data. Moreover, the IPCC assessments are based on surface temperature datasets and theoretical simulations derived from GCMs that appear flawed in many ways and that incorporate equally problematic low-variability TSI forcing functions. These models contradict each other regarding the ECS value (Figure 5) and appear to conflict with a substantial body of empirical evidence spanning the entire Holocene. Notably, they fail to accurately reconstruct the secular-scale warm periods of the past including the MWP, RWP and HTM (Figures 10, 11), which should be a prerequisite for trusting the GCM-based climate attributions for the period from 1850–1900 to 2011–2020 depicted in Figure 2, underestimate the warming from the 1900s to the 1940s (Figure 8) and overestimate the global surface warming of the last 40 years (Figure 6).

In contrast, semi-empirical and empirical modeling approaches, which try to account for natural variability, emphasize a significant role of solar variability in climate change. The IPCC tends to ignore the efforts of empirical modelings of the climate system. Yet, holistic empirical models are necessary to properly guiding the research, in particular when the reductionist ones are demonstrated to poorly reconstruct natural climate variability in key patterns. The discussed empirical models project moderate warming trajectories for the 21st century, diverging from the CMIP6 GCM projections, and would not support the necessity of Net-Zero by 2050 policies to satisfy the climatic targets of the Paris Agreement (2016) because the global surface warming may remain approximately below 2°C throughout the 21st century also under realistic and moderate development scenarios, such as the SSP2-4.5 (Figure 21). More specifically, the proposed empirical evidence could suggest

that the observed global surface warming likely results from multiple contributing factors such as:

- *warm bias* — around 20% of reported global warming may stem from non-climatic warm biases in the global surface temperature records;
- *solar contribution* — natural solar-induced variability, operating through multiple mechanisms, could account for up to 50% of the reported warming;
- *anthropogenic contribution* — human activities are estimated to contribute roughly 30% to the reported warming.

The above empirical assessment is compatible with a low climate sensitivity to anthropogenic emissions, where ECS estimates are as low as 1.1 ± 0.4 °C. If correct, climate risks may be significantly lower than those projected by the CMIP6 GCMs, supporting adaptive strategies and cost-effective mitigation technologies instead of expensive Net-Zero policies (Scafetta, 2024).

Climate science remains far from settled, yet trillions of dollars continue to be allocated toward policies aimed at mitigating extreme hypothetical warming scenarios based on potentially flawed GCM outputs. Historically, atmospheric CO₂ levels have been 10 to 20 times higher than current concentrations during approximately 95% of Earth's history since complex life emerged 600 million years ago (Davis, 2017). Notably, CO₂ concentrations often lag temperature changes across different timescales, suggesting temperature fluctuations may drive CO₂ variations rather than vice versa (Shakun et al., 2012; Koutsoyiannis, 2024).

Since 1900, atmospheric CO₂ concentrations have increased from 295 ppm to 425 ppm, primarily due to human emissions and, to a lesser extent, rising sea surface temperatures. While higher CO₂ levels can negatively impact marine biodiversity by lowering the pH of the sea surface microlayer (Davis, 2023), they also contribute to planetary greening through fertilization effects, enhancing crop yields (Zhu et al., 2016; Piao et al., 2019; McKittrick, 2025).

As CO₂ is a greenhouse gas, climate hazard assessments related to its future emissions depend largely on the Equilibrium Climate Sensitivity (ECS) and Transient Climate Response (TCR) values of the climate system, as well as on the projected emission scenarios. Notably, extreme concentration pathways — such as SSP3-7.0 and SSP5-8.5 — are increasingly regarded as “*unlikely*” and “*very unlikely*”, respectively, and emphasizing climate model simulation based on such scenarios could be misleading (Ritchie and Dowlatabadi, 2017; Hausfather and Peters, 2020; Pielke et al., 2022; Burgess et al., 2023). This fact should be taken into account when developing climate related policies for not harming the economy with unnecessary mitigation policies, which should be based on realistic risks. In this regards, the meta economic analysis by Tol (2023) appears particularly compelling when comparing the costs and benefits of the Paris climate targets.

Advancing climate science requires directly confronting uncertainties in detection, attribution, and modeling. Further research on unresolved issues is critical for improving climate risk assessment and developing more effective strategies for addressing future environmental challenges.

Data Availability (accessed on April 10, 2025)

- Many climatic records can be downloaded from the cited references and from the KNMI Climate Explorer.
Available from: <https://climexp.knmi.nl/>
- CMIP6 GCM simulations. Available from https://climexp.knmi.nl/selectfield_cmip6_knmi23.cgi
- HadSST4. Available from: <https://www.metoffice.gov.uk/hadobs/hadsst4/>
- NOAA/CIRES/DOE 20th Century Reanalysis (V3).
Available from: https://www.psl.noaa.gov/data/gridded/data.20thC_ReanV3.html
- AMO unsmoothed from the Kaplan SST V2.
Available from: <https://psl.noaa.gov/data/correlation/amon.us.long.data>

- UAH MSU lt v 6.1
Available from: https://www.nsstc.uah.edu/data/msu/v6.1/tlt/uahncdc_lt_6.1.txt
- NOAA-STAR v. 5
Available from:
https://www.star.nesdis.noaa.gov/data/mscat/MSU_AMSU_v5.0/Monthly_Atmospheric_Layer_Mean_Temperature/Global_Mean_Anomaly_Time_Series/
- ISCCP Global Cloud Cover
Available from: <https://isccp.giss.nasa.gov/pub/data/D2BASICS/B8glbp.dat>

Declaration

- The author declares that he has no known competing financial interests or personal relationships that could have appeared to influence the work reported in this paper.
- The author is a Guest Editor of this journal and was not involved in the editorial review or the decision to publish this article.

References

- Agnihotri, R., Dutta, K., 2003. Centennial scale variations in monsoonal rainfall (Indian, east equatorial and Chinese monsoons): manifestations of solar variability. *Curr. Sci.*, 85, 459–463.
- Alley, R.B., 2000. The Younger Dryas cold interval as viewed from central Greenland. *Quat. Sci. Rev.*, 19, 213–226.
- Ardalan, A.A., Hashemi-Farahani, H., 2007. A harmonic approach to global ocean tide analysis based on TOPEX/Poseidon satellite. *Mar. Geophys. Res.*, 28, 235–255.
- Atwoli, L., Baqui, A.H., Benfield, T., Bosurgi, R., Godlee, F., et al., 2021. Call for Emergency Action to Limit Global Temperature Increases, Restore Biodiversity, and Protect Health. *N. Engl. J. Med.*, 385, 1134–1137.
- Bard, E., Raisbeck, G.M., Yiou, F., Jouzel, J., 2000. Solar irradiance during the last 1200 years based on cosmogenic nuclides. *Tellus B*, 52, 985–992.
- Bates, J.R., 2016. Estimating climate sensitivity using two-zone energy balance models. *Earth Sp. Sci.*, 3, 207–225.
- Benestad, R.E., Schmidt, G.A., 2009. Solar trends and global warming. *J. Geophys. Res.*, 114, D14101.
- Bereiter, B., Eggleston, S., Schmitt, J., Nehrbass-Ahles, C., Stocker, T.F., et al., 2015. Revision of the EPICA Dome-C CO₂ record from 800 to 600 kyr before present. *Geophys. Res. Lett.*, 42, 542–549.
- Black, D.E., Peterson, L.C., Overpeck, J.T., Kaplan, A., Evans, M.N., Kashgarian, M., 1999. Eight centuries of North Atlantic Ocean atmosphere. *Science*, 286, 1709–1713.
- Bond, G., Kromer, B., Beer, J., Muscheler, R., Evans, M.N., et al., 2001. Persistent solar influence on North Atlantic climate during the Holocene. *Science*, 294 (5549), 2130–2136.
- Bova, S., Rosenthal, Y., Liu, Z., Yan, M., 2021. Seasonal origin of the thermal maxima at the Holocene and the last interglacial. *Nature*, 589, 548–553.
- Bray, J.R., 1968. Glaciation and solar activity since the fifth century BC and the solar cycle. *Nature*, 220, 672–674.

- Brohan, P., Kennedy, J.J., Harris, I., Tett, S.F.B., Jones, P.D., 2006. Uncertainty estimates in regional and global observed temperature changes: A new dataset from 1850. *J. Geophys. Res.*, 111, D12106.
- Büntgen, U., Kirdyanov, A.V., Krusic, P.J., Shishov, V.V., Esper, J., 2021. Arctic aerosols and the 'Divergence Problem' in dendroclimatology. *Dendrochronologia*, 67, 125837.
- Burgess, M.G., Ritchie, J., Shapland, J., Pielke, R., 2023. IPCC baseline scenarios have over-projected CO₂ emissions and economic growth. *Environ. Res. Lett.*, 16(1), 014016.
- Cai, M., Lu, J., 2023. Research progress on the divergence problem of tree ring growth-climate relationship. *J. Sichuan For. Sci. Technol.*, 44(6), 7–13.
- Camuffo, D., Bertolin, C., Barriendos, M., Dominguez-Castro, F., Cocheo, C., et al., 2010. 500-year temperature reconstruction in the Mediterranean Basin by means of documentary data and instrumental observations. *Clim. Change*, 101, 169–199.
- Cardoso, R.D.S., Dorigon, L.P., Teixeira, D.C.F., Amorim, M.C.d.C.T., 2017. Assessment of Urban Heat Islands in Small- and Mid-Sized Cities in Brazil. *Climate*, 5(1), 14.
- Cartapanis, O., Jonkers, L., Moffa-Sanchez, P., Jaccard, S.L., de Vernal, A., 2022. Complex spatio-temporal structure of the Holocene Thermal Maximum. *Nat. Commun.*, 13, 5662.
- Chambers, D.P., Merrifield, M.A., Nerem, R.S., 2012. Is there a 60-year oscillation in global mean sea level? *Geophys. Res. Lett.*, 39, L18607.
- Charney, J.G., Arakawa, A., Baker, D.J., Bolin, B., Dickinson, R.E., et al., 1979. Carbon dioxide and climate: A scientific assessment. *Natl. Acad. Sci. Wash. DC*. Available at: <https://doi.org/10.17226/12181>, accessed on April 10, 2025.
- Christiansen, B., Ljungqvist, F.C., 2012. The extra-tropical Northern Hemisphere temperature in the last two millennia: Reconstructions of low-frequency variability. *Clim. Past*, 8, 765–786.
- Christy, J.R., Spencer, R.W., Braswell, W.D., Junod, R., 2018. Examination of space-based bulk atmospheric temperatures used in climate research. *Int. J. Remote Sens.*, 39, 3580–3607.
- Chylek, P., Klett, J.D., Lesins, G., Dubey, M.K., Hengartner, N., 2014. The Atlantic Multidecadal Oscillation as a dominant factor of oceanic influence on climate. *Geophys. Res. Lett.*, 41, 1689–1697.
- Climate Action Tracker: 2024. The CAT Thermometer, CAT Emissions Gap. Available at: <https://climateactiontracker.org>, accessed on April 10, 2025.
- Coddington, O., Lean, J.L., Pilewskie, P., Snow, M., Lindholm, D., 2016. A Solar Irradiance Climate Data Record. *Bull. Am. Meteorol. Soc.*, 97, 1265.
- Connolly, R., Connolly, M., Soon, W., Legates, D.R., Cionco, R.G., Velasco Herrera, V.M., 2019. Northern hemisphere snow-cover trends (1967-2018): A comparison between climate models and observations. *Geosci.*, 9(3), 135.
- Connolly, R., Connolly, M., Carter, R.M., Soon, W., 2020. How much human-caused global warming should we expect with business-as-usual (BAU) climate policies? *Energies*, 13(6), 1365.
- Connolly, R., Soon, W., Connolly, M., Baliunas, S., Berglund, J., et al., 2023. Challenges in the detection and attribution of Northern Hemisphere surface temperature trends since 1850. *Res. Astron. Astrophys.*, 23, 105015.
- Connolly, R., Soon, W., Connolly, M., Cionco, R.G., Elias, A.G., et al., 2024. Multiple new or updated satellite total solar irradiance (TSI) composites (1978–2023). *Astrophys. J.*, 975, 102.

- Cook, J., Nuccitelli, D., Green, S.A., Richardson, M., Winkler, B., et al., 2013. Quantifying the consensus on anthropogenic global warming in the scientific literature. *Environ. Res. Lett.*, 8, 024024.
- Creel, R.C., Austermann, J., Kopp, R.E., Khan, N.S., Albrecht, T., Kingslake, J., 2024. Global mean sea level likely higher than present during the Holocene. *Nat. Commun.*, 15, 10731.
- Crowley, T.J., 2000. Causes of climate change over the past 1000 years. *Science*, 289, 270–277.
- Cruz-Silva, E., Harrison, S.P., Prentice, I.C., Marinova, E., Bartlein, P.J., et al., 2023. Pollen-based reconstructions of Holocene climate trends in the eastern Mediterranean region. *Clim. Past*, 19, 2093–2108.
- Curry, J., 2023. *Climate Uncertainty and Risk: Rethinking Our Response*. Anthem Press.
- Czymzik, M., Muscheler, R., Brauer, A., 2016. Solar modulation of flood frequency in central Europe during spring and summer on interannual to multi-centennial timescales. *Clim. Past*, 12, 799–805.
- D'Aleo, J.S., 2016. A critical look at surface temperature records. In *Evid.-Based Clim. Sci.*, 2nd ed.; Easterbrook, D.J., Ed.; Elsevier: Amsterdam, The Netherlands; pp. 11–48.
- Davis, J.C., Bohling, G., 2001. The search for patterns in ice-core temperature curves. In *Geol. Perspect. Glob. Clim. Change*; Gerhard, L.C., Harrison, W.E., Hanson, B.M. (Eds.), pp. 213–229.
- Davis, W.J., 2017. The relationship between atmospheric carbon dioxide concentration and global temperature for the last 425 million years. *Climate*, 5(4), 76.
- Davis, W.J., 2023. Mass extinctions and their relationship with atmospheric carbon dioxide concentration: Implications for Earth's future. *Earth's Future*, 11, e2022EF003336.
- deMenocal, P.B., Tierney, J.E., 2012. Green Sahara: African humid periods paced by Earth's orbital changes. *Nat. Educ. Knowl.*, 3(10), 12.
- Deming, D., 2006. US Senate Hearing on Climate Change and the Media (December 6, 2006 09:30 AM). Available at: https://www.epw.senate.gov/public/index.cfm/hearings?Id=BFE4D91D-802A-23AD-4306-B4121BF7ECED&Statement_id=361256C4-11DC-4E5D-8D1D-9FEDF082D081, accessed on April 10, 2025.
- Denton, G.H., Karlén, W., 1973. Holocene climatic variations – their pattern and possible cause. *Quat. Res.*, 3, 155–205.
- de Wit, T.D., Kopp, G., Fröhlich, C., Schöll, M., 2017. Methodology to create a new total solar irradiance record: Making a composite out of multiple data records. *Geophys. Res. Lett.*, 44(3), 1196–1203.
- Diamond, J., 2005. *Collapse: How Societies Choose To Fail Or Succeed*. Penguin. ISBN 978-0241958681.
- Dong, Y., Wu, N., Li, F., Zhang, D., Zhang, Y., et al., 2022. The Holocene temperature conundrum answered by mollusk records from East Asia. *Nat. Commun.*, 13, 5153.
- Easterbrook, D.J., 2019. *Solar Magnetic Cause of Climate Changes and Origin of the Ice Ages*. Independently Published, ISBN: 9781691061631.
- Eddy, J.A., 1976. The Maunder Minimum. *Science*, 192, 1189–1202.
- Eddy, J.A., 1977. Climate and the changing Sun. *Clim. Change*, 1, 173–190.
- Egorova, T., Schmutz, W., Rozanov, E., Shapiro, A.I., Usoskin, I., et al., 2018. Revised historical solar irradiance forcing. *Astron. Astrophys.*, 615, A85.
- Esper, J., St. George, S., Anchukaitis, K., D'Arrigo, R., Ljungqvist, F.C., et al., 2018. Large-scale, millennial-length temperature reconstructions from tree-rings. *Dendrochronologia*, 50, 81–90.

- Esper, J., Smerdon, J.E., Anchukaitis, K.J., Cook, E.R., D'Arrigo, R., et al., 2024. The IPCC's reductive Common Era temperature history. *Commun. Earth Environ.*, 5, 222.
- Etminan, M., Myhre, G., Highwood, E.J., Shine, K.P., 2016. Radiative forcing of carbon dioxide, methane, and nitrous oxide: A significant revision of the methane radiative forcing. *Geophys. Res. Lett.*, 43, 12,614–12,623.
- European Union, 2024. European Green Deal. Available at: https://commission.europa.eu/strategy-and-policy/priorities-2019-2024/european-green-deal_en, accessed on April 10, 2025.
- European Commission, 2024. GHG emissions of all world countries. Available at: https://edgar.jrc.ec.europa.eu/report_2024, accessed on April 10, 2025.
- Eyring, V., Bony, S., Meehl, G.A., Senior, C.A., Stevens, B., et al., 2016. Overview of the coupled model intercomparison project phase 6 (CMIP6) experimental design and organization. *Geosci. Model Dev.*, 9(5), 1937–1958.
- Fagan, B., 2008. *The Great Warming: Climate Change and the Rise and Fall of Civilizations*. Bloomsbury Press. ISBN 978-1596913929.
- Filippelli, G., Beal, L., Rajaram, H., AghaKouchak, A., Balikhin, M.A., et al., 2021. Geoscientists, who have documented the rapid and accelerating climate crisis for decades, are now pleading for immediate collective action. *Geophys. Res. Lett.*, 48, e2021GL096644.
- Forster, P., Gregory, J.M., 2006. The climate sensitivity and its components diagnosed from Earth Radiation Budget data. *J. Clim.*, 19, 39–52.
- Fröhlich, C., 2012. Total solar irradiance observations. *Surv. Geophys.*, 33(3–4), 453–473.
- Fyfe, J., Gillett, N., Zwiers, F., 2013. Overestimated global warming over the past 20 years. *Nature Clim. Change* 3, 767–769.
- Ge, Q.S., Liu, H.L., Ma, X., Zheng, J.Y., Hao, Z.X., 2017. Characteristics of temperature change in China over the last 2000 years and spatial patterns of dryness/wetness during cold and warm periods. *Adv. Atmos. Sci.*, 34, 941–951.
- Gervais, F., 2016. Anthropogenic CO₂ warming challenged by 60-year cycle. *Earth-Sci. Rev.*, 155, 129–135.
- Global Coal Plant Tracker: 2024. Available at: <https://globalenergymonitor.org/projects/global-coal-plant-tracker/tracker/>, accessed on April 10, 2025.
- Golaz, J.-C., Caldwell, P.M., Van Roekel, L.P., Petersen, M.R., Tang, Q., et al., 2019. The DOE E3SM coupled model version 1: Overview and evaluation at standard resolution. *J. Adv. Model. Earth Syst.*, 11, 2089–2129.
- Gore, A., 2006. *The Inconvenient Truth* (film documentary). Paramount Classics. Available at: <https://participant.com/campaign/inconvenient-truth/>, accessed on April 10, 2025.
- Groves, D.I., Santosh, M., Yang, C.-X., 2023. Net zero climate remediations and potential terminal depletion of global critical metal resources: A synoptic geological perspective. *Geosyst. Geoenviron.*, 2(1), 100136.
- Hansen, J., Sato, M., Ruedy, R., Kharecha, P., Lacis, A., et al., 2007. Climate simulations for 1880–2003 with GISS modelE. *Clim. Dyn.*, 29, 661–696.
- Harde, H., 2014. Advanced two-layer climate model for the assessment of global warming by CO₂. *Open J. Atmos. Clim. Change*, 1(3), 1–51.
- Harris, I., Osborn, T.J., Jones, P., Lister, D., 2020. Version 4 of the CRU TS monthly high-resolution gridded multivariate climate dataset. *Sci. Data*, 7, 109.

- Hausfather, Z., Peters, G.P., 2020. Emissions — the ‘business as usual’ story is misleading. *Nature*, 577(7792), 618–620.
- Hausfather, Z., Marvel, K., Schmidt, G.A., Nielsen-Gammon, J.W., Zelinka, M., 2022. Climate simulations: recognize the ‘hot model’ problem. *Nature*, 605(7908), 26–29.
- Helbling, M., Meierrieks, D., 2023. Global warming and urbanization. *J. Popul. Econ.*, 36, 1187–1223.
- Hellmuth, F., Carlsen, T., Daloz, A.S., David, R.O., Che, H., Storelvmo, T., 2025. Evaluation of biases in mid-to-high-latitude surface snowfall and cloud phase in ERA5 and CMIP6 using satellite observations. *Atmos. Chem. Phys.*, 25, 1353–1383.
- Hoyt, D.V., Schatten, K.H., 1993. A discussion of plausible solar irradiance variations, 1700–1992. *J. Geophys. Res. Space Phys.*, 98(A11), 18895–18906.
- Hoyt, D.V., Schatten, K.H., 1997. *The Rule of the Sun in Climate Change*. Oxford University Press. ISBN: 9780195094145.
- Hudson, R., 2023. The problem of tropospheric temperature trend measurements for global climate models: Complex versus direct empiricism. *New Techno Humanit.*, 3(2), 117–123.
- IEA, 2024. *World Energy Outlook 2024*. International Energy Agency (IEA), Paris, France. Available at: <https://www.iea.org/reports/world-energy-outlook-2024> (accessed January 23, 2025).
- IPCC, 1990. *Clim. Change: IPCC Sci. Assess. Contribution of Working Group I*. [J.T. Houghton, G.J. Jenkins, J.J. Ephraums (eds.)]. Cambridge Univ. Press.
- IPCC, 1995. *Second Assess. Clim. Change. Contribution of Working Group I*. [J.T. Houghton, L.G. Meira Filho, B.A. Callander, N. Harris, A. Kattenberg, K. Maskell (eds.)]. Cambridge Univ. Press.
- IPCC, 2001. *Clim. Change 2001: Sci. Basis. Contribution of Working Group I to the Third Assessment Report*. [J.T. Houghton, Y. Ding, D.J. Griggs, M. Noguer, et al. (eds.)]. Cambridge Univ. Press.
- IPCC, 2007. *Clim. Change 2007: Phys. Sci. Basis. Contribution of Working Group I to the Fourth Assessment Report*. [S. Solomon, D. Qin, M. Manning, Z. Chen, et al. (eds.)]. Cambridge Univ. Press.
- IPCC, 2013. *Clim. Change 2013: Phys. Sci. Basis. Contribution of Working Group I to the Fifth Assessment Report*. [T.F. Stocker, D. Qin, G.-K. Plattner, M. Tignor, et al. (eds.)]. Cambridge Univ. Press.
- IPCC, 2021. *Clim. Change 2021: Phys. Sci. Basis. Contribution of Working Group I to the Sixth Assessment Report*. [V. Masson-Delmotte, P. Zhai, A. Pirani, S.L. Connors, et al. (eds.)]. Cambridge Univ. Press.
- IPCC, 2023. *Clim. Change 2023: Synth. Report. Contribution of Working Groups I, II & III*. [Core Writing Team, H. Lee, J. Romero (eds.)]. IPCC, Geneva, Switzerland.
- Jenkins, S., Smith, C., Allen, M., Grainger, R., 2023. Tonga eruption increases chance of temporary surface temperature anomaly above 1.5 °C. *Nat. Clim. Change.*, 13(2), 127–129.
- Jevrejeva, S., Moore, J.C., Grinsted, A., Woodworth, P.L., 2008. Recent global sea level acceleration started over 200 years ago? *Geophys. Res. Lett.*, 35, L08715.
- Jones, T.R., Cuffey, K.M., Roberts, W.H.G., Markle, B.R., Steig, E.J., et al., 2023. Seasonal temperatures in West Antarctica during the Holocene. *Nature*, 613, 292–297.
- Judge, P.G., Egeland, R., Henry, G.W., 2020. Sun-like stars shed light on solar climate forcing. *Astrophys. J.*, 891(1), 96.

- Katata, G., Connolly, R., O'Neill, P., 2023. Evidence of urban blending in homogenized temperature records in Japan and the United States: implications for the reliability of global land surface air temperature data. *J. Appl. Meteorol. Climatol.*, 62(8), 1095–1114.
- Kaufman, D., McKay, N., Routson, C., Erb, M., Dätwyler, C., et al., 2020. Holocene global mean surface temperature: a multi-method reconstruction. *Sci. Data*, 7, 201.
- Kaufman, D.S., Broadman, E., 2023. Revisiting the Holocene global temperature conundrum. *Nature*, 614, 425–435.
- Kennedy, J.J., Rayner, N.A., Atkinson, C.P., Killick, R.E., 2019. An ensemble dataset of sea-surface temperature change from 1850: the Met Office Hadley Centre HadSST.4.0.0.0 data set. *J. Geophys. Res. Atmos.*, 124, 7719–7763.
- Kerr, R.A., 2001. A variable sun paces millennial climate. *Science*, 294(5546), 1431–1433.
- Kim, D., Christy, J.R., 2022. Detecting impacts of surface development near weather stations since 1895 in the San Joaquin Valley of California. *Theor. Appl. Climatol.*, 149, 1223–1238.
- Kirkby, J., 2007. Cosmic rays and climate. *Surv. Geophys.*, 28(5–6), 333–375.
- Kirkby, J., Curtius, J., Almeida, J., Dunne, E., Duplissy, J., et al., 2011. Role of sulphuric acid, ammonia and galactic cosmic rays in atmospheric aerosol nucleation. *Nature*, 476, 429–433.
- Klimenko, V.V., Matskovsky, V.V., Dahlmann, D., 2014. Multi-archive temperature reconstruction of the Russian Arctic for the past two millennia. *Geogr. Environ. Sustain.*, 4(12), 84–95.
- Klyashtorin, L.B., Borisov, V., Lyubushin, A., 2008. Cyclic changes of climate and major commercial stocks of the Barents Sea. *Mar. Biol. Res.*, 5(1), 4–17.
- Knight, J., Kennedy, J.J., Folland, C., Harris, G., Jones, G.S., et al., 2009. Do global temperature trends over the last decade falsify climate predictions? *Bull. Am. Meteorol. Soc.*, 90(8), S22–S23.
- Knudsen, M., Seidenkrantz, M.S., Jacobsen, B., Kuijpers, A., 2011. Tracking the Atlantic Multidecadal Oscillation over 8,000 years. *Nat. Commun.*, 2, 178.
- Knutti, R., Rugenstein, M.A., Hegerl, G.C., 2017. Beyond equilibrium climate sensitivity. *Nat. Geosci.*, 10, 727–736.
- Kopp, G., Krivova, N., Wu, C.J., Lean, J., 2016. The Impact of the Revised Sunspot Record on Solar Irradiance Reconstructions. *Sol. Phys.* 291, 2951–2965.
- Koutsoyiannis, D., 2024. Stochastic assessment of temperature–CO₂ causal relationship in climate from the Phanerozoic through modern times. *Math. Biosci. Eng.*, 21(7), 6560–6602.
- Kutschera, W., Patzelt, G., Schaefer, J.M., Schlüchter, C., Steier, P., Wild, E.M., 2020. The movements of Alpine glaciers throughout the last 10,000 years as sensitive proxies of temperature and climate changes. *EPJ Web Conf.*, 232, 02002.
- Lamb, H.H., 1965. The early medieval warm epoch and its sequel. *Palaeogeogr. Palaeoclimatol. Palaeoecol.*, 1, 13–37.
- Lamb, H.H., 1972. *Climate: Present, Past, and Future*. Vol. 1. Methuen.
- Lawrimore, J.H., Menne, M.J., Gleason, B.E., Williams, C.N., Wuertz, D.B., et al., 2011. An overview of the Global Historical Climatology Network monthly mean temperature data set, version 3. *J. Geophys. Res.*, 116, D19121.

- Lean, J., Beer, J., Bradley, R., 1995. Reconstruction of solar irradiance since 1610: implications for climate change. *Geophys. Res. Lett.*, 22, 3195–3198.
- Lean, J., 2000. Evolution of the sun's spectral irradiance since the Maunder Minimum. *Geophys. Res. Lett.*, 27, 2425–2428.
- Lean, J., Wang, Y.M., Sheeley, N.R., 2005. SORCE contributions to new understanding of global change and solar variability. *Sol. Phys.*, 230, 27–53.
- Legates, D.R., Soon, W., Briggs, W.M., Monckton, C., 2015. Climate Consensus and 'Misinformation': A Rejoinder to Agnotology, Scientific Consensus, and the Teaching and Learning of Climate Change. *Sci. Educ.*, 24, 299–318.
- Lasher, G.E., Axford, Y., 2019. Medieval warmth confirmed at the Norse Eastern Settlement in Greenland. *Geology*, 47(3), 267–270.
- Laskar, J., Fienga, A., Gastineau, M., Manche, H., 2011. La2010: a new orbital solution for the long-term motion of the Earth. *Astron. Astrophys.*, 532, A89.
- Le Roy Ladurie, E., 1967. *Histoire du Climat depuis l'an mil*. Flammarion, Paris (translated by B. Bray, Doubleday & Co., 1971).
- Lewis, N., 2023. Objectively combining climate sensitivity evidence. *Clim. Dyn.*, 60, 3139–3165.
- Li, Y., Wu, D., Wang, T., Chen, L., Zhang, C., Guo, S., 2023. Late Holocene temperature and precipitation variations in an alpine region of the northeastern Tibetan Plateau and their response to global climate change. *Palaeogeogr. Palaeoclimatol. Palaeoecol.*, 615, 111442.
- Li, Z., Liu, T., Huang, Y., Peng, J., Ling, Y., 2022. Evaluation of the CMIP6 precipitation simulations over global land. *Earth's Future*, 10, e2021EF002500.
- Lin, Y.C., Fan, C.Y., Damon, P.E., Wallick, E.J., 1975. Long-Term Modulation of Cosmic-Ray Intensity and Solar Activity Cycle. At the 14th Int. Cosmic Ray Conf., 3, 995–999.
- Lindzen, R.S., Chou, M.-D., Hou, A.Y., 2001. Does the Earth have an adaptive infrared iris?. *Bull. Am. Meteorol. Soc.* 82, 417–432.
- Lindzen, R.S., Choi, Y.-S., 2011. On the observational determination of climate sensitivity and its implications. *Asia-Pac. J. Atmos. Sci.*, 47, 377–390.
- Liu, Z., Zhu, J., Rosenthal, Y., Timm, O.E., 2014. The Holocene temperature conundrum. *Proc. Natl. Acad. Sci. USA*, 111(34), E3501–E3505.
- Ljungqvist, F.C., 2010. A new reconstruction of temperature variability in the extra-tropical northern hemisphere during the last two millennia. *Geogr. Ann. Ser. A Phys. Geogr.*, 92, 339–351.
- Lockwood, M., Stamper, R., Wild, M., 1999. A doubling of the Sun's coronal magnetic field during the past 100 years. *Nature*, 399, 437–439.
- Lüdecke, H.J., Müller-Plath, G., Lüning, S., 2024. Central-European sunshine hours, relationship with the Atlantic Multidecadal Oscillation, and forecast. *Sci. Rep.*, 14, 25152.
- Lüning, S., 2022. Climate reconstructions of the 'Medieval Warm Period' 1000–1200 AD. Online map available at: <http://t1p.de/mwp>
- Luterbacher, J., Xoplaki, E., Dietrich, D., Jones, P.D., Davies, T.D., et al., 2002. Extending North Atlantic Oscillation reconstructions back to 1500. *Atmos. Sci. Lett.*, 2(1–4), 114–124.

- Luterbacher, J., Werner, J.P., Smerdon, J.E., Fernández-Donado, L., González-Rouco, F.J., et al., 2016. European summer temperatures since Roman times. *Environ. Res. Lett.*, 11, 024001.
- Lutsko, N.J., Luongo, M.T., Wall, C.J., Myers, T.A., 2022. Correlation between cloud adjustments and cloud feedbacks responsible for larger range of climate sensitivities in CMIP6. *J. Geophys. Res. Atmos.*, 127, e2022JD037486.
- Lynas, M., Houlton, B.Z., Perry, S., 2021. Greater than 99% consensus on human-caused climate change in the peer-reviewed scientific literature. *Environ. Res. Lett.*, 16, 114005.
- Ma, N., Zhang, Y., Yang, Y., 2025. Recent decline in global ocean evaporation due to wind stilling. *Geophys. Res. Lett.*, 52, e2024GL114256.
- Ma, P.-L., Harrop, B.E., Larson, V.E., Neale, R.B., Gettelman, A., et al., 2022. Better calibration of cloud parameterizations and subgrid effects increases the fidelity of the E3SM Atmosphere Model version 1. *Geosci. Model Dev.*, 15, 2881–2916.
- Maibach, E., Perkins, D., Francis, Z., Myers, T., Engblom, A., et al., 2016. A 2016 National Survey of American Meteorological Society Member Views on Climate Change: Initial Findings. George Mason Univ., Center for Clim. Change Commun.
- Manabe, S., Wetherald, R.T., 1975. The effects of doubling the CO₂ concentration on the climate of a general circulation model. *J. Atmos. Sci.*, 32, 3–15.
- Mann, M.E., Bradley, R.S., Hughes, M.K., 1999. Northern hemisphere temperatures during the past millennium: inferences, uncertainties, and limitations. *Geophys. Res. Lett.*, 26, 759–762.
- Mann, M., Zhang, Z., Hughes, M., Bradley, R., Miller, S., et al., 2008. Proxy-based reconstructions of hemispheric and global surface temperature variations over the past two millennia. *Proc. Natl. Acad. Sci. USA*, 105(36), 13252–13257.
- Mann, M.E., Zhang, Z., Rutherford, S., Bradley, R.S., Malcolm K., et al., 2009. Global signatures and dynamical origins of the Little Ice Age and Medieval Climate Anomaly. *Science*, 326(5957), 1256–1260.
- Matsumoto, H., Svensmark, H., Enghoff, M.B., 2022. Effects of Forbush decreases on clouds determined from PATMOS-x. *J. Atmos. Sol.-Terr. Phys.*, 230, 105845.
- Matthes, K., Funke, B., Andersson, M.E., Barnard, L., Beer, J., et al., 2017. Solar forcing for CMIP6 (v3.2). *Geosci. Model Dev.*, 10, 2247–2302.
- Mauritsen, T., Bader, J., Becker, T., Behrens, J., Bittner, M., et al., 2019. Developments in the MPI-M Earth System Model version 1.2 (MPI-ESM1.2) and its response to increasing CO₂. *J. Adv. Model. Earth Syst.*, 11, 998–1038.
- Mazzarella, A., Scafetta, N., 2012. Evidences for a quasi 60-year North Atlantic Oscillation since 1700 and its meaning for global climate change. *Theor. Appl. Climatol.*, 107, 599–609.
- McCracken, K.G., Beer, J., Steinhilber, F., 2014. Evidence for planetary forcing of the cosmic ray intensity and solar activity throughout the past 9400 years. *Sol. Phys.*, 289, 3207–3229.
- McIntyre, S., McKittrick, R., 2003. Corrections to the Mann et al. (1998) proxy database and Northern Hemispheric average temperature series. *Energy Environ.*, 14(6), 751–771.
- McKittrick, R.R., Michaels, P.J., 2007. Quantifying the influence of anthropogenic surface processes and inhomogeneities on gridded global climate data. *J. Geophys. Res.*, 112, D24S09.
- McKittrick, R., Christy, J., 2018. A test of the tropical 200- to 300-hPa warming rate in climate models. *Earth Space Sci.*, 5, 529–536.

- McKittrick, R., Christy, J., 2020. Pervasive warming bias in CMIP6 tropospheric layers. *Earth Space Sci.*, 7, e2020EA001281.
- McKittrick, R., 2025. Extended crop yield meta-analysis data do not support upward SCC revision. *Sci. Rep.*, 15, 5575.
- McNutt, M., 2015. The beyond-two-degree inferno. *Science*, 349, 7.
- McSweeney, R., Hausfather, Z., 2018. Q&A: How do climate models work? Available at: <https://www.carbonbrief.org/qa-how-do-climate-models-work/#tune>
- Mears, C.A., Wentz, F.J., 2016. Sensitivity of satellite-derived tropospheric temperature trends to the diurnal cycle adjustment. *J. Clim.*, 29(10), 3629–3646.
- Melo, M., Lapin, M., Pecho, J., 2022. Climate in the Past and Present in the Slovak Landscapes—The Central European Context. In: Lehotský, M., Boltižiar, M. (eds.) *Landscapes Landforms Slovakia*, Springer, Cham. https://doi.org/10.1007/978-3-030-89293-7_3
- Menne, M.J., Williams, C.N., Gleason, B.E., Rennie, J.J., Lawrimore, J.H., 2018. The Global Historical Climatology Network monthly temperature dataset, version 4. *J. Clim.*, 31(24), 9835–9854.
- Mitchell, D.M., Lo, Y.T.E., Seviour, W.J.M., Haimberger, L., Polvani, L.M., 2020. The vertical profile of recent tropical temperature trends: Persistent model biases in the context of internal variability. *Environ. Res. Lett.*, 15(10), 1040b4.
- Miyahara, H., Kusano, K., Kataoka, R., Shima, S.-i., Touber, E., 2023. Response of high-altitude clouds to galactic cosmic ray cycles in tropical regions. *Front. Earth Sci.*, 11, 1157753.
- Moberg, A., Sonechkin, D.M., Holmgren, K., Datsenko, N.M., Karlén, W., 2005. Highly variable Northern Hemisphere temperatures reconstructed from proxy data. *Nature*, 433, 613–617.
- Mohajerani, A., Bakaric, J., Jeffrey-Bailey, T., 2017. The urban heat island effect, its causes, and mitigation, with reference to the thermal properties of asphalt concrete. *J. Environ. Manage.*, 197, 522–538.
- Möller, F., 1963. Influence of changes in CO₂ concentration on the radiation balance of Earth's surface and on the climate. *J. Geophys. Res.*, 68, 3877–3886.
- Monckton, C., Soon, W.-H., Legates, D.R., Briggs, W.M., 2015. Why models run hot: results from an irreducibly simple climate model. *Sci. Bull.*, 60(1), 122–135.
- Montford, A., 2013. Consensus? What consensus? GWPF Note 5. Available at <https://www.thegwpf.org/content/uploads/2013/09/Montford-Consensus.pdf>, accessed on April 10, 2025.
- Morice, C.P., Kennedy, J.J., Rayner, N.A., Jones, P.D., 2012. Quantifying uncertainties in global and regional temperature change using an ensemble of observational estimates: the HadCRUT4 dataset. *J. Geophys. Res.*, 117, D08101.
- Morice, C.P., Kennedy, J.J., Rayner, N.A., Winn, J.P., Hogan, E., et al., 2021. An updated assessment of near-surface temperature change from 1850: the HadCRUT5 data set. *J. Geophys. Res. Atmos.*, 126, e2019JD032361.
- Murata, A., Mori, T., Kato, H., Hu, H.-M., Shen, C.-C., et al., 2025. Holocene Temperature Trend Inferred From Oxygen and Carbonate Clumped Isotope Profiles of a Stalagmite Collected From a Maritime Area of Central Honshu, Japan. *Island Arc*, 34, e70002.

- Myhre, G., 1998. New estimates of radiative forcing due to well-mixed greenhouse gases. *Geophys. Res. Lett.*, 25(14), 2715–2718.
- Neff, U., Burns, S.J., Mangini, A., Mudelsee, M., Fleitmann, D., Matter, A., 2001. Strong coherence between solar variability and the monsoon in Oman between 9 and 6 kyr ago. *Nature*, 411, 290–293.
- ÓhAiseadha, C., Quinn, G., Connolly, R., Connolly, M., Soon, W., 2020. Energy and climate policy — an evaluation of global climate change expenditure 2011–2018. *Energies*, 13(18), 4839.
- O'Neill, P., Connolly, R., Connolly, M., Soon, W., Chimani, B., Crok, M., et al., 2022. Evaluation of the homogenization adjustments applied to European temperature records in the Global Historical Climatology Network dataset. *Atmosphere*, 13(2), 285.
- Osborn, T.J., Jones, P.D., Lister, D.H., Morice, C.P., Simpson, I.R., et al., 2021. Land surface air temperature variations across the globe updated to 2019: the CRUTEM5 dataset. *J. Geophys. Res. Atmos.*, 126, e2019JD032352.
- PAGES-2K Consortium, 2019. Consistent multi-decadal variability in global temperature reconstructions and simulations over the Common Era. *Nat. Geosci.*, 12(8), 643–649.
- Paris Agreement, 2016. The Paris Agreement is a legally binding international treaty on climate change. It was adopted by 196 Parties at the UN Climate Change Conference (COP21) in Paris, France, on 12 December 2015. It entered into force on 4 November 2016. Available at: <https://unfccc.int/process-and-meetings/the-paris-agreement>, accessed on April 10, 2025.
- Patterson, R.T., Prokoph, A., Chang A., 2004. Late Holocene sedimentary response to solar and cosmic ray activity influenced climate variability in the NE Pacific. *Sediment. Geol.*, 172, 67–84.
- Penza, V., Berrilli, F., Bertello, L., Cantoresi, M., Criscuoli, S., Giobbi, P., 2022. Total solar irradiance during the last five centuries. *Astrophys. J.*, 937(2), 84.
- Piao, S., Wang, X., Park, T., Chen, C., Lian, X., et al., 2019. Characteristics, drivers and feedbacks of global greening. *Nat. Rev. Earth Environ.*, 1(1), 14–27.
- Pielke, R., Burgess, M.G., Ritchie, J., 2022. Plausible 2005–2050 emissions scenarios project between 2°C and 3°C of warming by 2100. *Environ. Res. Lett.*, 17, 024027.
- Pinho, O., Orgaz, M., 2000. The urban heat island in a small city in coastal Portugal. *Int. J. Biometeorol.*, 44, 198–203.
- Plavcová, E., Lhotka, O., Beranová, R., Dubrovský, M., Skalák, P., 2025. Precipitation variability in CMIP6 climate models across the North Atlantic–European region and their links to atmospheric circulation. *Clim. Dyn.*, 63, 98.
- Rahmstorf, S., 2008. Anthropogenic climate change: revisiting the facts. In: Zedillo, E. (Ed.), *Global Warming: Looking Beyond Kyoto*. Brookings Institution Press, Washington, Ch.3, pp. 34–53.
- Rasool, S.I., Schneider, S.H., 1971. Atmospheric carbon dioxide and aerosols: effects of large increases on global climate. *Science*, 173, 138–141.
- Ritchie, J., Dowlatabadi, H., 2017. Why do climate change scenarios return to coal? *Energy*, 140, 1276–1291.
- Royer, D.L., Berner, R.A., Beerling, D.J., 2001. Phanerozoic atmospheric CO₂ change: evaluating geochemical and paleobiological approaches. *Earth-Sci. Rev.*, 54(4), 349–392.
- Rugenstein, M., Zelinka, M. D., Karnauskas, K. B., Ceppi, P., Andrews, T., 2023. Patterns of Surface Warming Matter for Climate Sensitivity. *Eos*, 104. American Geophysical Union (AGU). doi:10.1029/2023eo230411.

- Santer, B., Fyfe, J., Pallotta, G., Flato, G.M., Meehl, G.A., et al., 2017. Causes of differences in model and satellite tropospheric warming rates. *Nat. Geosci.*, 10, 478–485.
- Scafetta, N., Grigolini, P., Imholt, T., Roberts, J., West, B. J., 2004. Solar turbulence in earth's global and regional temperature anomalies. *Phys. Rev. E* 69, 026303.
- Scafetta, N., West, B.J., 2006a. Phenomenological solar contribution to the 1900–2000 global surface warming. *Geophys. Res. Lett.*, 33, L05708.
- Scafetta, N., West, B.J., 2006b. Phenomenological solar signature in 400 years of reconstructed Northern Hemisphere temperature record. *Geophys. Res. Lett.*, 33, L17718.
- Scafetta, N., West, B.J., 2007. Phenomenological reconstructions of the solar signature in the Northern Hemisphere surface temperature records since 1600. *J. Geophys. Res.*, 112, D24S03.
- Scafetta, N., West, B.J., 2008. Is climate sensitive to solar variability? *Phys. Today*, 61(3), 50–51.
- Scafetta, N., 2009. Empirical analysis of the solar contribution to global mean air surface temperature change. *J. Atmos. Sol.-Terr. Phys.*, 71, 17–18.
- Scafetta, N., 2010. Empirical evidence for a celestial origin of the climate oscillations and its implications. *J. Atmos. Sol.-Terr. Phys.*, 72, 951–970.
- Scafetta, N., 2012a. Testing an astronomically based decadal-scale empirical harmonic climate model versus the IPCC (2007) general circulation climate models. *J. Atmos. Sol.-Terr. Phys.*, 80, 124–137.
- Scafetta, N., 2012b. Multi-scale harmonic model for solar and climate cyclical variation throughout the Holocene based on Jupiter-Saturn tidal frequencies plus the 11-year solar dynamo cycle. *J. Atmos. Sol.-Terr. Phys.*, 80, 296–311.
- Scafetta, N., 2012c. A shared frequency set between the historical mid-latitude aurora records and the global surface temperature. *J. Atmos. Sol.-Terr. Phys.*, 74, 145–163.
- Scafetta, N., 2012d. Does the Sun work as a nuclear fusion amplifier of planetary tidal forcing? A proposal for a physical mechanism based on the mass-luminosity relation. *J. Atmos. Sol.-Terr. Phys.*, 81–82, 27–40.
- Scafetta, N., 2013a. Discussion on climate oscillations: CMIP5 general circulation models versus a semi-empirical harmonic model based on astronomical cycles. *Earth Sci. Rev.*, 126, 321–357.
- Scafetta, N., 2013b. Discussion on common errors in analyzing sea level accelerations, solar trends and global warming. *Pattern Recognit. Phys.*, 1, 37–57.
- Scafetta, N., 2014a. Multi-scale dynamical analysis (MSDA) of sea level records versus PDO, AMO, and NAO indexes. *Clim. Dyn.*, 43(1–2), 175–192.
- Scafetta, N., 2014b. Discussion on the spectral coherence between planetary, solar and climate oscillations: a reply to some critiques. *Astrophys. Space Sci.*, 354, 275–299.
- Scafetta, N., Milani, F., Bianchini, A., Ortolani, S., 2016. On the astronomical origin of the Hallstatt oscillation found in radiocarbon and climate records throughout the Holocene. *Earth-Sci. Rev.*, 162, 24–43.
- Scafetta, N., Ouyang, S., 2019. Detection of UHI bias in China climate network using Tmin and Tmax surface temperature divergence. *Glob. Planet. Change*, 181, 102989.
- Scafetta, N., Willson, R.C., Lee, J.N., Wu, D.L., 2019. Modeling quiet solar luminosity variability from TSI satellite measurements and proxy models during 1980–2018. *Remote Sens.*, 11(21), 2569.

- Scafetta, N., 2020. Solar oscillations and the orbital invariant inequalities of the solar system. *Sol. Phys.*, 295(2), 33.
- Scafetta, N., Milani, F., Bianchini, A., 2020. A 60-year cycle in the meteorite fall frequency suggests a possible interplanetary dust forcing of the Earth's climate driven by planetary oscillations. *Geophys. Res. Lett.*, 47(18), e2020GL089954.
- Scafetta, N., 2021. Detection of non-climatic biases in land surface temperature records by comparing climatic data and their model simulations. *Clim. Dyn.*, 56(9–10), 2959–2982.
- Scafetta, N., 2021b. Reconstruction of the interannual to millennial scale patterns of the global surface temperature. *Atmosphere*, 12, 147.
- Scafetta, N., 2021c. Testing the CMIP6 GCM simulations versus surface temperature records from 1980–1990 to 2011–2021: High ECS is not supported. *Climate*, 9, 161.
- Scafetta, N., 2022. Advanced testing of low, medium, and high ECS CMIP6 GCM simulations versus ERA5-T2m. *Geophys. Res. Lett.*, 49(6), e2022GL097716.
- Scafetta, N., Bianchini, A., 2022. The planetary theory of solar activity variability: a review. *Front. Astron. Space Sci.*, 9, 937930.
- Scafetta, N., 2023a. Empirical assessment of the role of the Sun in climate change using balanced multi-proxy solar records. *Geosci. Front.*, 14(6), 101650.
- Scafetta, N., 2023b. CMIP6 GCM ensemble members versus global surface temperatures. *Clim. Dyn.*, 60, 3091–3120.
- Scafetta, N., 2023c. CMIP6 GCM validation based on ECS and TCR ranking for 21st-century temperature projections and risk assessment. *Atmosphere*, 14, 345.
- Scafetta, N., Bianchini, A., 2023. Overview of the spectral coherence between planetary resonances and solar and climate oscillations. *Climate*, 11(4), 77.
- Scafetta, N., 2024. Impacts and risks of “realistic” global warming projections for the 21st century. *Geosci. Front.*, 15(2), 101774.
- Scafetta, N., Milani, F., 2025. Spectral Structure of the Solar Inertial Motion from 12999 BC to 16998 AD. *Publ. Astron. Soc. Pac.*, under press.
- Schildknecht, D., 2020. Saturation of the infrared absorption by carbon dioxide in the atmosphere. *Int. J. Mod. Phys. B*, 34, 30.
- Schlesinger, M., Ramankutty, N., 1994. An oscillation in the global climate system of period 65–70 years. *Nature*, 367, 723–726.
- Schmutz, W.K., 2021. Changes in the total solar irradiance and climatic effects. *J. Space Weather Space Clim.*, 11, 40.
- Schoeberl, M.R., Wang, Y., Taha, G., Zawada, D.J., Ueyama, R., Dessler, A., 2024. Evolution of the climate forcing during the two years after the Hunga Tonga-Hunga Ha'apai eruption. *J. Geophys. Res. Atmos.*, 129, e2024JD041296.
- Shakun, J., Clark, P., He, F., Marcott, S.A., Mix, A.C., Liu, Z., et al., 2012. Global warming preceded by increasing carbon dioxide concentrations during the last deglaciation. *Nature*, 484, 49–54.
- Shaviv, N.J., Veizer, J., 2003. Celestial driver of Phanerozoic climate? *GSA Today*, 13(7), 4–10.

- Shaviv, N.J., 2008. Using the oceans as a calorimeter to quantify the solar radiative forcing. *J. Geophys. Res. Space Phys.*, 113(A11), A11101.
- Shaviv, N.J., Svensmark, H., Veizer, J., 2023. The Phanerozoic climate. *Ann. N.Y. Acad. Sci.*, 1519, 7–19.
- Sherwood, S., Webb, M., Annan, J., Armour, K., Forster, P., et al., 2020. An assessment of Earth's climate sensitivity using multiple lines of evidence. *Rev. Geophys.*, 58, e2019RG000678.
- Simpson, I.R., McKinnon, K.A., Kennedy, D., Lawrence, D.M., Lehner, F., Seager, R., 2024. Observed humidity trends in dry regions contradict climate models. *Proc. Natl. Acad. Sci. USA*, 121(1), e2302480120.
- Soon, W., Posmentier, E., Baliunas, S., 2000. Climate hypersensitivity to solar forcing? *Ann. Geophys.*, 18(5), 583–588.
- Soon, W., Baliunas, S., 2003. Proxy climatic and environmental changes of the past 1000 years. *Clim. Res.*, 23(2), 89–110.
- Soon, W., Baliunas, S., Idso, C., Idso, S., Legates, D., 2003. Reconstructing climatic and environmental changes of the past 1000 years: A reappraisal. *Energy Environ.*, 14(2–3), 233–296.
- Soon, W., Legates, D.R., 2013. Solar irradiance modulation of equator-to-pole (Arctic) temperature gradients: Empirical evidence for climate variation on multi-decadal timescales. *J. Atmos. Sol.-Terr. Phys.*, 93, 45–56.
- Soon, W., Connolly, R., Connolly, M., Akasofu, S.-I., Baliunas, S., et al., 2023. The detection and attribution of Northern Hemisphere land surface warming (1850–2018) in terms of human and natural factors: Challenges of inadequate data. *Climate*, 11, 179.
- Spencer, R.W., Christy, J.R., Braswell, W.D., 2017. UAH version 6 global satellite temperature products: Methodology and results. *Asia-Pac. J. Atmos. Sci.*, 53(1), 121–130.
- Squintu, A.A., van der Schrier, G., Štěpánek, P., Zahradníček, P., Tank, A.K., 2020. Comparison of homogenization methods for daily temperature series against an observation-based benchmark dataset. *Theor. Appl. Climatol.*, 140, 285–301.
- Stefani, F., 2021. Solar and anthropogenic influences on climate: Regression analysis and tentative predictions. *Climate*, 9, 163.
- Stefani, F., Horstmann, G.M., Klevs, M., Mamatsashvili, G., Weier, T., 2024. Rieger, Schwabe, Suess-de Vries: the sunny beats of resonance. *Sol. Phys.*, 299, 51.
- Steinhilber, F., Abreu, J.A., Beer, J., Brunner, I., Christl, M., et al., 2012. 9,400 years of cosmic radiation and solar activity from ice cores and tree rings. *Proc. Natl. Acad. Sci. USA*, 109(16), 5967–5971.
- Stewart, I.D., Oke, T.R., 2012. Local climate zones for urban temperature studies. *Bull. Am. Meteorol. Soc.*, 93, 1879–1900.
- Svensmark, H., Friis-Christensen, E., 1997. Variation of cosmic ray flux and global cloud coverage — a missing link in solar-climate relationships. *J. Atmos. Sol.-Terr. Phys.*, 59(11), 1225–1232.
- Svensmark, J., Enghoff, M.B., Shaviv, N.J., Svensmark, H., 2016. The response of clouds and aerosols to cosmic ray decreases. *J. Geophys. Res. Space Phys.*, 121(9), 8152–8181.
- Svensmark, H., 2019. Force Majeure: The Sun's Role in Climate Change. The Global Warming Policy Foundation. ISBN 978-0993119095. Available at <https://www.thegwpcf.org/content/uploads/2019/03/SvensmarkSolar2019-1.pdf>
- Svensmark, H., 2022. Supernova rates and burial of organic matter. *Geophys. Res. Lett.*, 49(1), e2021GL096376.

- Tol, R., 2023. Costs and benefits of the Paris climate targets. *Clim. Change Econ.*, 14, 2340003.
- Toohey, M., Sigl, M., 2017. Volcanic stratospheric sulfur injections and aerosol optical depth from 500 BCE to 1900 CE. *Earth Syst. Sci. Data*, 9, 809–831.
- Undorf, S., Pulkkinen, K., Wikman-Svahn, P., Bender, F.A.-M., 2022. How do value-judgments enter model-based assessments of climate sensitivity? *Clim. Change*, 174, 19.
- van Wijngaarden, W.A., Happer, W., 2023. Atmosphere and greenhouse gas primer. arXiv, DOI: 10.48550/arXiv.2303.00808.
- van Wijngaarden, W.A., Happer, W., 2025. Radiation transport in clouds. *Sci. Clim. Change*, 5(1), 1–12.
- von Storch, H., Zorita, E., Jones, J.M., Dimitriev, Y., González-Rouco, F., Tett, S.F.B., 2004. Reconstructing past climate from noisy data. *Science*, 306, 679–682.
- Watts, A., 2022. Corrupted Climate Stations: The Official U.S. Temperature Record Remains Fatally Flawed. Heartland Inst., Available at: https://heartland.org/wp-content/uploads/documents/2022_Surface_Station_Report.pdf, accessed on April 10, 2025.
- WCRP Coupled Model Intercomparison Project (CMIP). Available at: <https://wcrp-cmip.org/>.
- Westhoff, J., Sinnl, G., Svensson, A., Freitag, J., Kjær, H.A., et al., 2022. Melt in the Greenland EastGRIP ice core reveals Holocene warm events. *Clim. Past*, 18, 1011–1034.
- Willson, R.C., Mordvinov, A.V., 2003. Secular total solar irradiance trend during solar cycles 21–23. *Geophys. Res. Lett.*, 30, 1199.
- Wu, C.-J., Krivova, N.A., Solanki, S.K., Usoskin, I.G., 2018. Solar total and spectral irradiance reconstruction over the last 9000 years. *Astron. Astrophys.*, 620, A120.
- Wyatt, M., Curry, J., 2014. Role of Eurasian Arctic shelf sea ice in a secularly varying hemispheric climate signal during the 20th century. *Clim. Dyn.*, 42, 2763–2782.
- Xiao, Z., Zhao, L., Zhou, L., Huo, W., Mironova, I., Miyahara, H., 2024. Editorial: Impact of solar activities on weather and climate. *Front. Earth Sci.*, 11, 1338416.
- Yeo, K.L., Krivova, N.A., Solanki, S.K., Glassmeier, K.H., 2014. Reconstruction of total and spectral solar irradiance from 1974 to 2013 based on KPVT, SoHO/MDI and SDO/HMI observations. *Astron. Astrophys.*, 570, A85.
- Yeo, K.L., Solanki, S.K., Krivova, N.A., Rempel, M., Anusha, L.S., et al., 2020. The dimmest state of the Sun. *Geophys. Res. Lett.*, 47(19), e2020GL090243.
- Zanchettin, D., Timmreck, C., Khodri, M., Schmidt, A., Toohey, M., et al., 2022. Effects of forcing differences and initial conditions on inter-model agreement in the VolMIP volc-pinatubo-full experiment. *Geosci. Model Dev.*, 15, 2265–2292.
- Zander, P.D., Böhl, D., Sirocko, F., Auderset, A., Haug, G.H., Martínez-García, A., 2024. Reconstruction of warm-season temperatures in central Europe during the past 60,000 years from lacustrine branched glycerol dialkyl glycerol tetraethers (brGDGTs). *Clim. Past*, 20, 841–864.
- Zhang, B., Song, S., Wang, H., Guo, T., Ding, Y., 2025. Evaluation of the performance of CMIP6 models in simulating extreme precipitation and its projected changes in global climate regions. *Nat. Hazards*, 121, 1737–1763.
- Zhu, Z., Piao, S., Myneni, R.B., Huang, M., Zeng, Z., et al., 2016. Greening of the Earth and its drivers. *Nat. Clim. Change*, 6(8), 791–795.

- Ziskin, S., Shaviv, N.J., 2012. Quantifying the role of solar radiative forcing over the 20th century. *Adv. Space Res.*, 50(6), 762–776.
- Zou, C.-Z., Xu, H., Hao, X., Liu, Q., 2023. Mid-tropospheric layer temperature record derived from satellite microwave sounder observations with backward merging approach. *J. Geophys. Res. Atmos.*, 128, e2022JD037472.